Chapter 6

ASAP Supplement

Lead Authors: Debra Weisenstein, Slimane Bekki
Authors: Giovanni Pitari, Claudia Timmreck, Michael Mills
Contributors: Joyce Penner, J.C. Wilson, Mian Chin, E. Mancini, Beiping Luo, Mark Hervig, Fok-Yan Leung

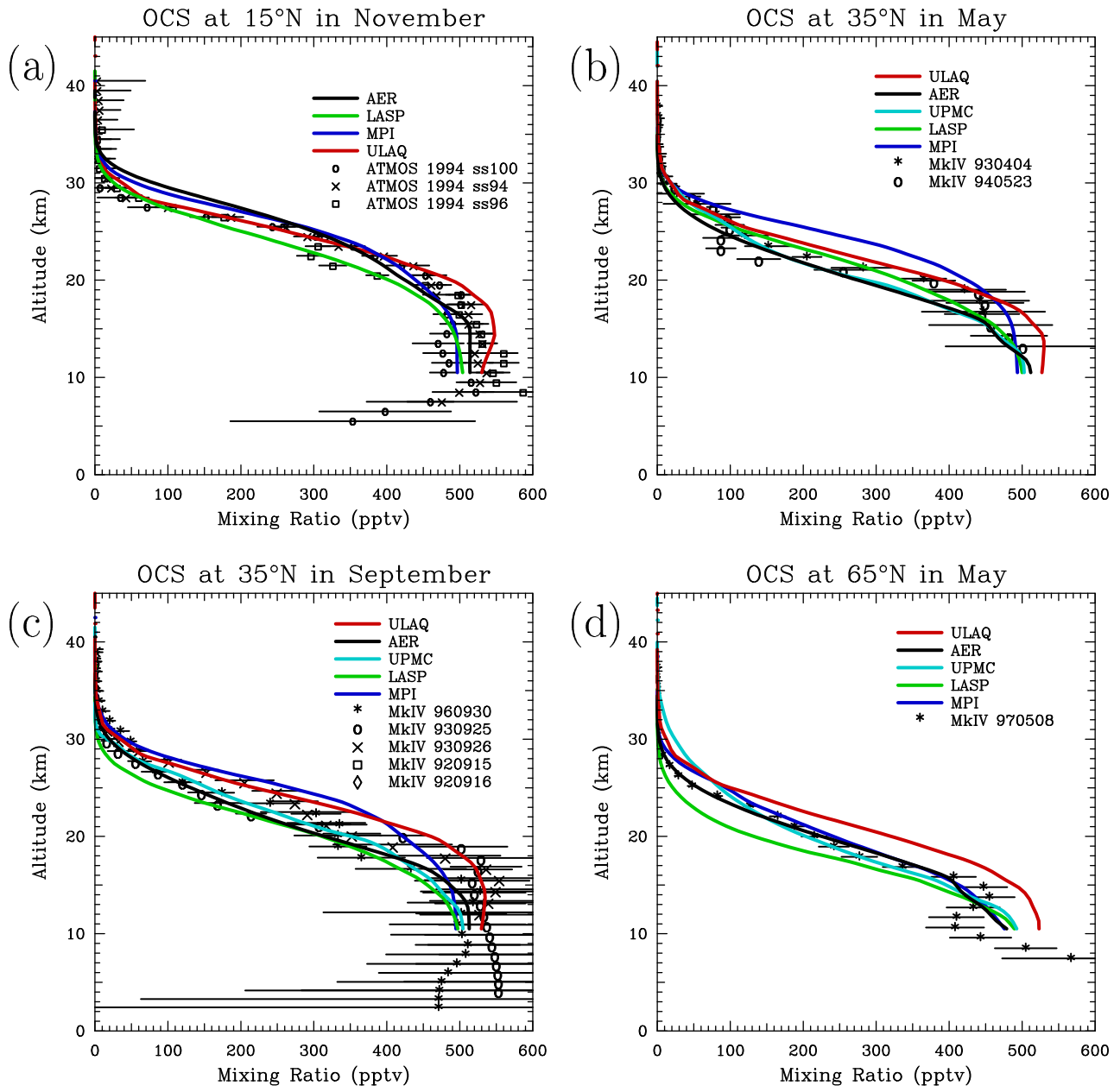

Figure 6.1: OCS calculated mixing ratio profiles at (a) 15°N in November compared to 1994 ATMOS observations [Gunson et al., 1996; Rinsland et al., 1996] and at (b) 35°N in May, (c) 35°N in September, and (d) 65°N in May compared to MkIV balloon observations [Leung et al., 2002] taken between 1992 and 1997.

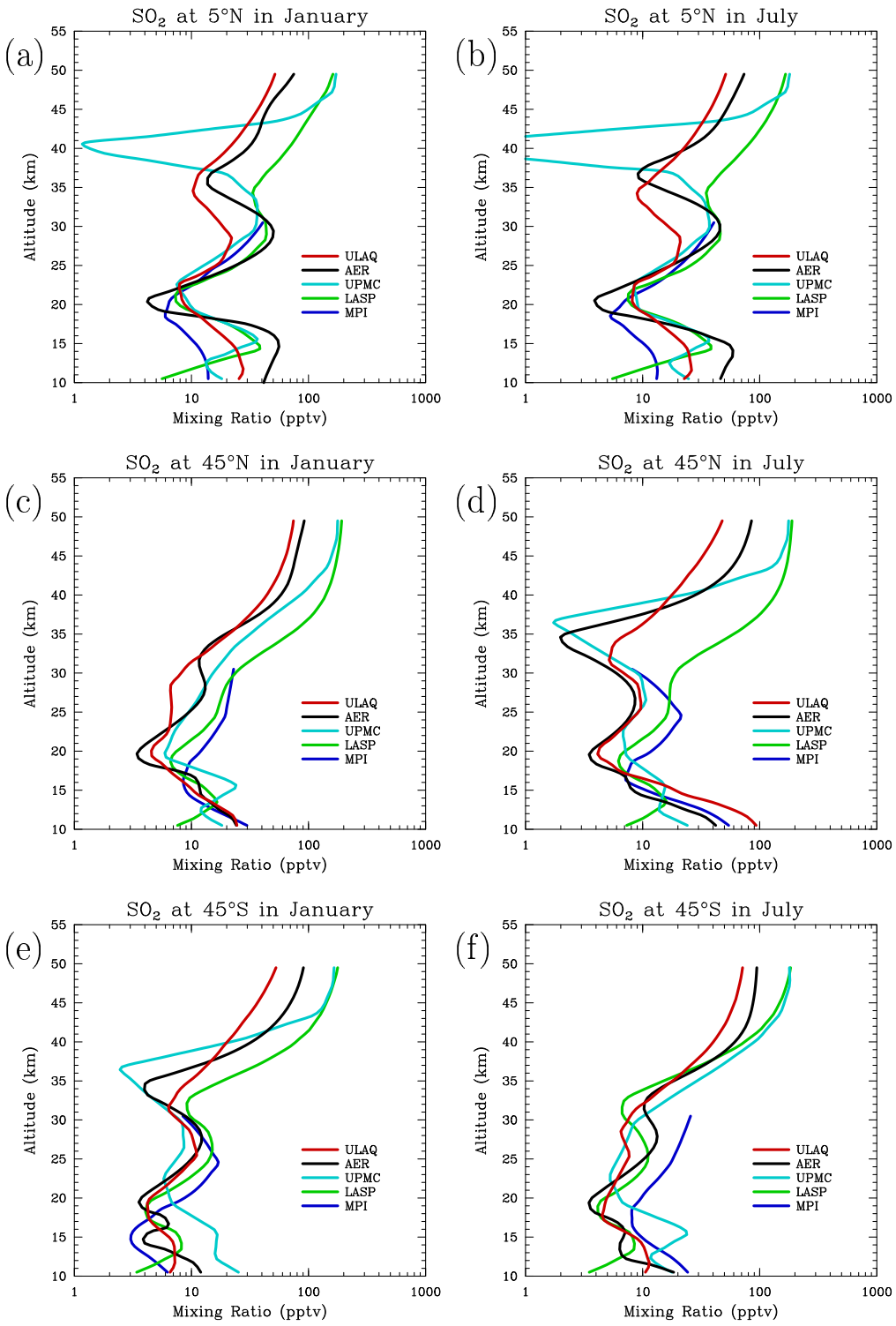

Figure 6.2: Model-calculated SO_2 mixing ratio profiles for January (left panels) and July (right panels) of 2000 at (a and b) 5°N, at (c and d) 45°N, and at (e and f) 45°S.

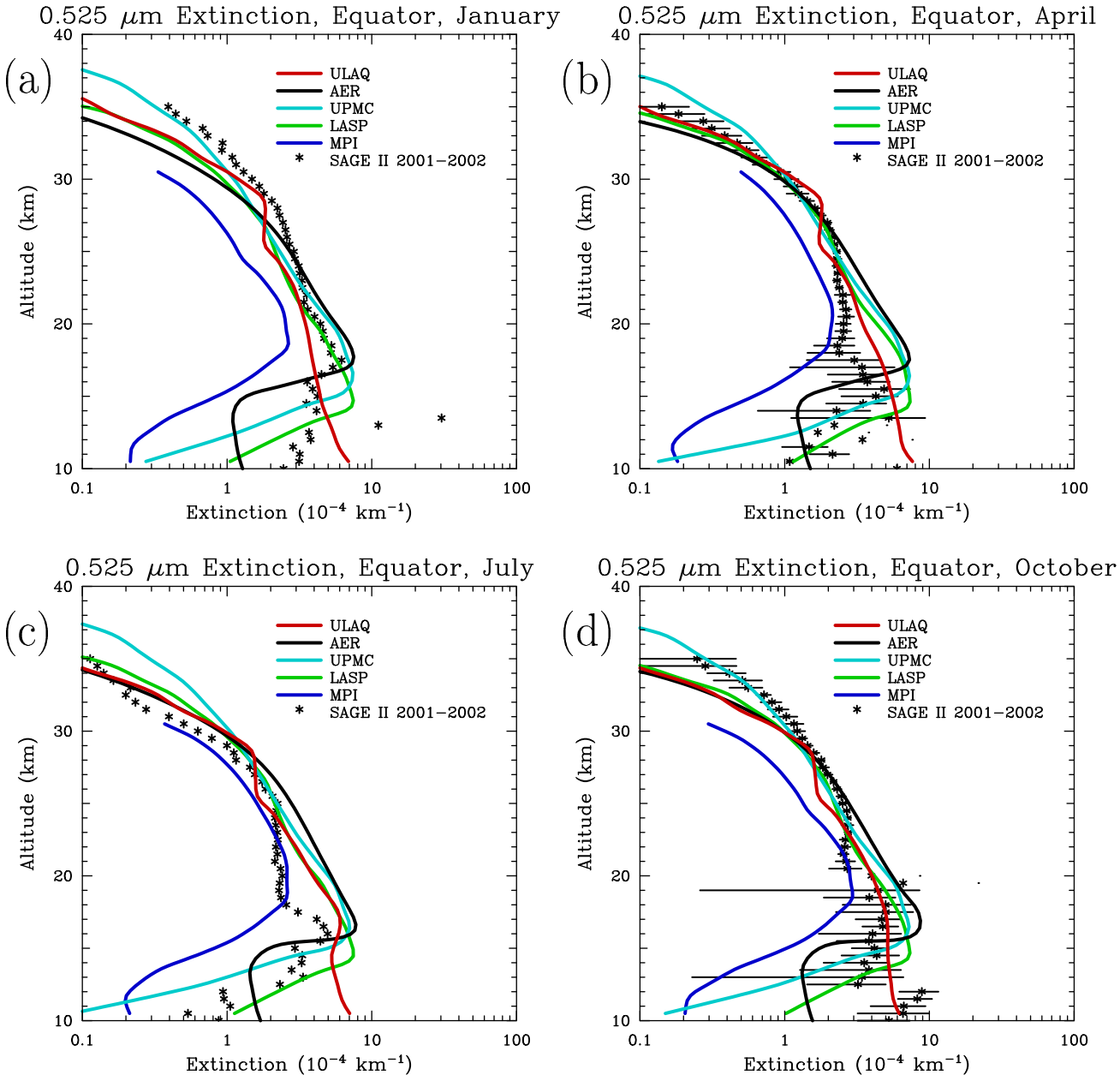

Figure 6.3: Comparison of SAGE II and model-calculated extinctions at 0.525 μm in (a) January, (b) April, (c) July, and (d) October of 2000 at the equator. SAGE II data are a composite of 2001 and 2002 observations as described in the text.

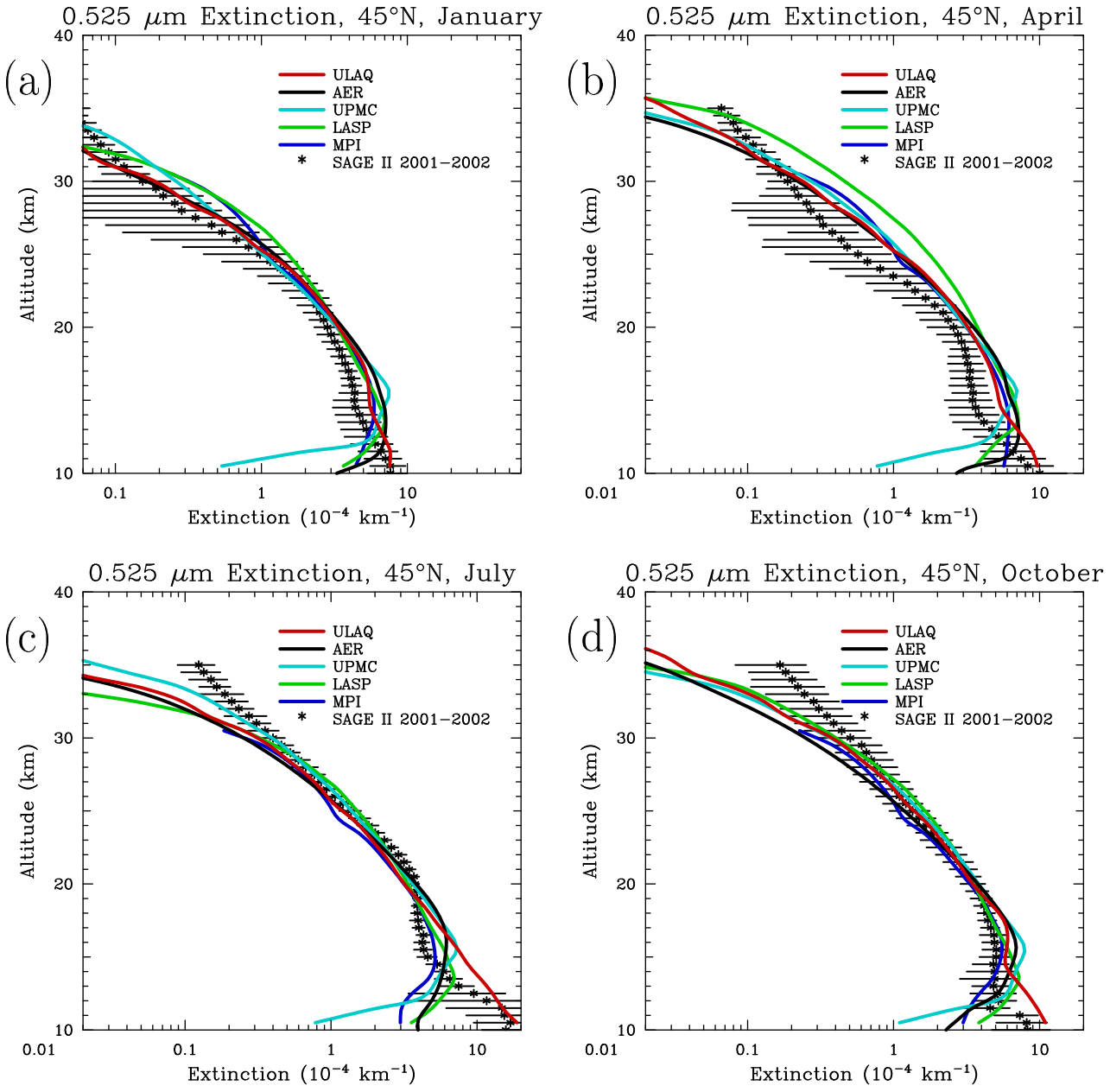

Figure 6.4: Comparison of SAGE II and model-calculated extinctions at 0.525 μm in (a) January, (b) April, (c) July, and (d) October of 2000 at 45°N. SAGE II data are a composite of 2001 and 2002 observations as described in the text.

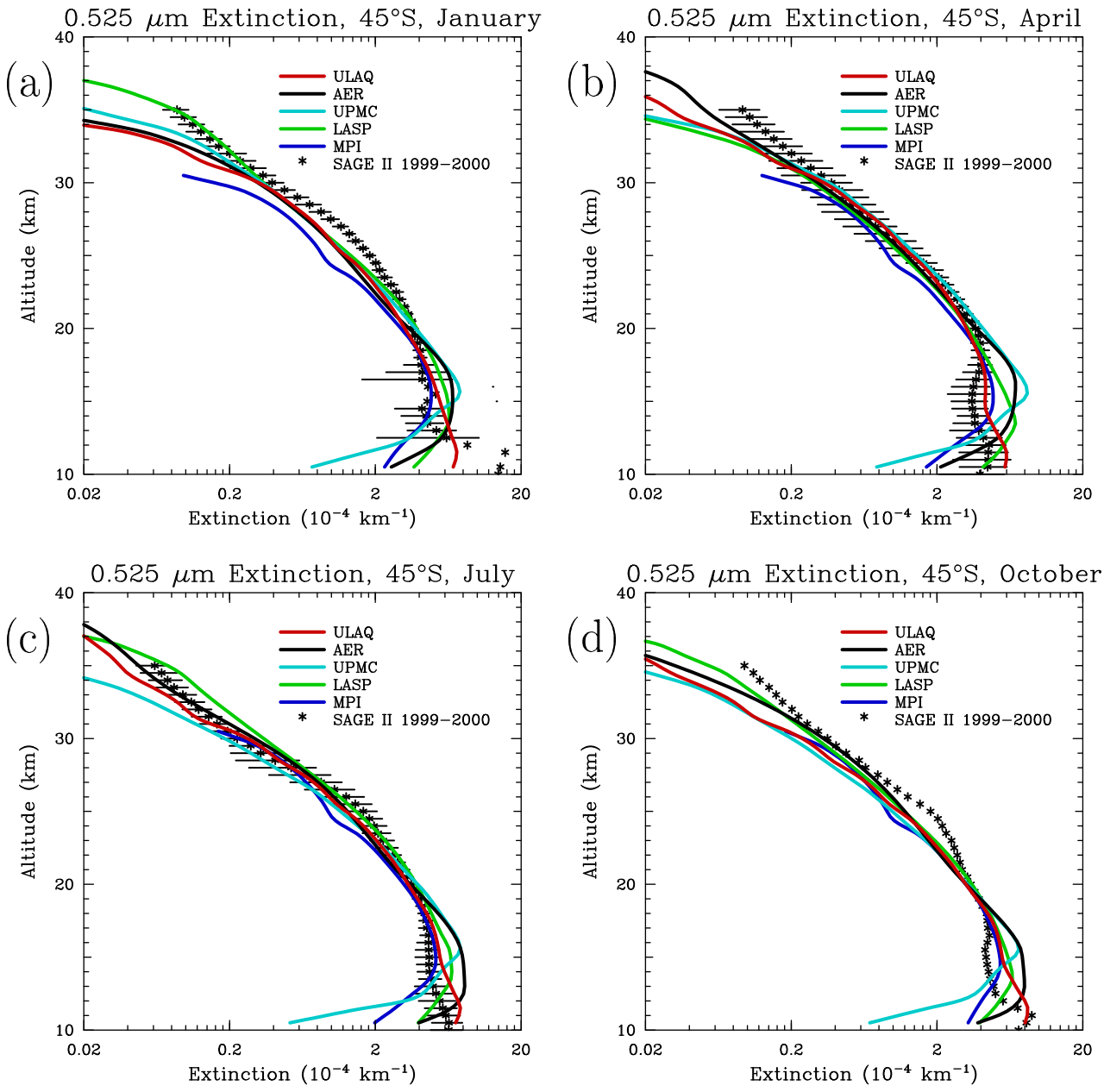

Figure 6.5: Comparison of SAGE II and model-calculated extinctions at 0.525 μm in (a) January, (b) April, (c) July, and (d) October of 2000 at 45°S. SAGE II data are a composite of 2001 and 2002 observations as described in the text.

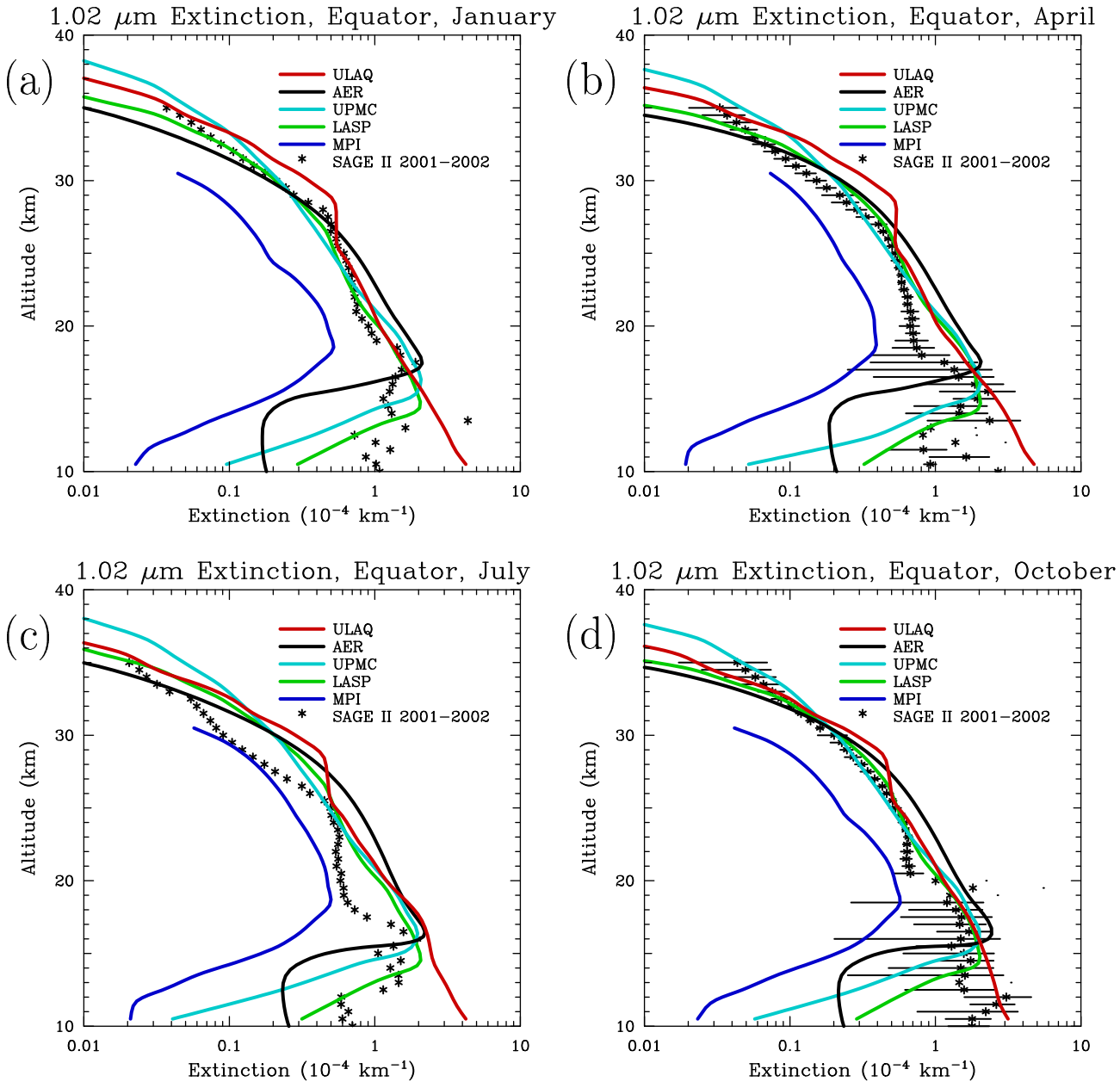

Figure 6.6: Comparison of SAGE II and model-calculated extinctions at 1.02 μm in (a) January, (b) April, (c) July, and (d) October of 2000 at the equator. SAGE II data are a composite of 2001 and 2002 observations as described in the text.

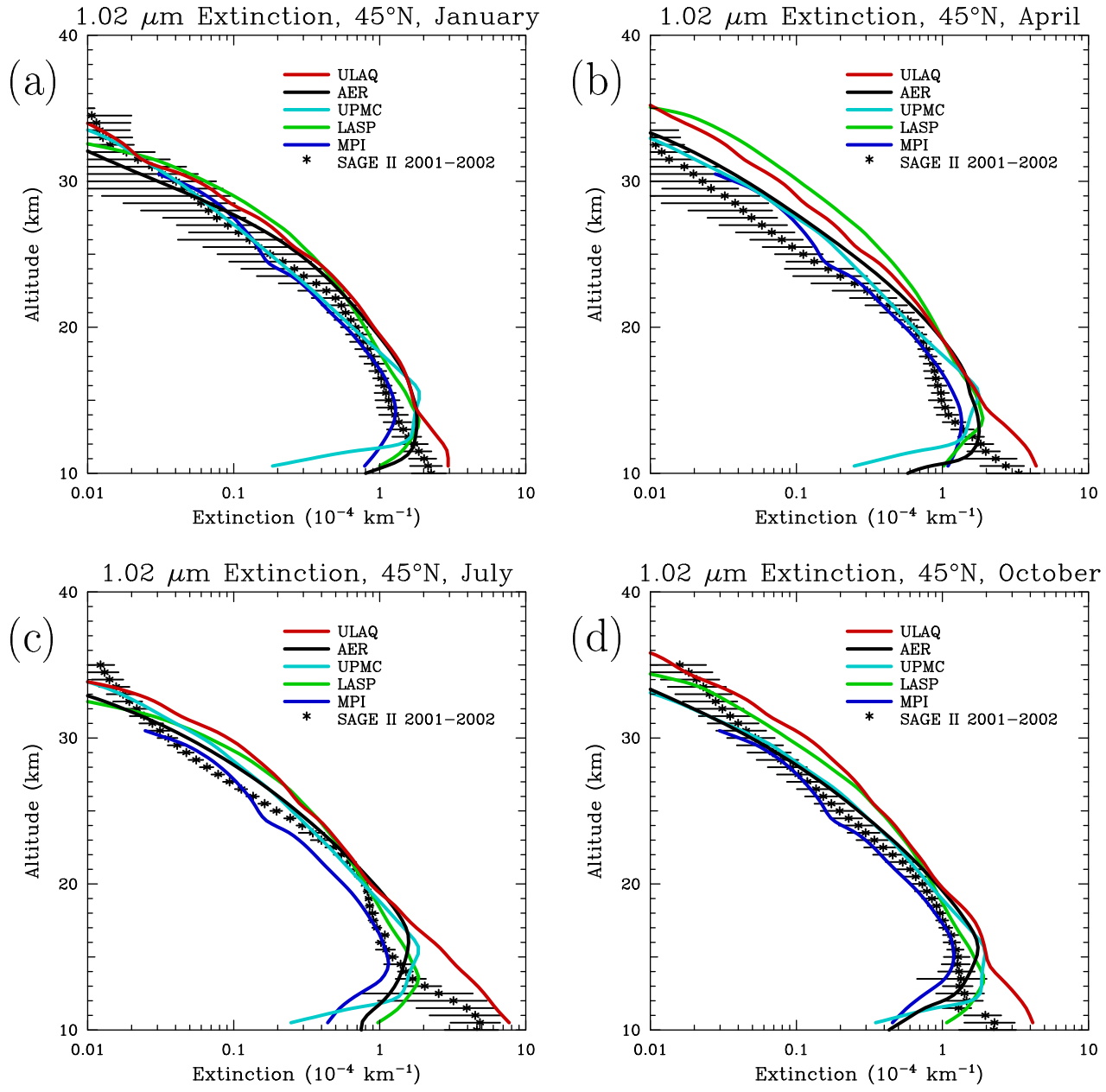

Figure 6.7: Comparison of SAGE II and model-calculated extinctions at 1.02 μm in (a) January, (b) April, (c) July, and (d) October of 2000 at 45°N. SAGE II data are a composite of 2001 and 2002 observations as described in the text.

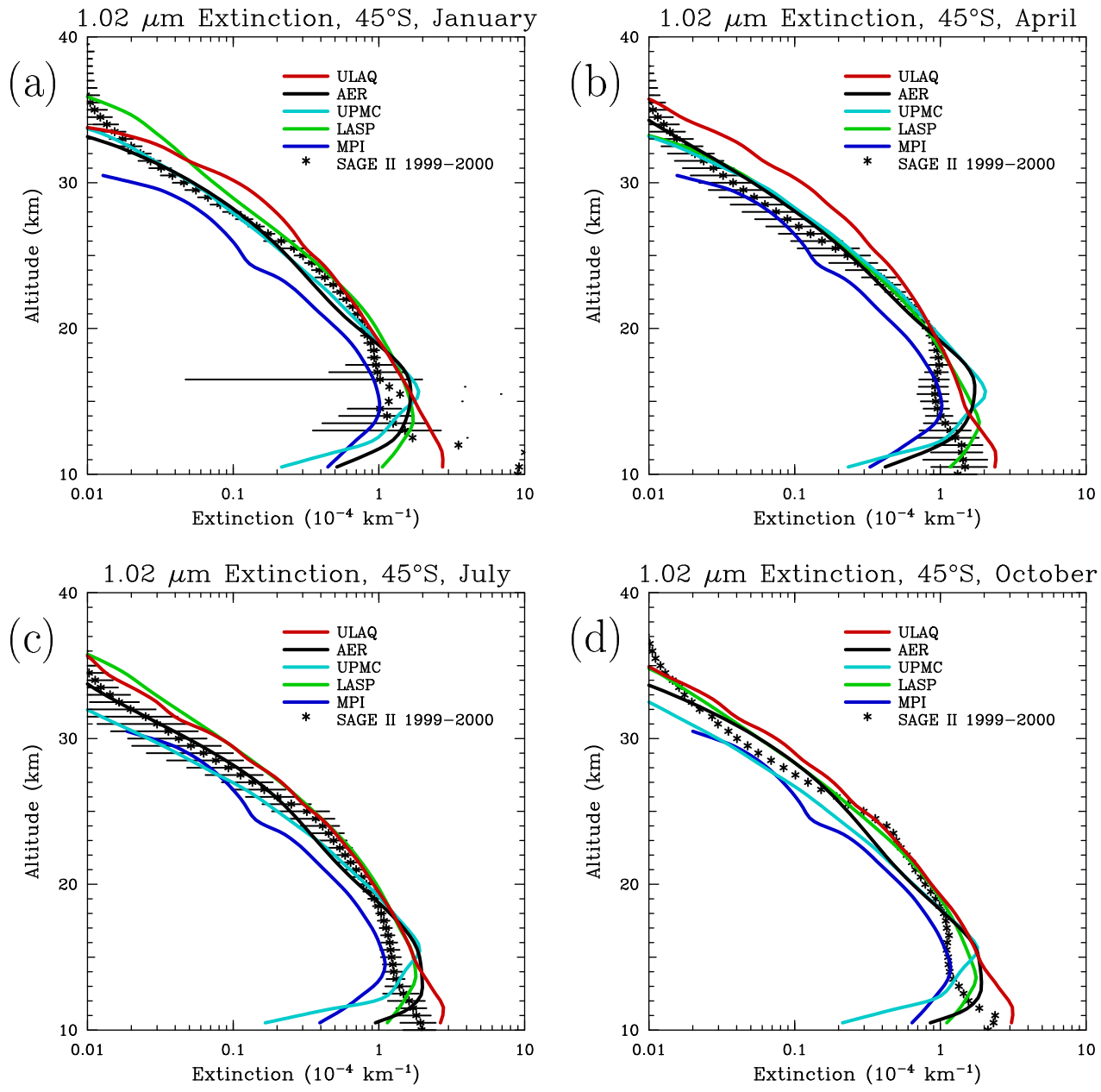

Figure 6.8: Comparison of SAGE II and model-calculated extinctions at 1.02 μm in (a) January, (b) April, (c) July, and (d) October of 2000 at 45°S. SAGE II data are a composite of 2001 and 2002 observations as described in the text.

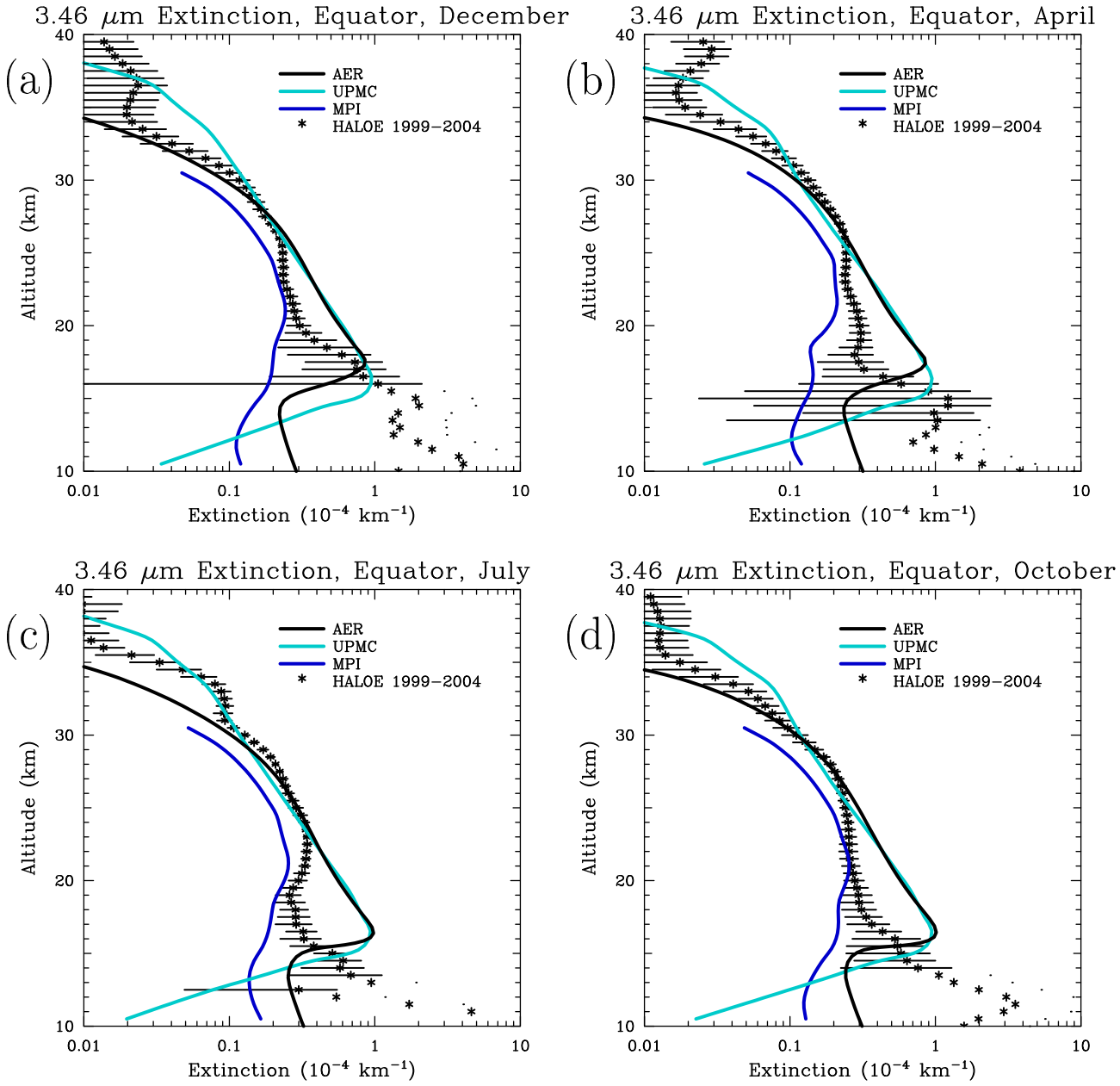

Figure 6.9: Comparison of HALOE and model-calculated extinctions at 3.46 μm in (a) December, (b) April, (c) July, and (d) October at the equator. HALOE observations are averaged over the 1999-2004 period.

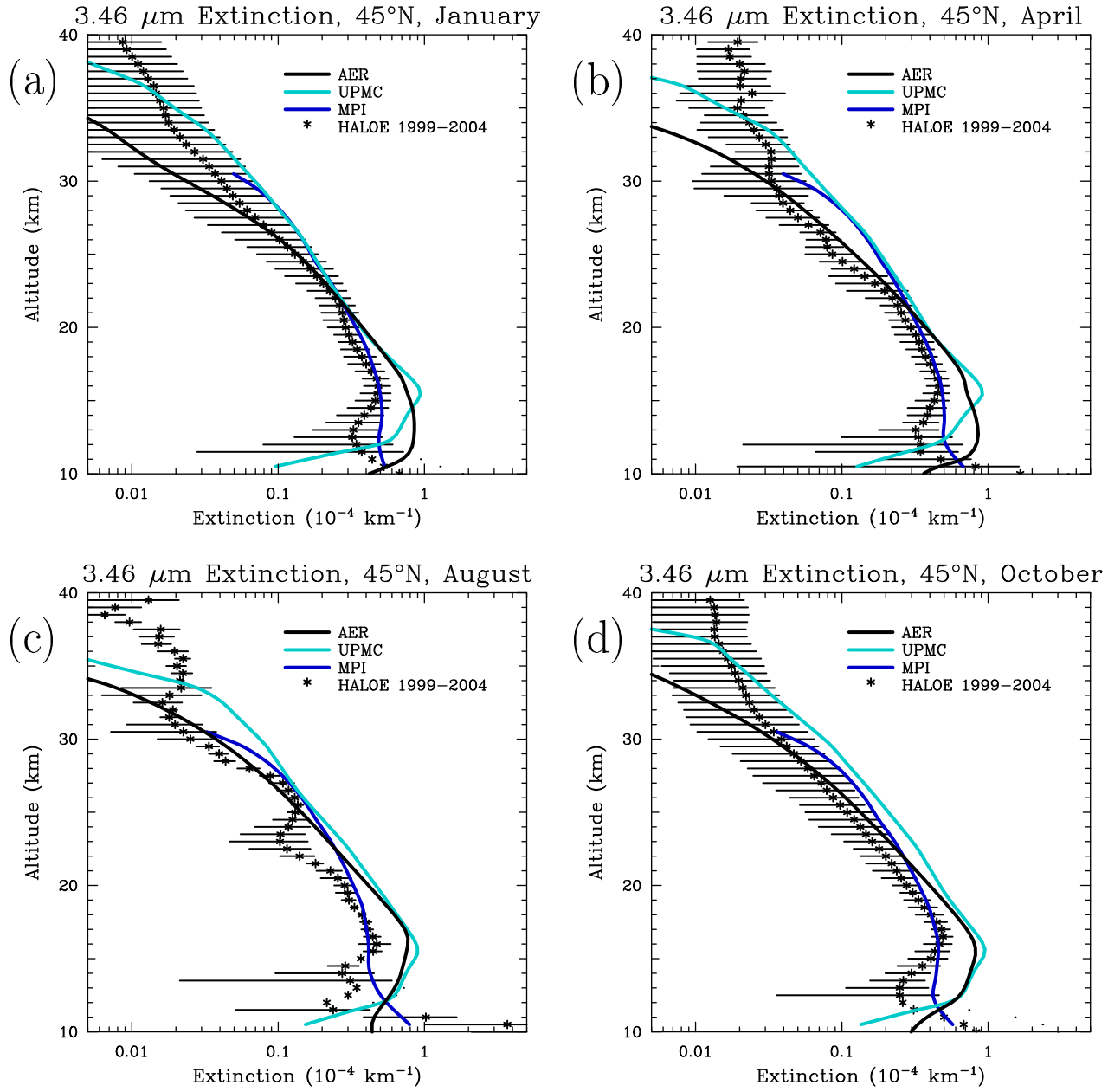

Figure 6.10: Comparison of HALOE and model-calculated extinctions at 3.46 μm in (a) January, (b) April, (c) August, and (d) October of 2000 at 45°N. HALOE observations are averaged over the 1999-2004 period.

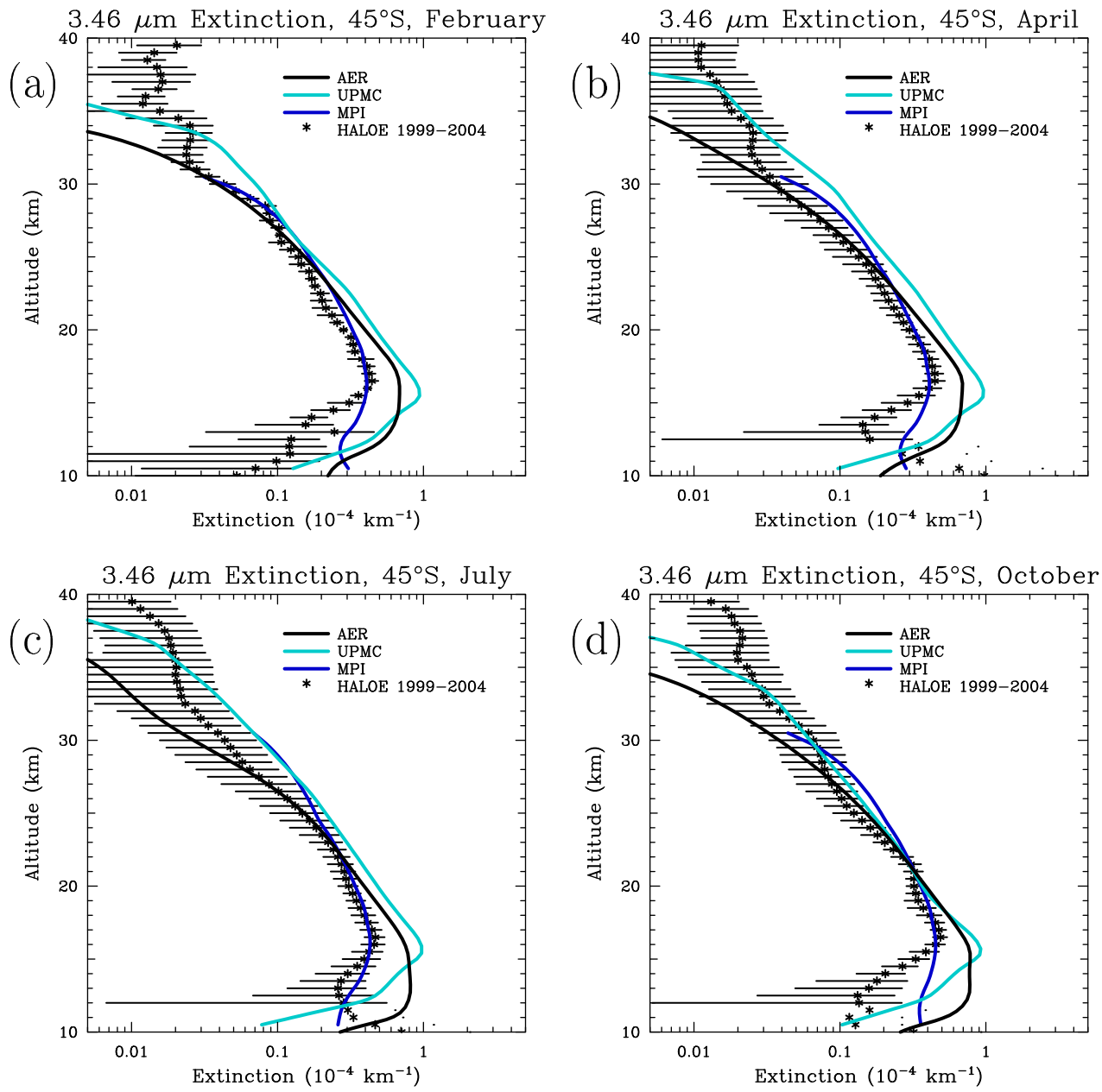

Figure 6.11: Comparison of HALOE and model-calculated extinctions at 3.46 μm in (a) February, (b) April, (c) July, and (d) October of 2000 at 45°S. HALOE observations are averaged over the 1999-2004 period.

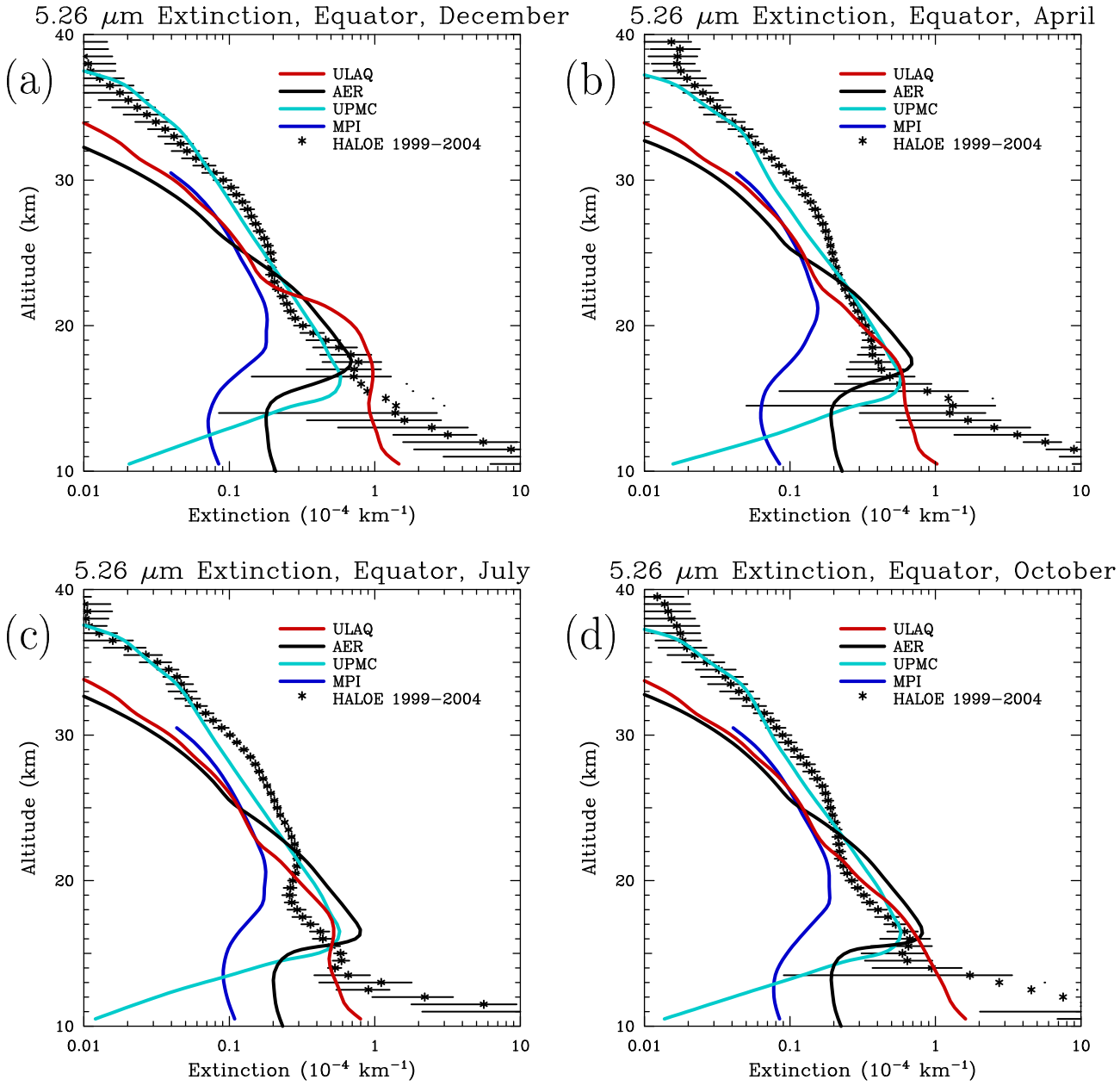

Figure 6.12: Comparison of HALOE and model-calculated extinctions at 5.26 μm in (a) December, (b) April, (c) July, and (d) October of 2000 at the equator. HALOE observations are averaged over the 1999-2004 period.

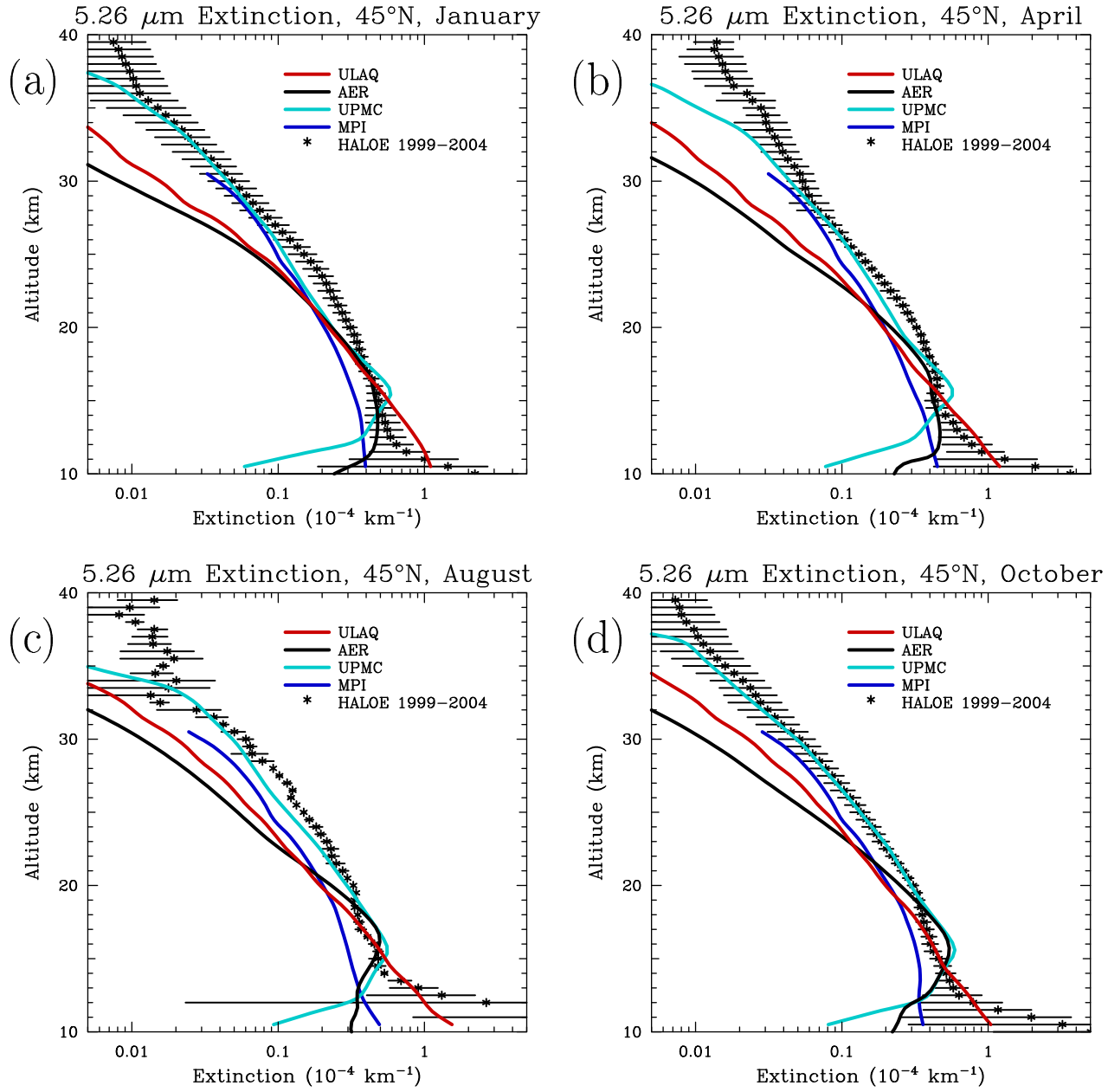

Figure 6.13: Comparison of HALOE and model-calculated extinctions at 5.26 μm in (a) January, (b) April, (c) August, and (d) October of 2000 at 45°N. HALOE observations are averaged over the 1999-2004 period.

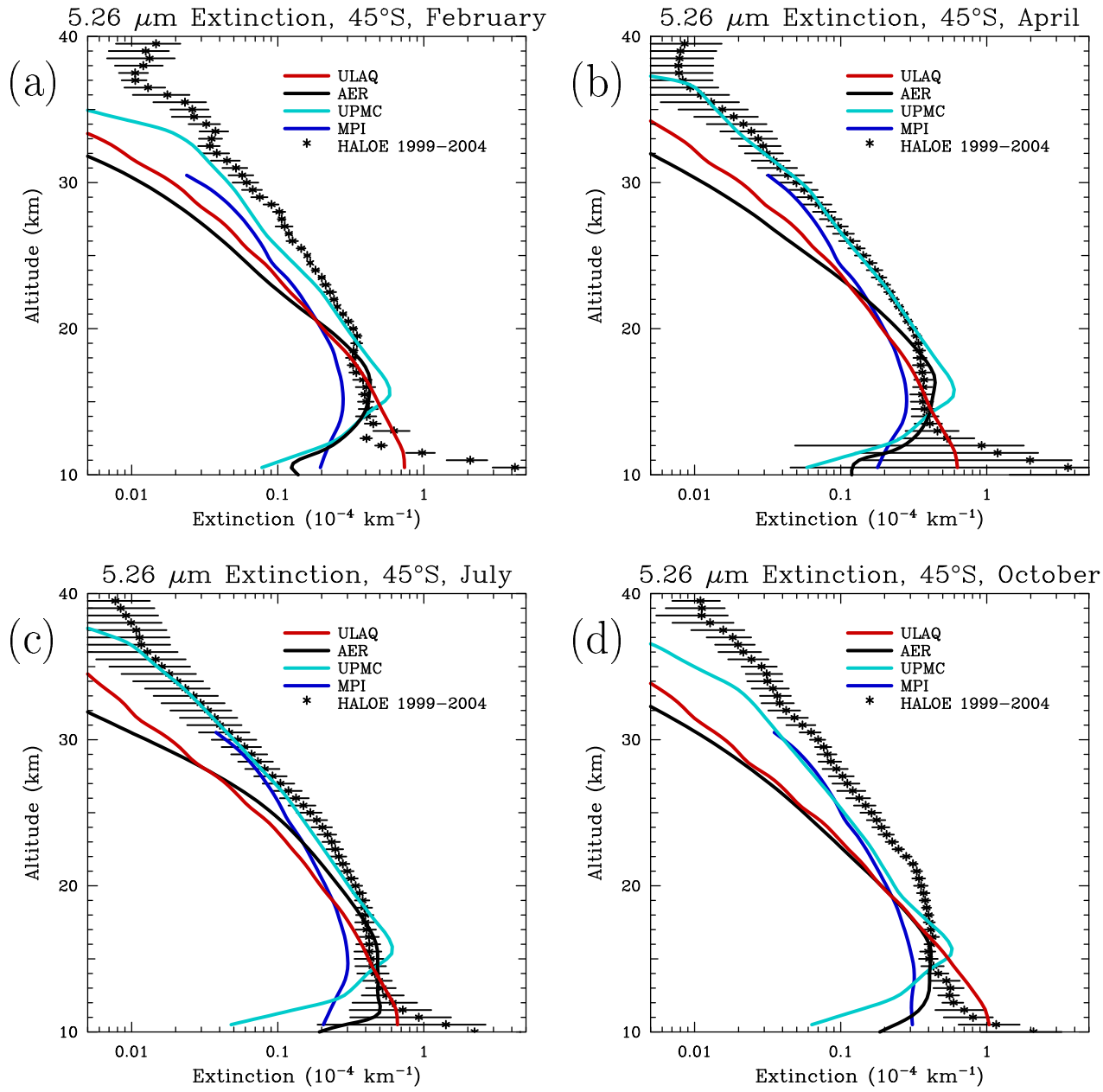

Figure 6.14: Comparison of HALOE and model-calculated extinctions at 5.26 μm in (a) February, (b) April, (c) July, and (d) October of 2000 at 45°S. HALOE observations are averaged over the 1999-2004 period.

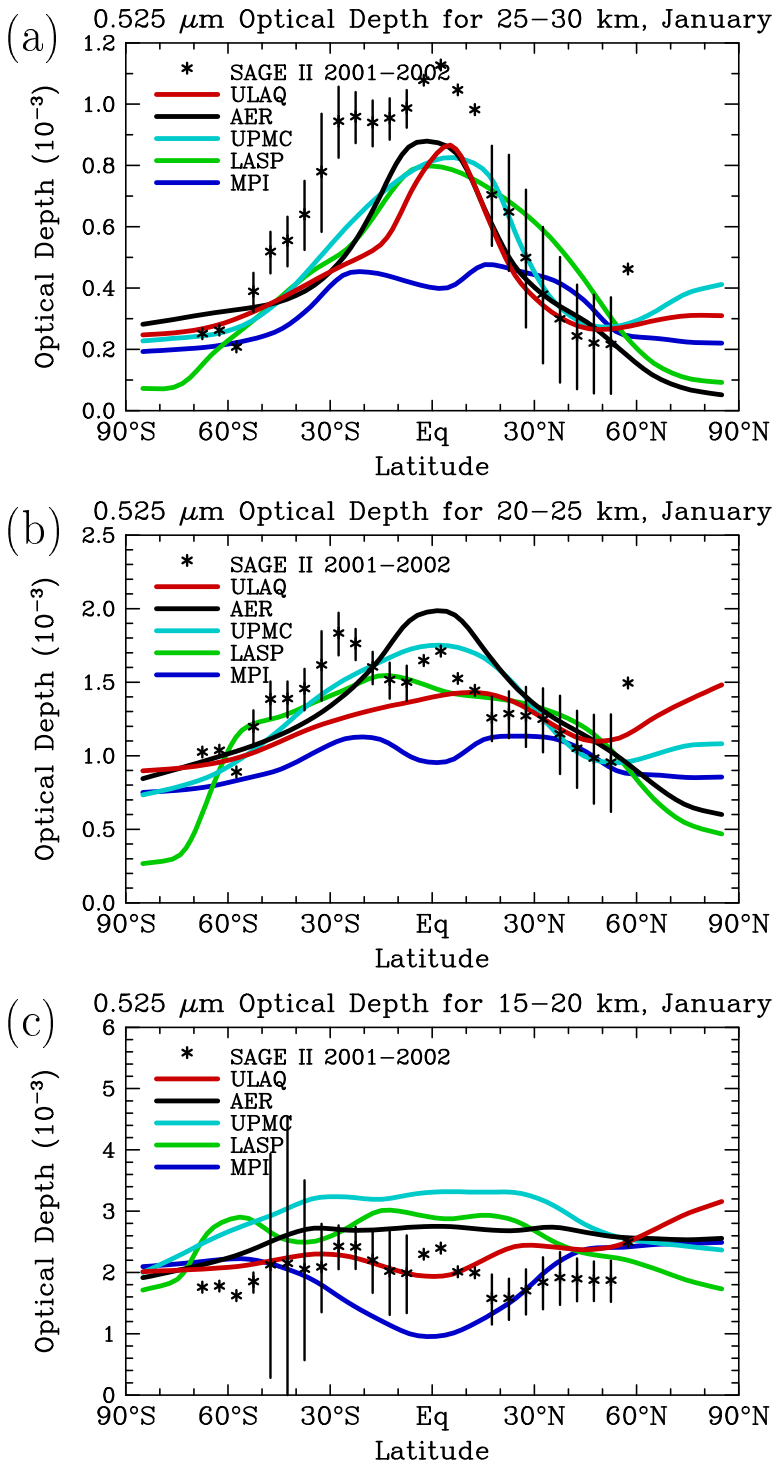

Figure 6.15: Aerosol optical depth at 0.525 μm for January of 2000 integrated from (a) 25 to 30 km, (b) 20 to 25 km and (c) 15 to 20 km. SAGE II data are shown by symbols, model results by colored lines.

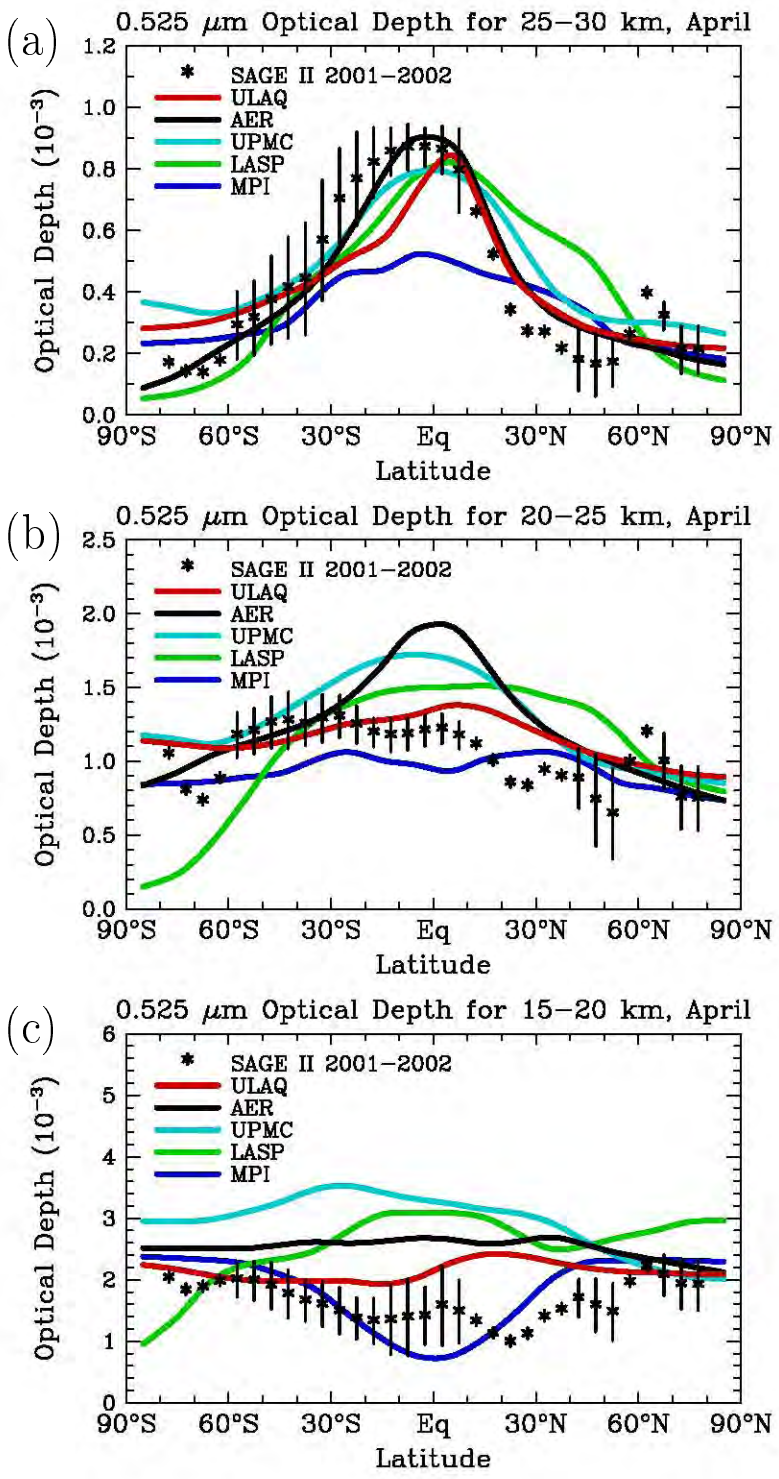

Figure 6.16: Aerosol optical depth at 0.525 μm for April of 2000 integrated from (a) 25 to 30 km, (b) 20 to 25 km and (c) 15 to 20 km. SAGE II data from the 2001-2002 composite background period are shown by symbols, model results by colored lines.

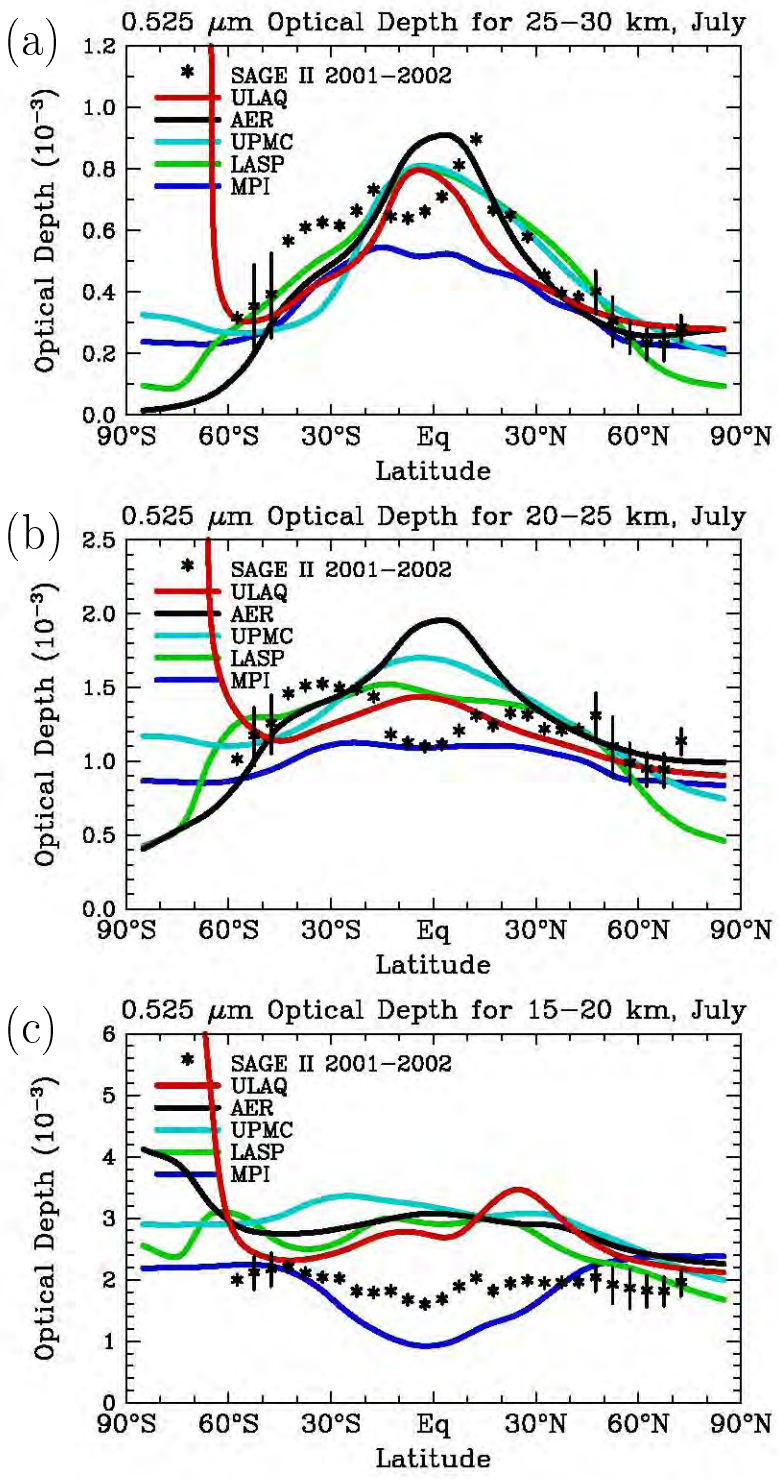

Figure 6.17: Aerosol optical depth at 0.525 μm for July of 2000 integrated from (a) 25 to 30 km, (b) 20 to 25 km and (c) 15 to 20 km. SAGE II data are shown by symbols, model results by colored lines. ULAQ optical depths include extinction due to PSC particles.

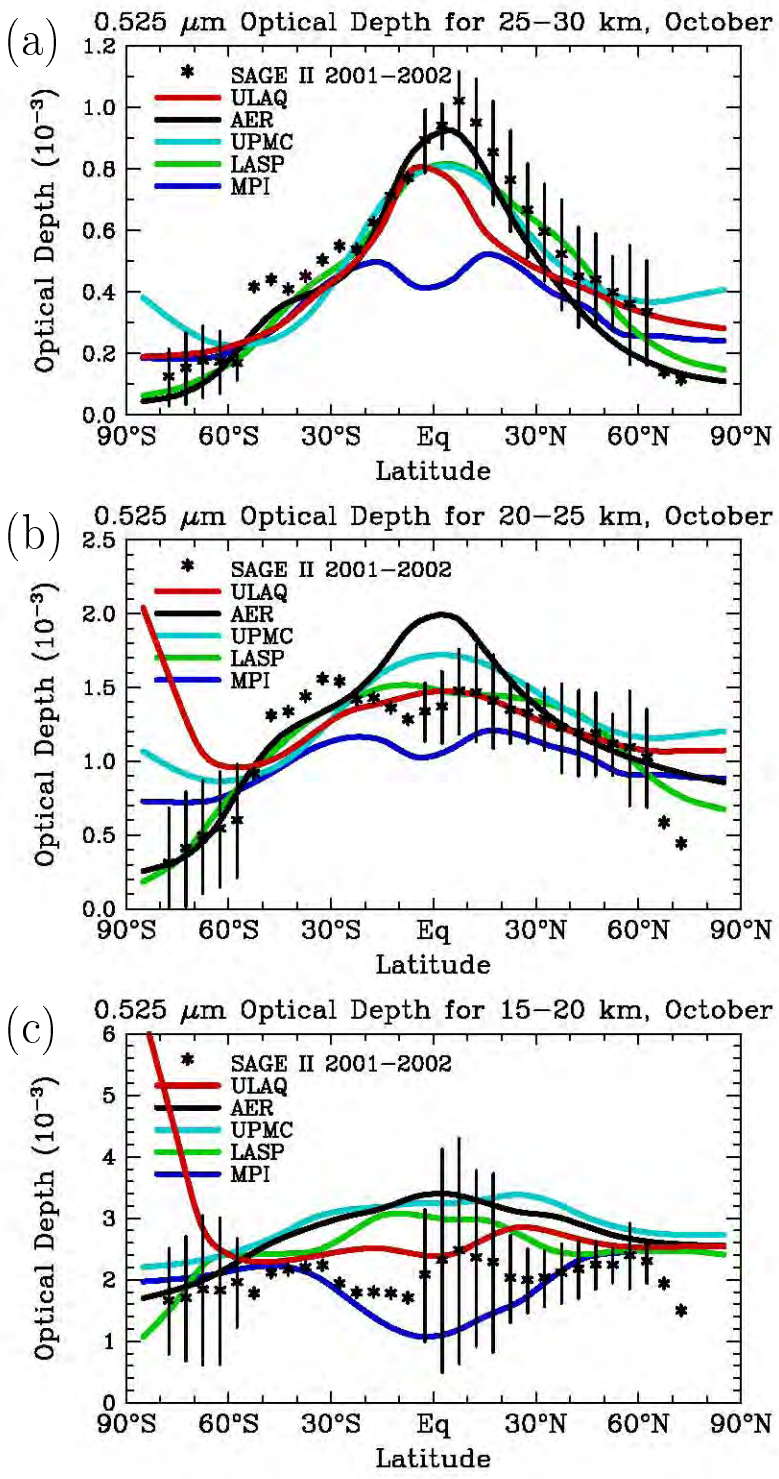

Figure 6.18: Aerosol optical depth at 0.525 μm for October of 2000 integrated from (a) 25 to 30 km, (b) 20 to 25 km and (c) 15 to 20 km. SAGE II data are shown by symbols, model results by colored lines. ULAQ optical depths include extinction due to PSC particles.

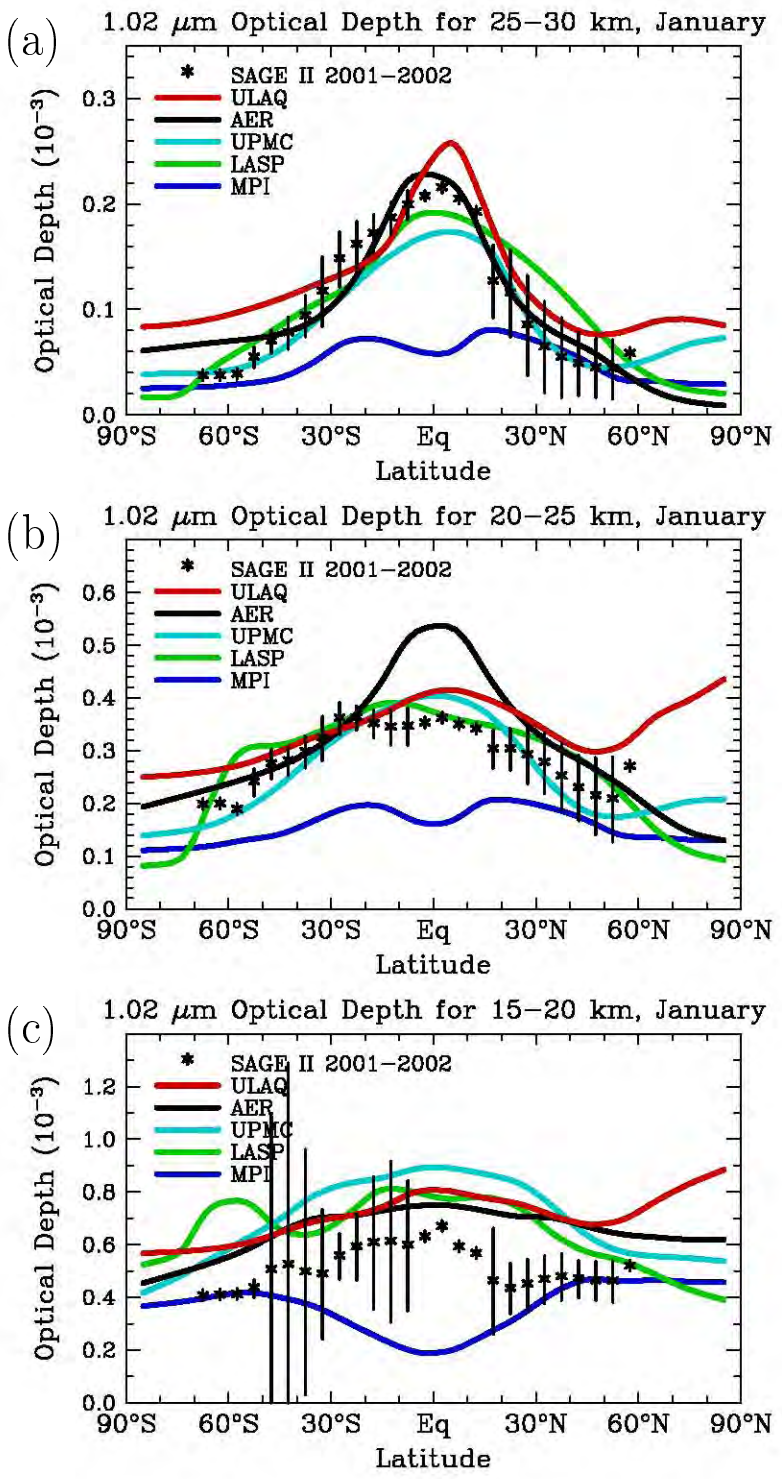

Figure 6.19: Aerosol optical depth at 1.02 μm for January of 2000 integrated from (a) 25 to 30 km, (b) 20 to 25 km and (c) 15 to 20 km. SAGE II data are shown by symbols, model results by colored lines.

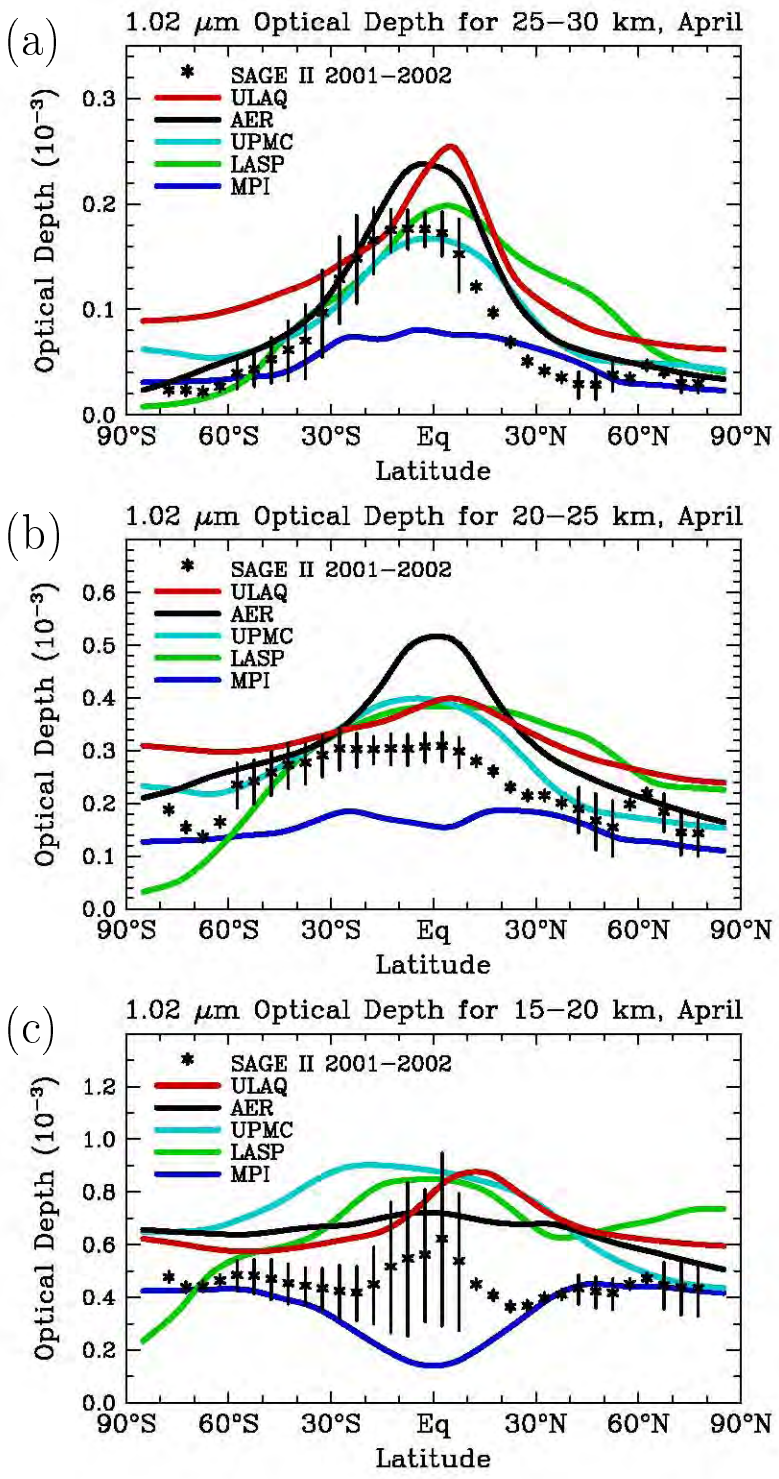

Figure 6.20: Aerosol optical depth at 1.02 μm for April of 2000 integrated from (a) 25 to 30 km, (b) 20 to 25 km and (c) 15 to 20 km. SAGE II data from the 2001-2002 composite background period are shown by symbols, model results by colored lines.

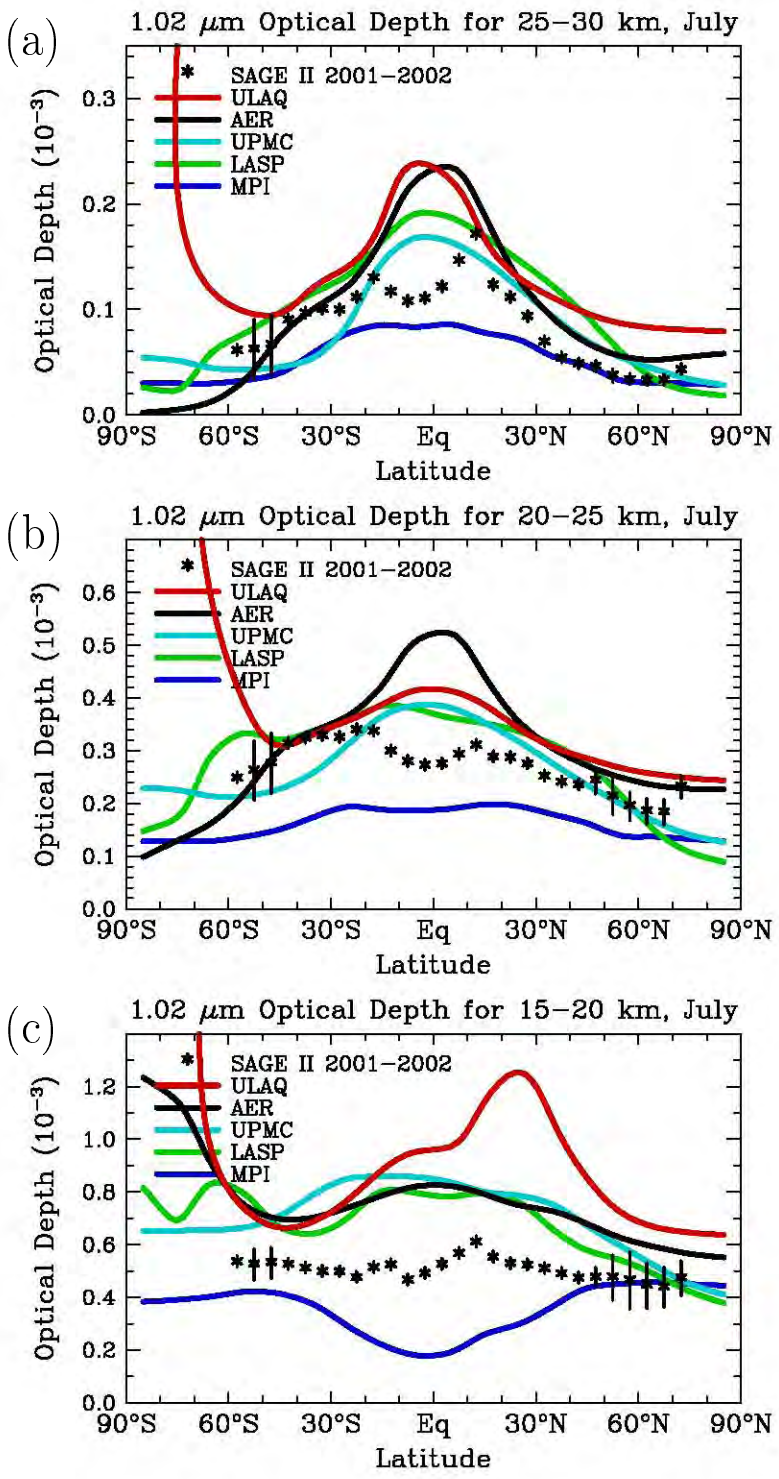

Figure 6.21: Aerosol optical depth at 1.02 μm for July of 2000 integrated from (a) 25 to 30 km, (b) 20 to 25 km and (c) 15 to 20 km. SAGE II data are shown by symbols, model results by colored lines. ULAQ optical depths include extinction due to PSC particles.

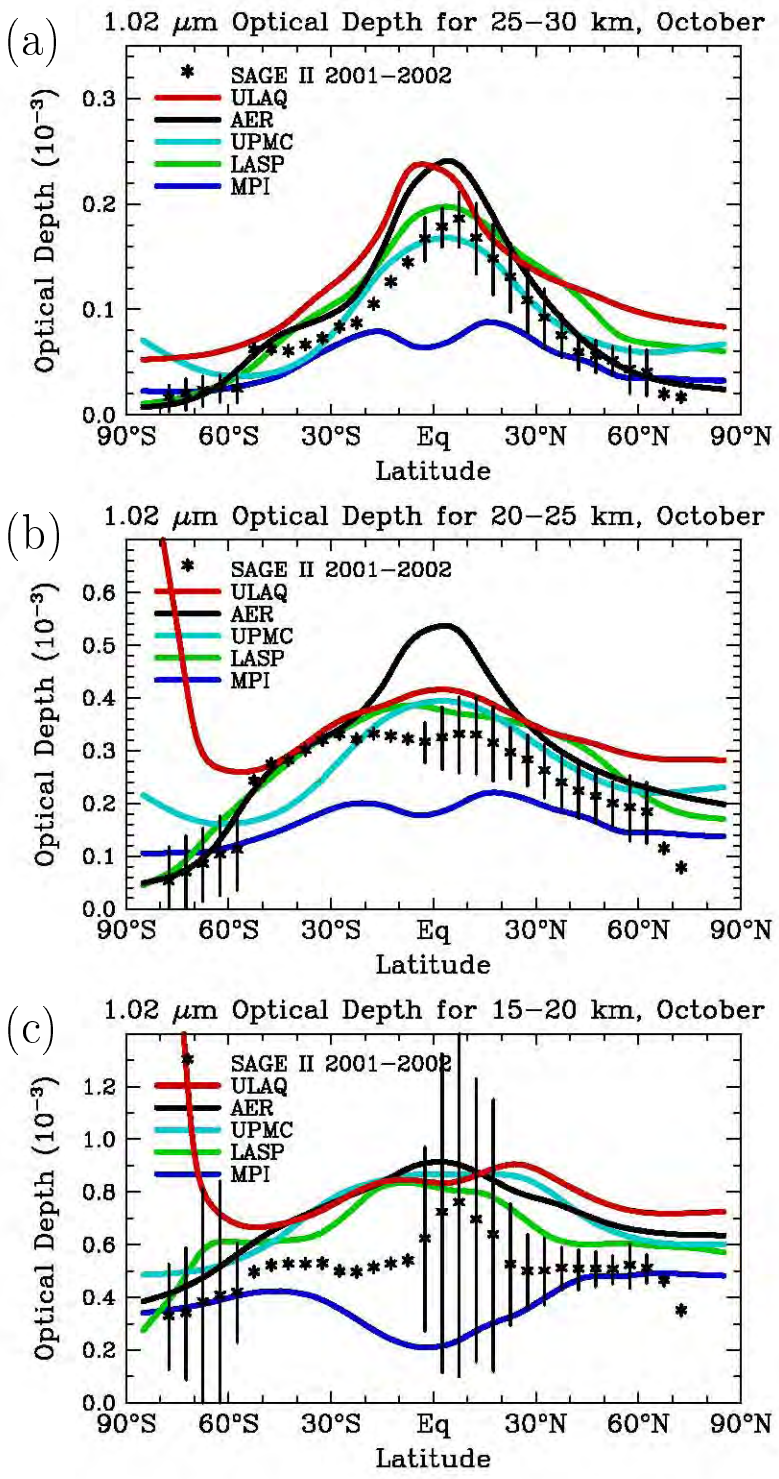

Figure 6.22: Aerosol optical depth at 1.02 μm for October of 2000 integrated from (a) 25 to 30 km, (b) 20 to 25 km and (c) 15 to 20 km. SAGE II data are shown by symbols, model results by colored lines. ULAQ optical depths include extinction due to PSC particles.

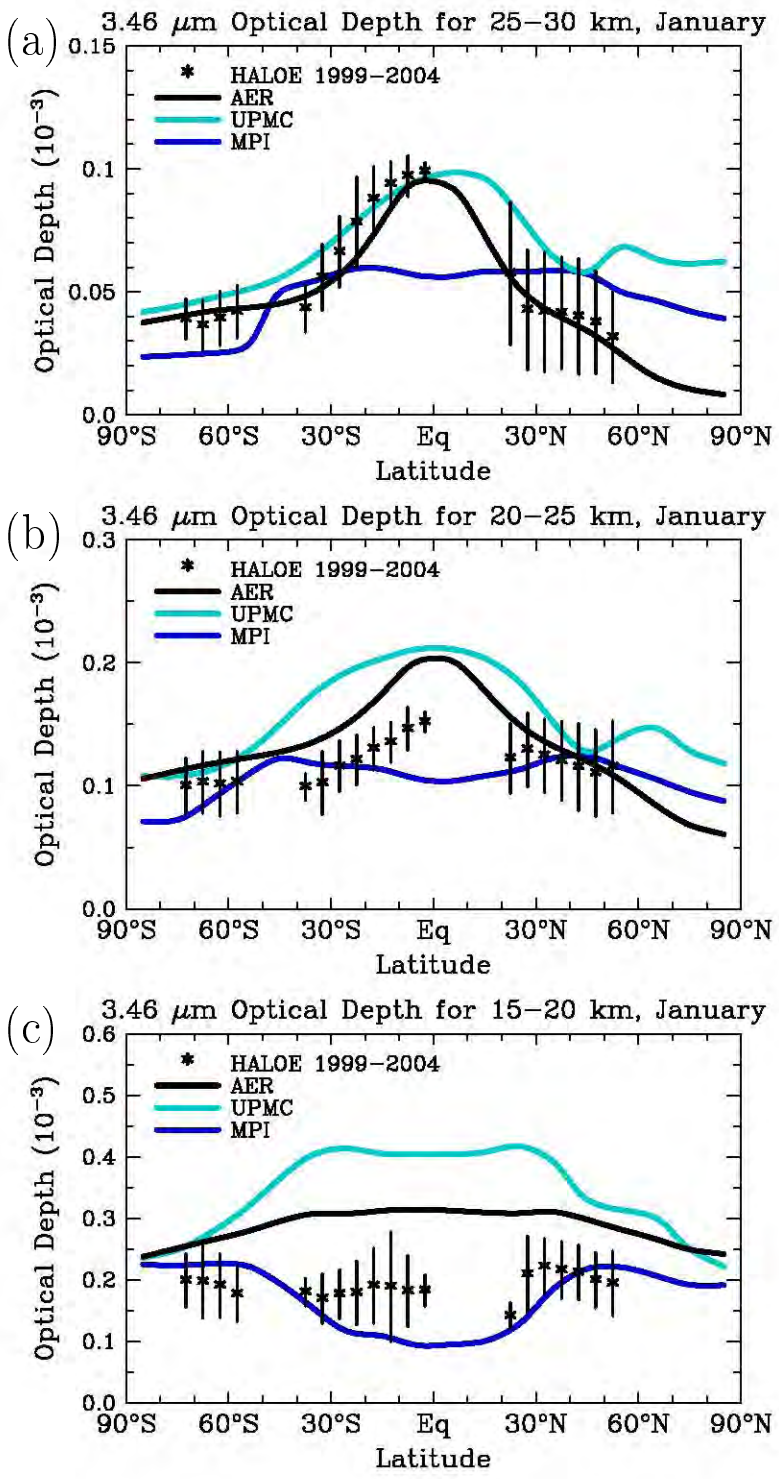

Figure 6.23: Aerosol optical depth at 3.46 μm for January of 2000 integrated from (a) 25 to 30 km, (b) 20 to 25 km and (c) 15 to 20 km. SAGE II data are shown by symbols, model results by colored lines.

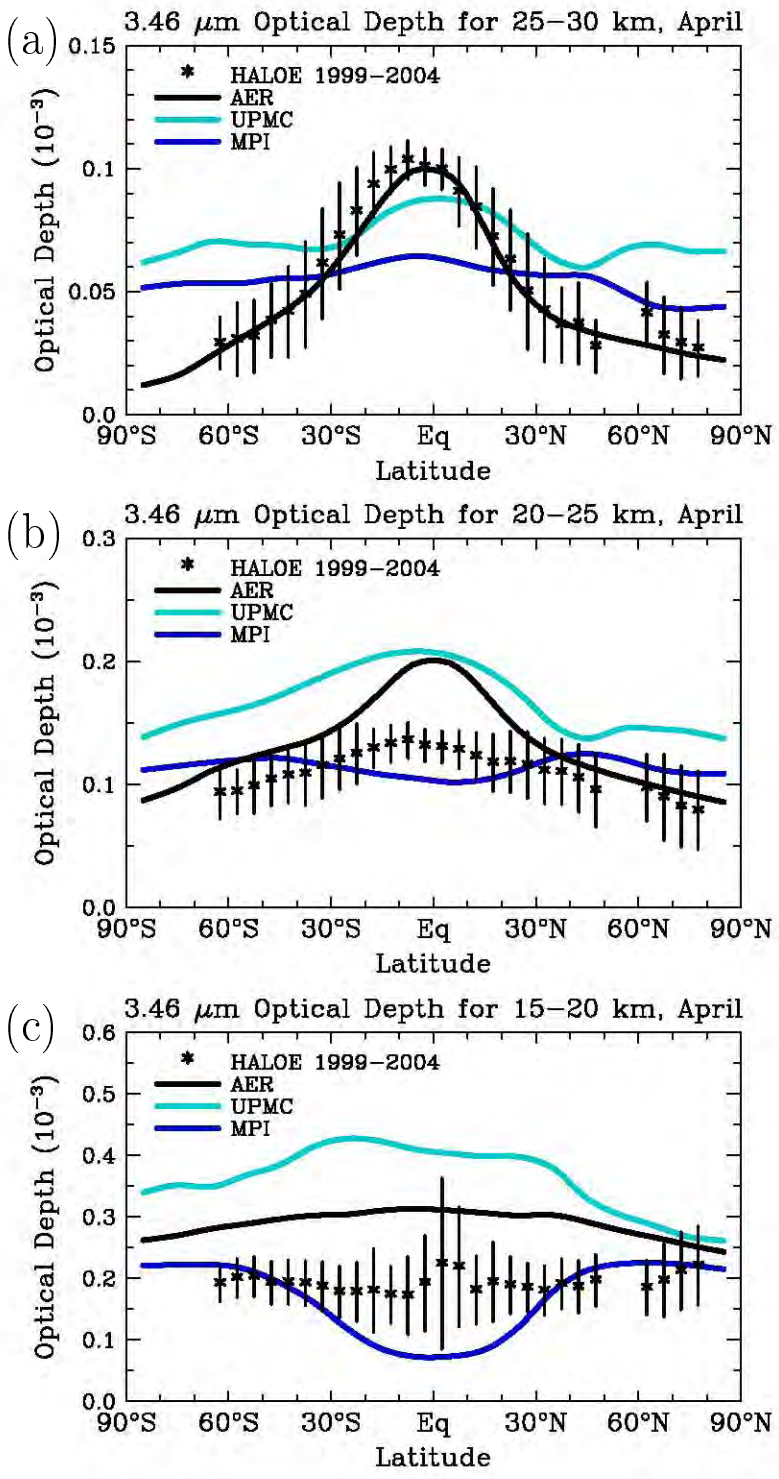

Figure 6.24: Aerosol optical depth at 3.46 μm for April of 2000 integrated from (a) 25 to 30 km, (b) 20 to 25 km and (c) 15 to 20 km. HALOE data from the 2001-2002 composite background period are shown by symbols, model results by colored lines.

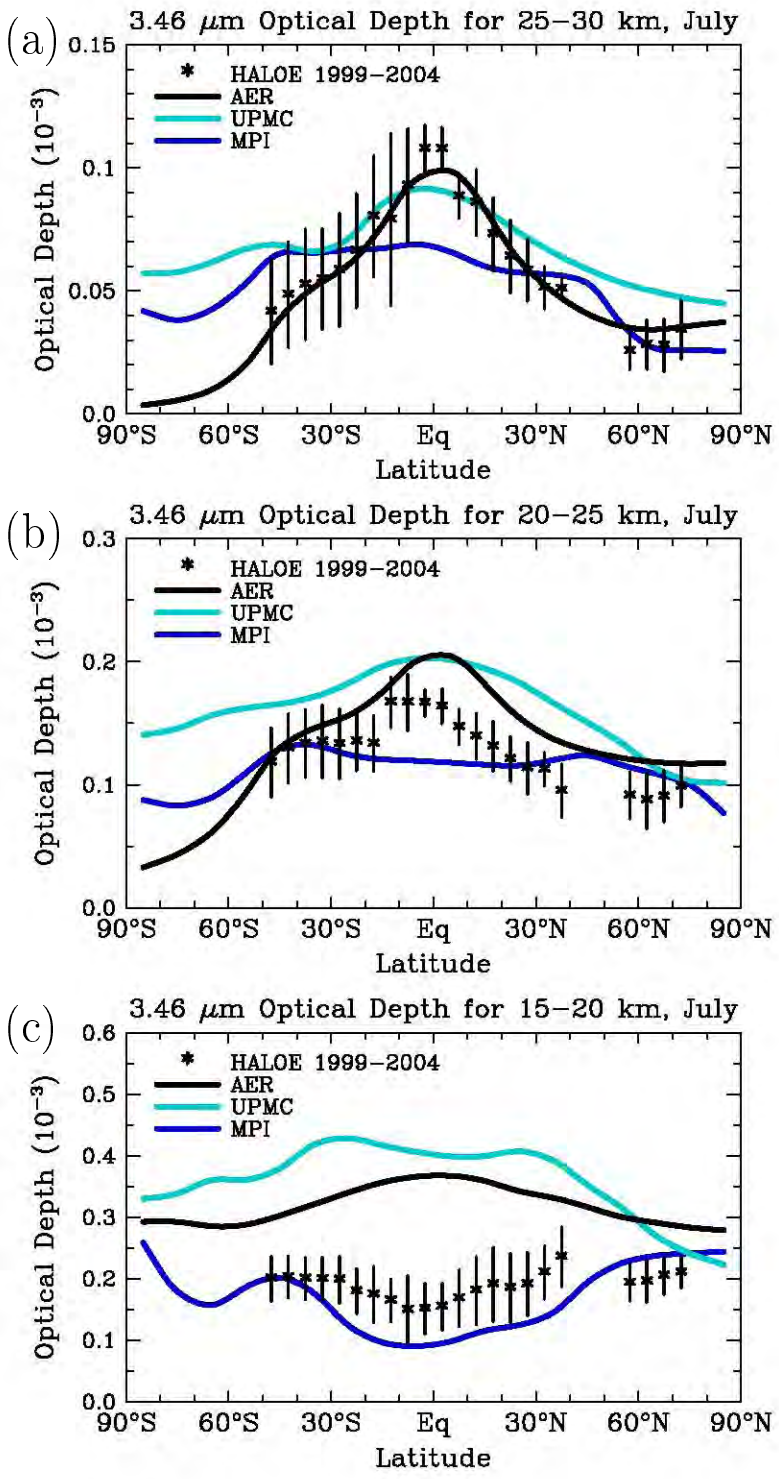

Figure 6.25: Aerosol optical depth at 3.46 μm for July of 2000 integrated from (a) 25 to 30 km, (b) 20 to 25 km and (c) 15 to 20 km. HALOE data are shown by symbols, model results by colored lines.

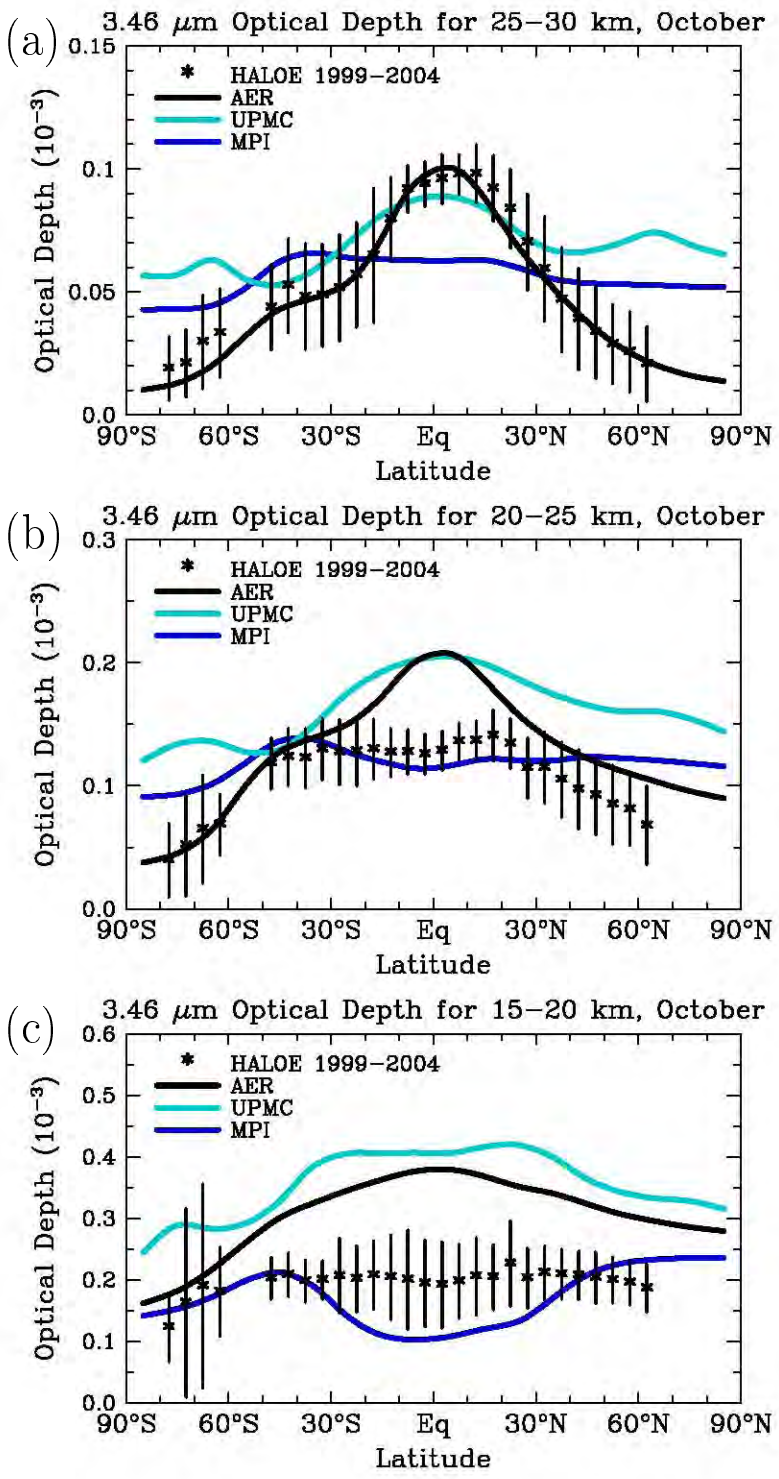

Figure 6.26: Aerosol optical depth at 3.46 μm for October of 2000 integrated from (a) 25 to 30 km, (b) 20 to 25 km and (c) 15 to 20 km. HALOE data are shown by symbols, model results by colored lines.

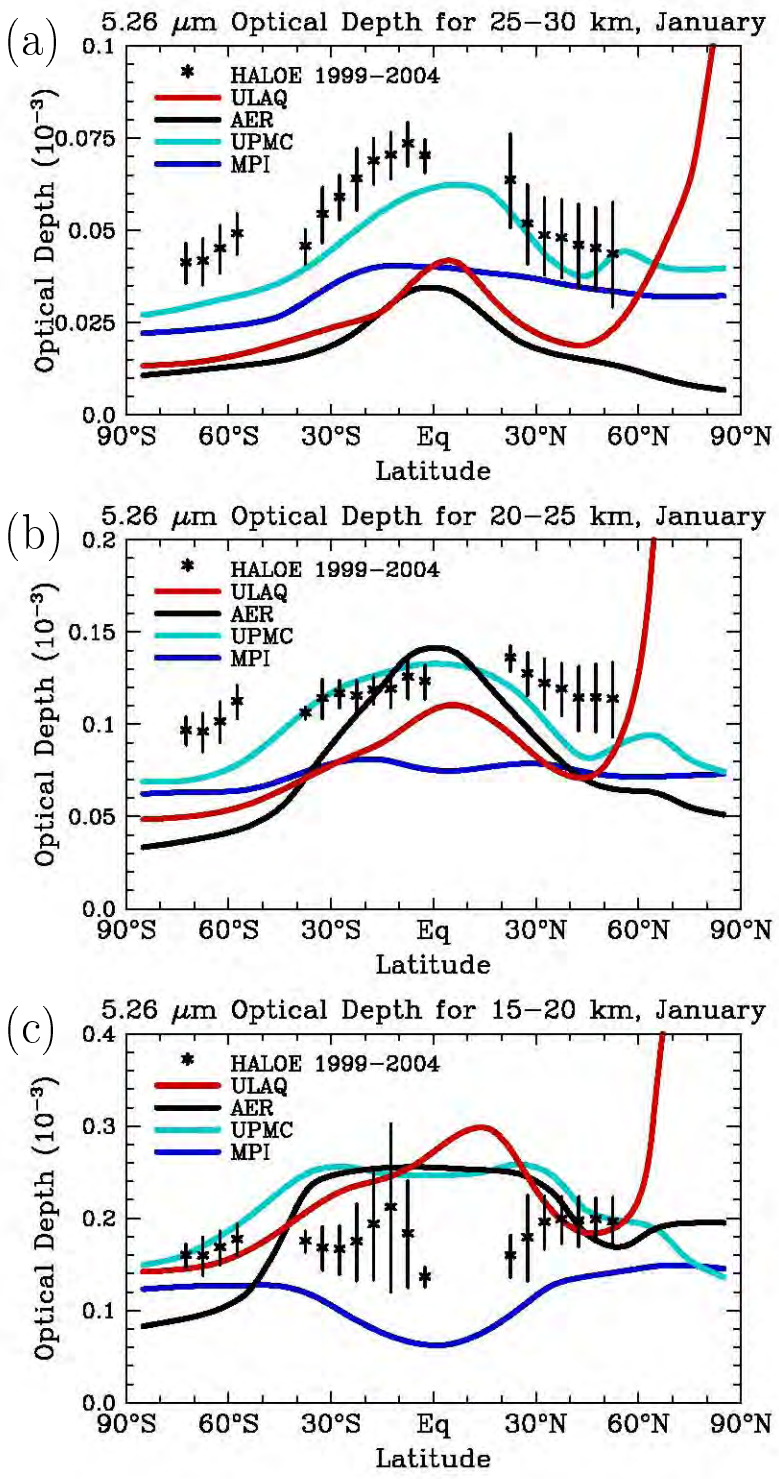

Figure 6.27: Aerosol optical depth at 5.26 μm for January of 2000 integrated from (a) 25 to 30 km, (b) 20 to 25 km and (c) 15 to 20 km. HALOE data are shown by symbols, model results by colored lines. ULAQ optical depths include extinction due to PSC particles.

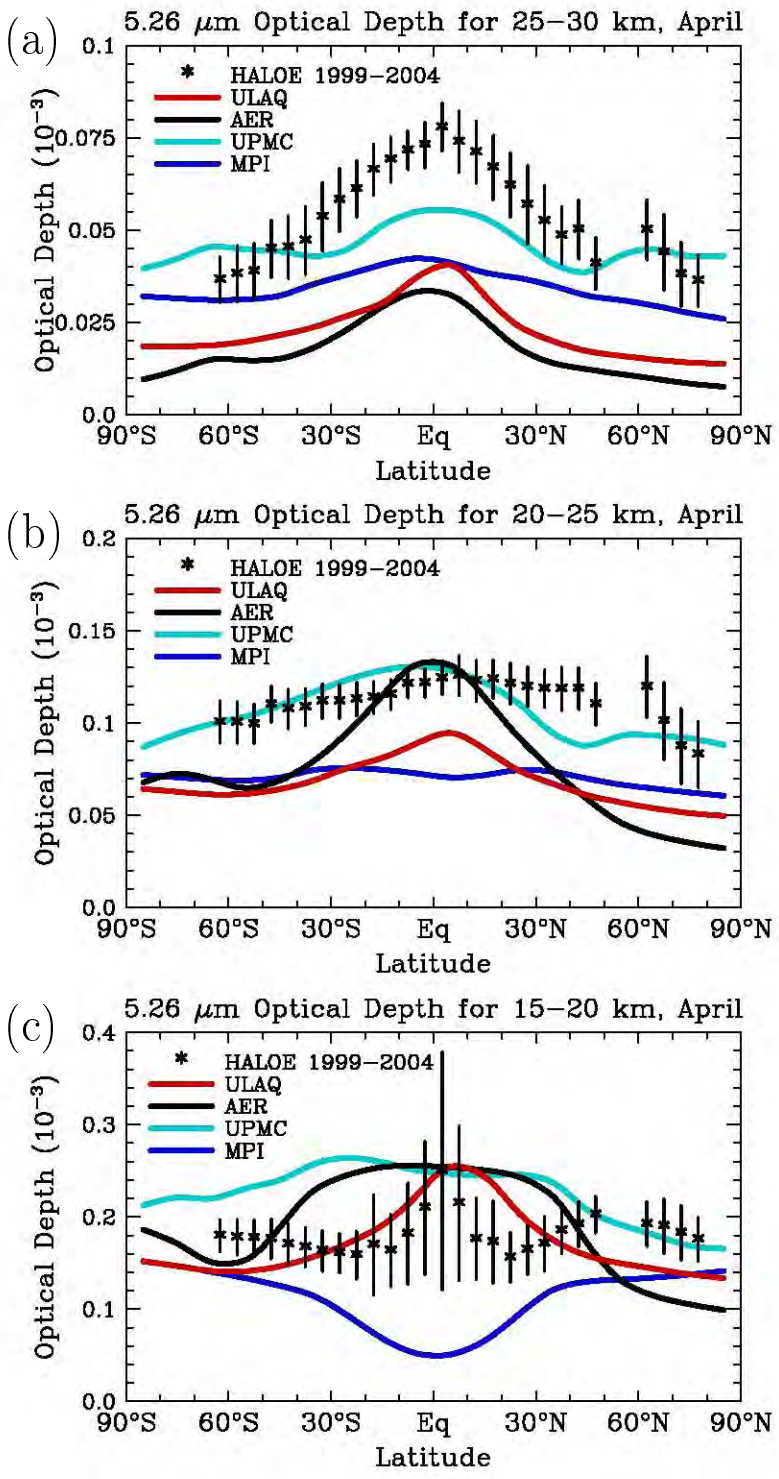

Figure 6.28: Aerosol optical depth at 5.26 μm for April of 2000 integrated from (a) 25 to 30 km, (b) 20 to 25 km and (c) 15 to 20 km. HALOE data are shown by symbols, model results by colored lines.

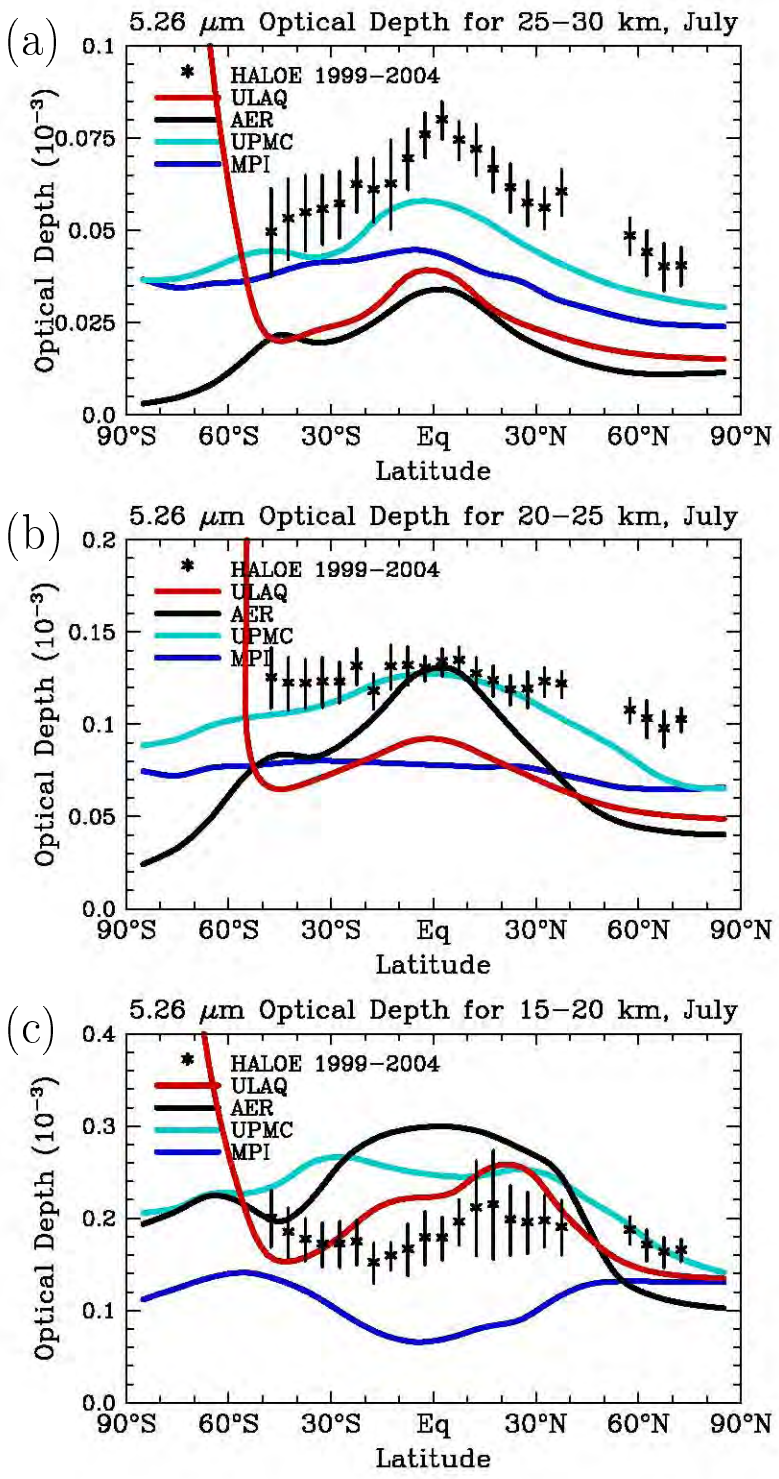

Figure 6.29: Aerosol optical depth at 5.26 μm for July of 2000 integrated from (a) 25 to 30 km, (b) 20 to 25 km and (c) 15 to 20 km. HALOE data are shown by symbols, model results by colored lines. ULAQ optical depths include extinction due to PSC particles.

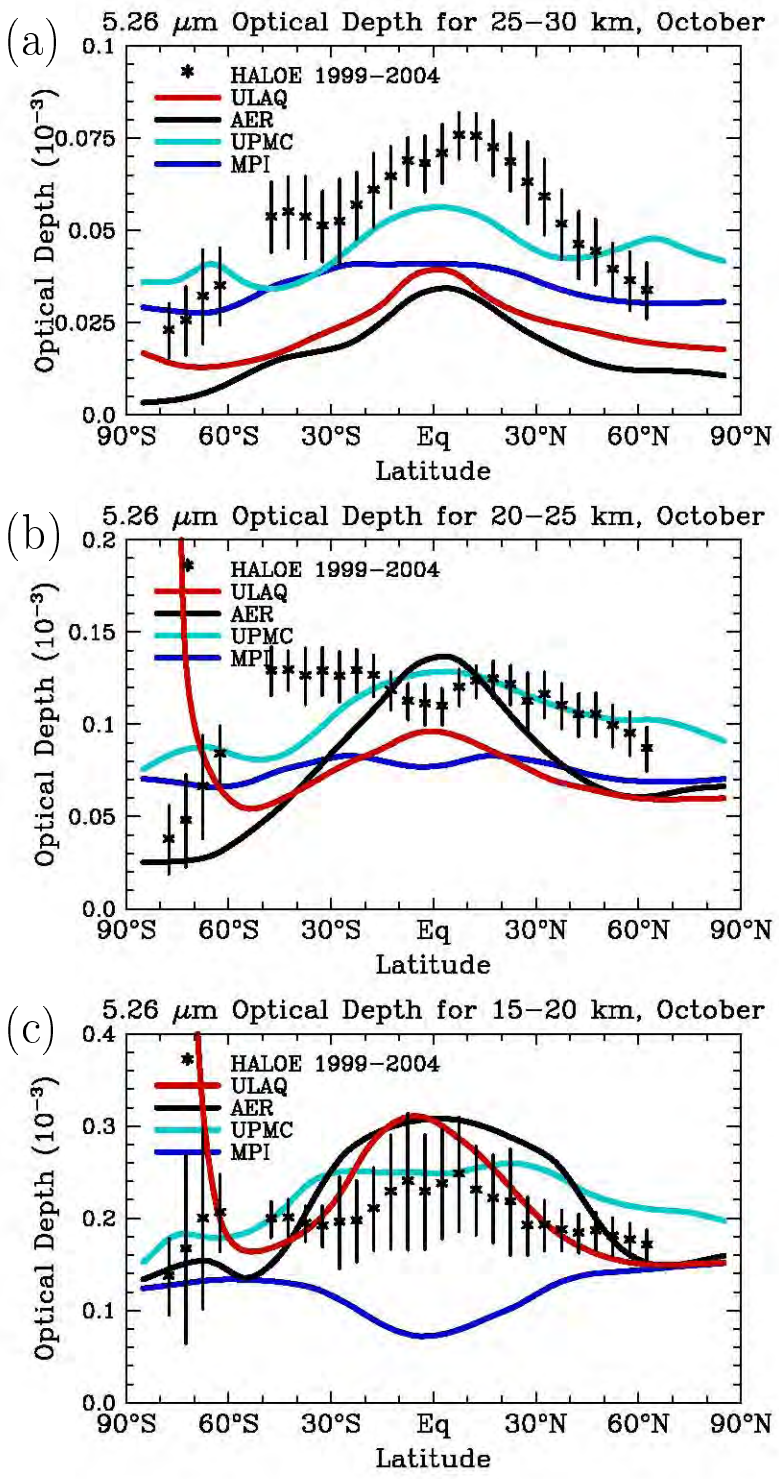

Figure 6.30: Aerosol optical depth at 5.26 μm for October of 2000 integrated from (a) 25 to 30 km, (b) 20 to 25 km and (c) 15 to 20 km. HALOE data are shown by symbols, model results by colored lines. ULAQ optical depths include extinction due to PSC particles.

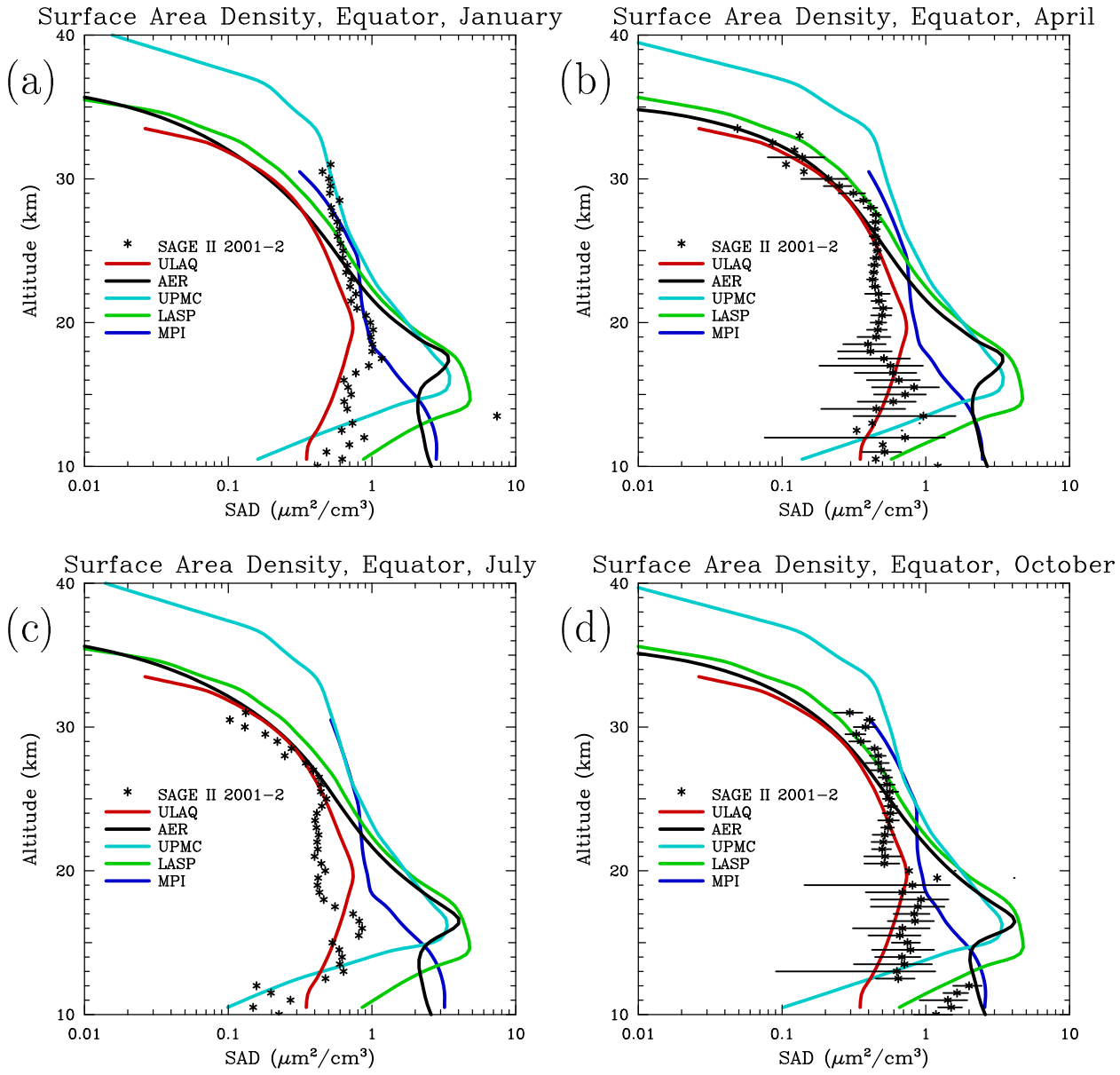

Figure 6.31: Comparison of surface area density derived from SAGE II observations and that calculated by the models at the equator in (a) January, (b) April, (c) July, and (d) October. SAGE II results use Equation 4.1 to obtain surface area from the 2001-2002 composite of 1.02 and 0.525 μm extinction. Model-calculated surface area density is integrated over the model's entire size distribution.

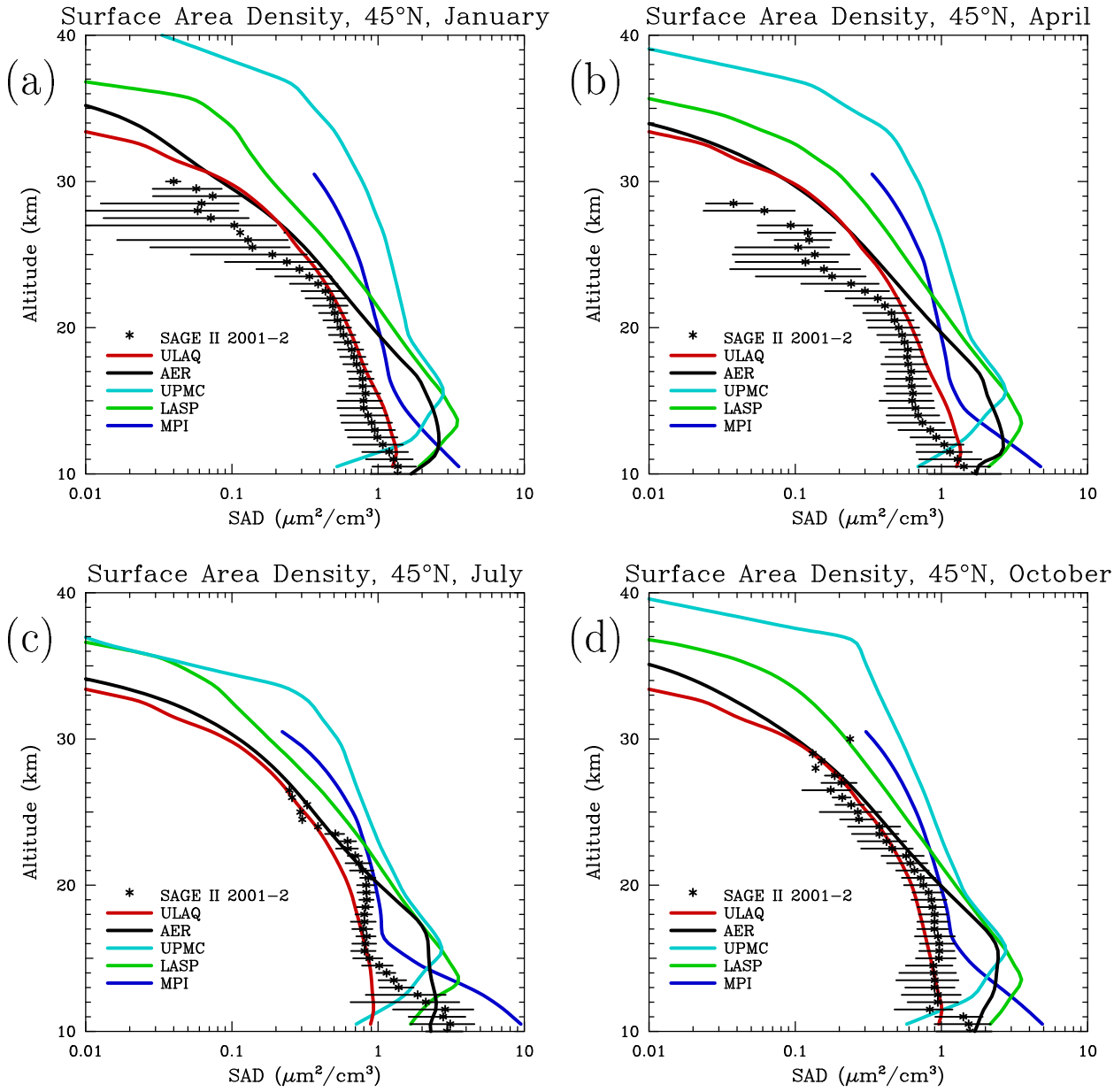

Figure 6.32: Comparison of surface area density derived from SAGE II observations and that calculated by the models at 45°N in (a) January, (b) April, (c) July, and (d) October. SAGE II results use Equation 4.1 to obtain surface area from the 2001-2002 composite of 1.02 and 0.525 μm extinction. Model-calculated surface area density is integrated over the model's entire size distribution.

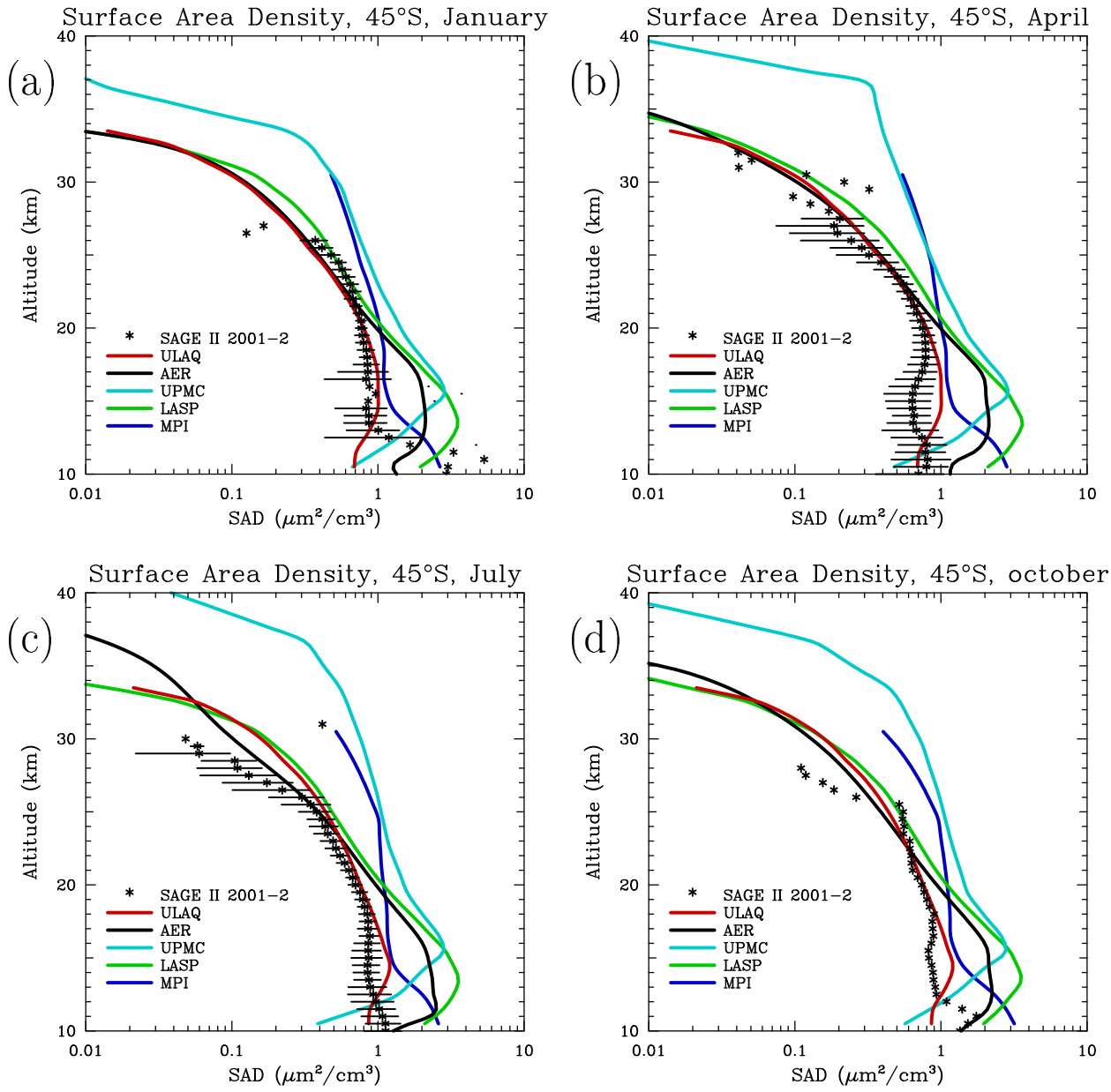

Figure 6.33: Comparison of surface area density derived from SAGE II observations and that calculated by the models at 45°S in (a) January, (b) April, (c) July, and (d) October. SAGE II results use Equation 4.1 to obtain surface area from the 2001-2002 composite of 1.02 and 0.525 μm extinction. Model-calculated surface area density is integrated over the model's entire size distribution.

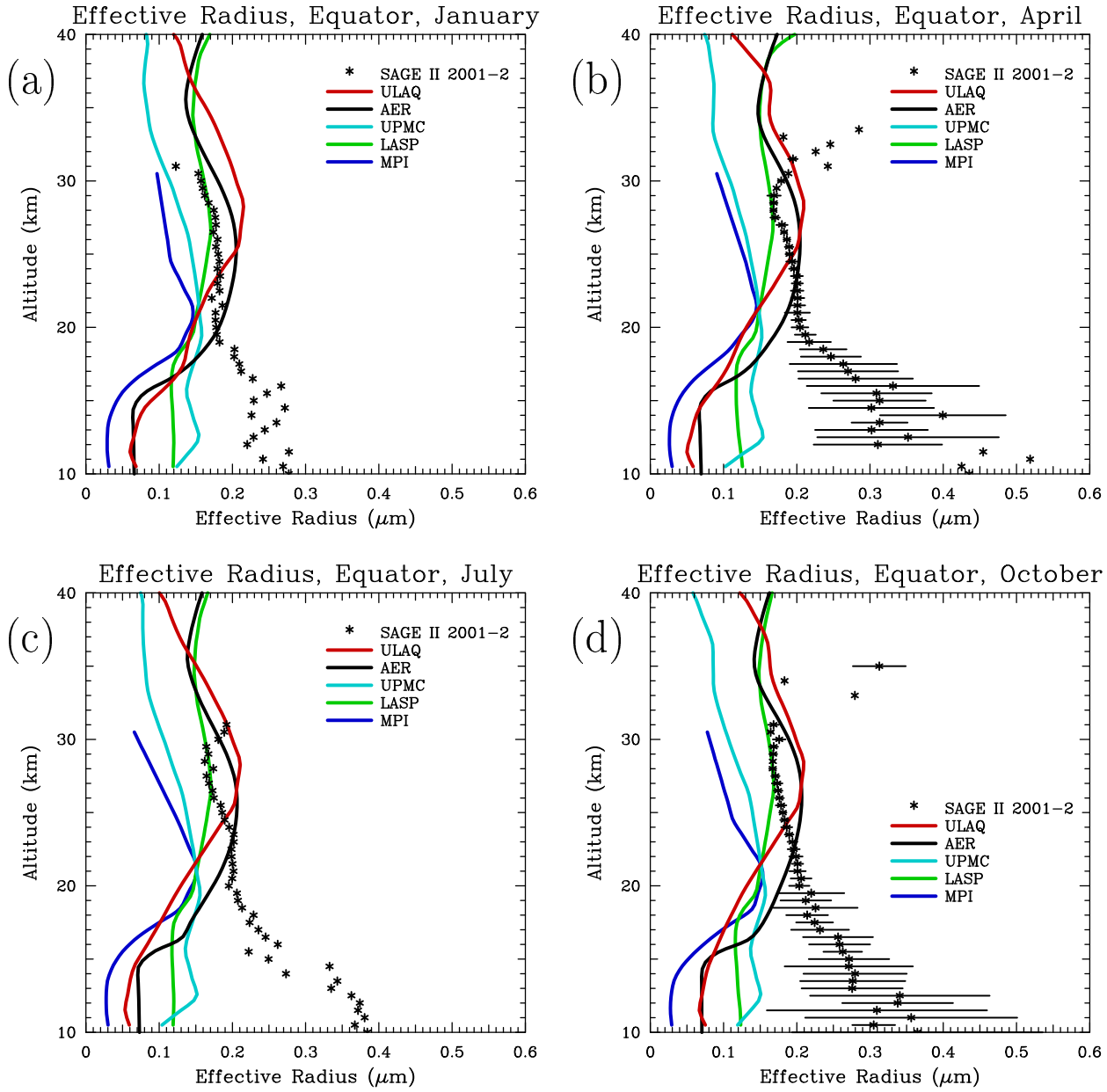

Figure 6.34: Comparison of effective radius derived from SAGE II observations and that calculated by the models at the equator in (a) January, (b) April, (c) July, and (d) October. SAGE II results use Equation 4.4 to obtain effective radius from the 2001-2002 composite of 1.02 μm extinction. Model-calculated effective radius is integrated over the model's entire size distribution.

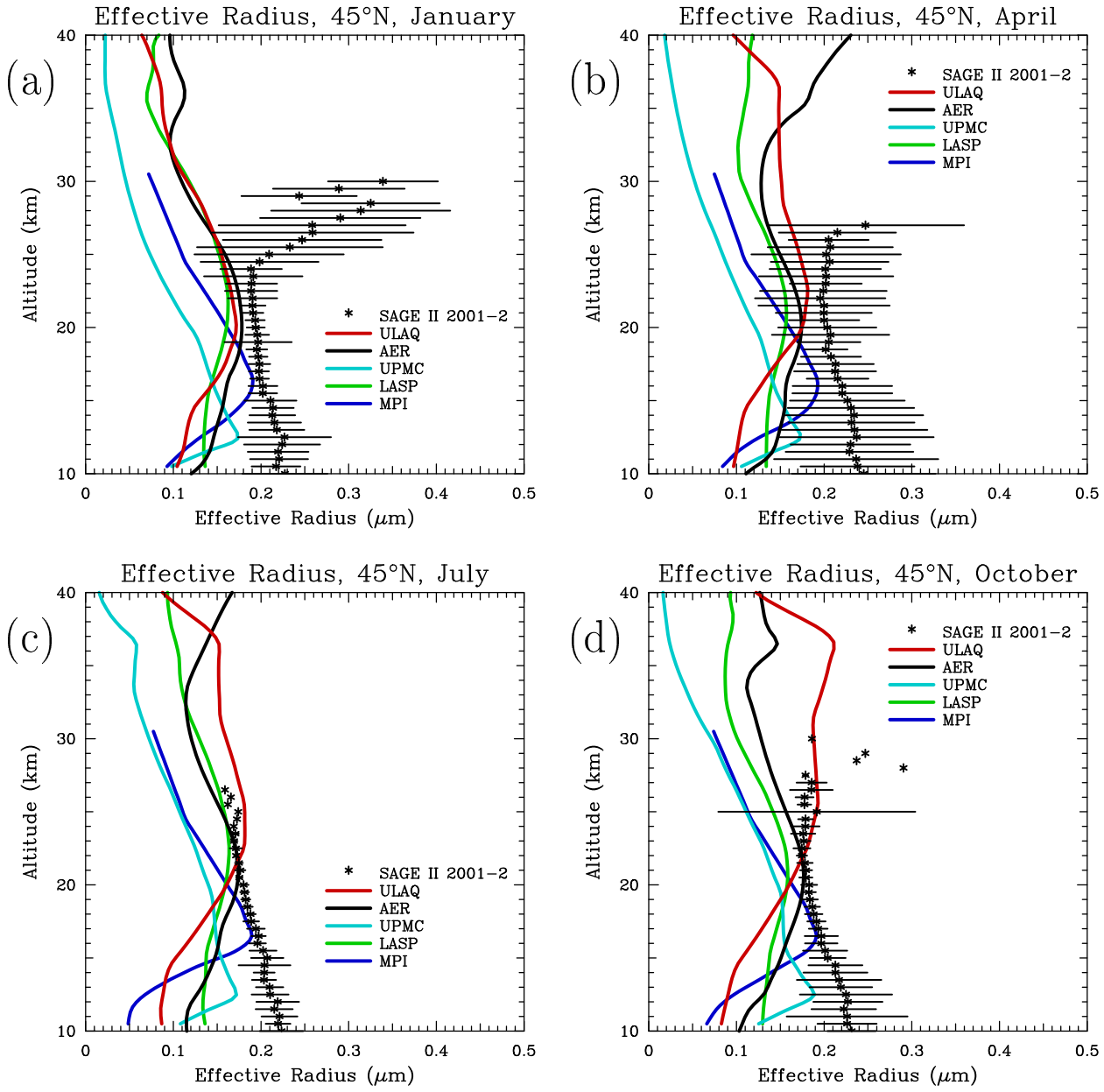

Figure 6.35: Comparison of effective radius derived from SAGE II observations and that calculated by the models at 45°N in (a) January, (b) April, (c) July, and (d) October. SAGE II results use Equation 4.4 to obtain effective radius from the 2001-2002 composite of 1.02 μm extinction. Model-calculated effective radius is integrated over the model's entire size distribution.

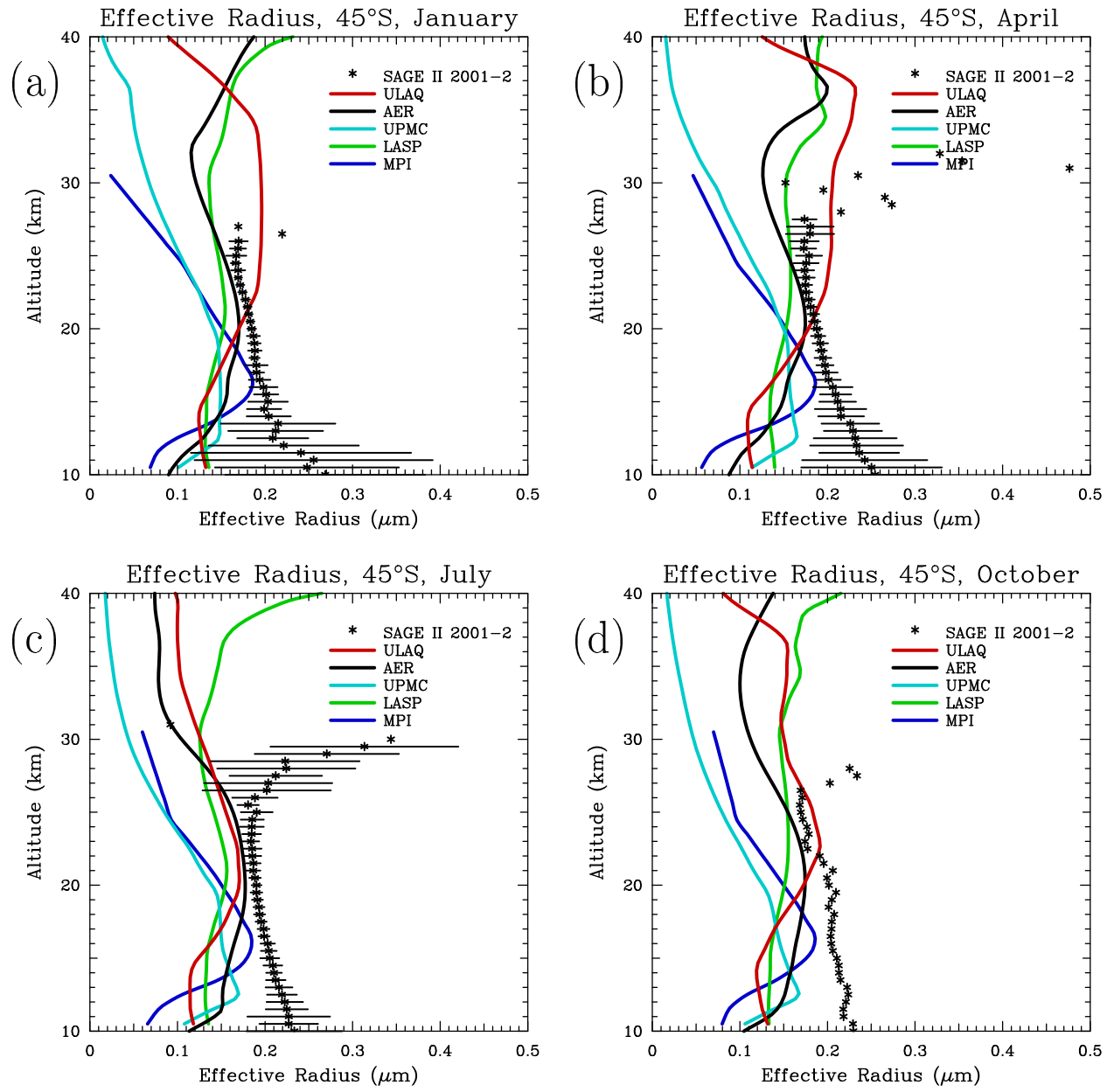

Figure 6.36: Comparison of effective radius derived from SAGE II observations and that calculated by the models at 45°S in (a) January, (b) April, (c) July, and (d) October. SAGE II results use Equation 4.4 to obtain effective radius from the 2001-2002 composite of 1.02 μm extinction. Model-calculated effective radius is integrated over the model's entire size distribution.

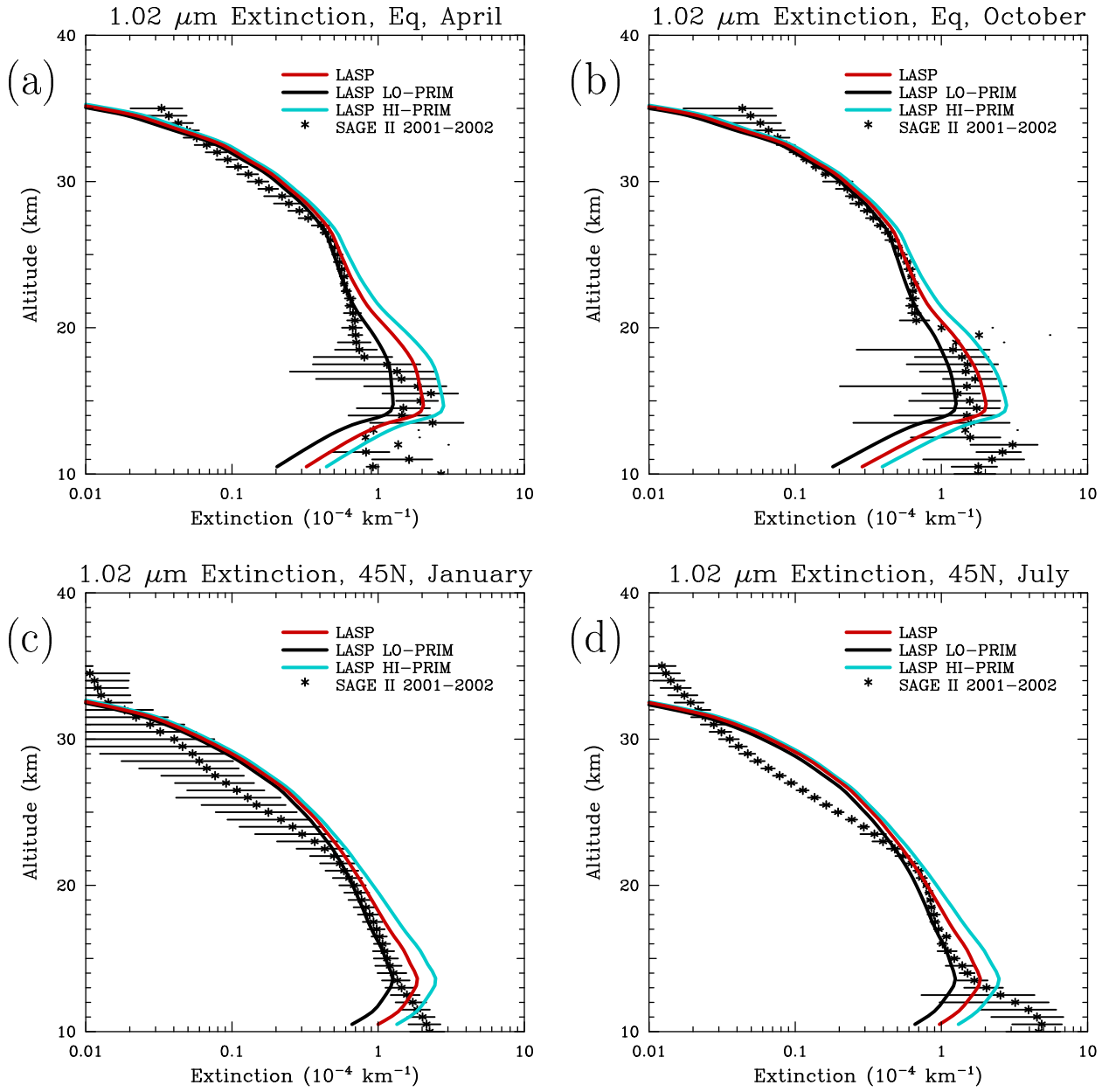

Figure 6.37: Comparison of SAGE II and calculated extinctions from the LASP model at 1.02 μm in (a) April and (b) October at the equator, and in (c) January and (d) July at 45°N. Model results are shown with primary aerosol at the tropopause increased (HI-PRIM) and decreased (LO-PRIM) by two standard deviations.

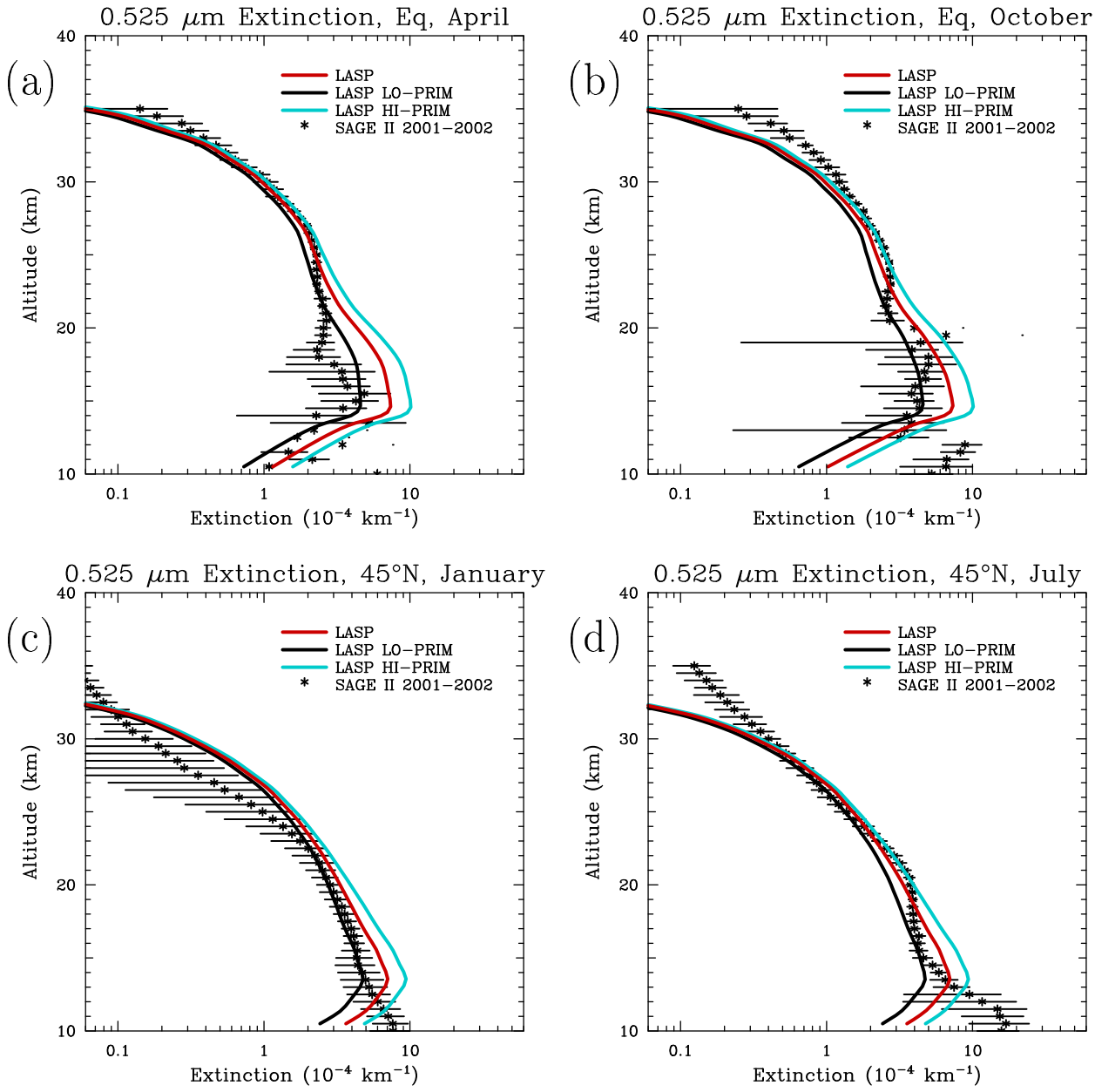

Figure 6.38: Comparison of SAGE II and calculated extinctions from the LASP model at 0.525 μm in (A) April and (B) October at the equator, and in (c) January and (d) July at 45°N. Model results are shown with primary aerosol at the tropopause increased (HI-PRIM) and decreased (LO-PRIM) by two standard deviations.

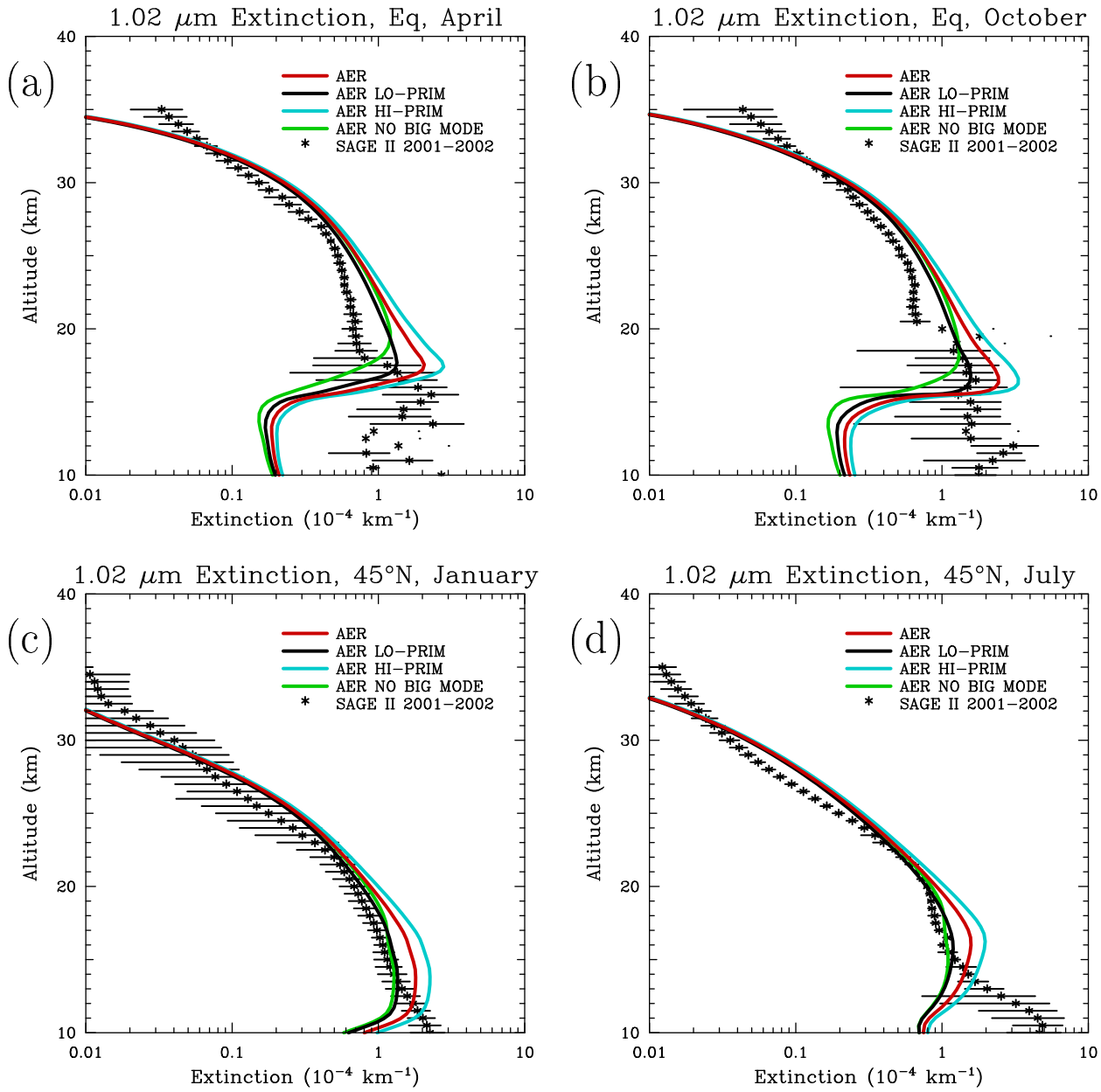

Figure 6.39: Comparison of SAGE II and calculated extinctions from the AER model at 1.02 μm in (a) April and (b) October at the equator, and in (c) January and (d) July at 45°N. Model results are shown with primary aerosol at the tropopause increased (HI-PRIM) and decreased (LO-PRIM) by two standard deviations and with the large mode (0.3-0.8 μm radius) of primary aerosol removed (NO BIG MODE).

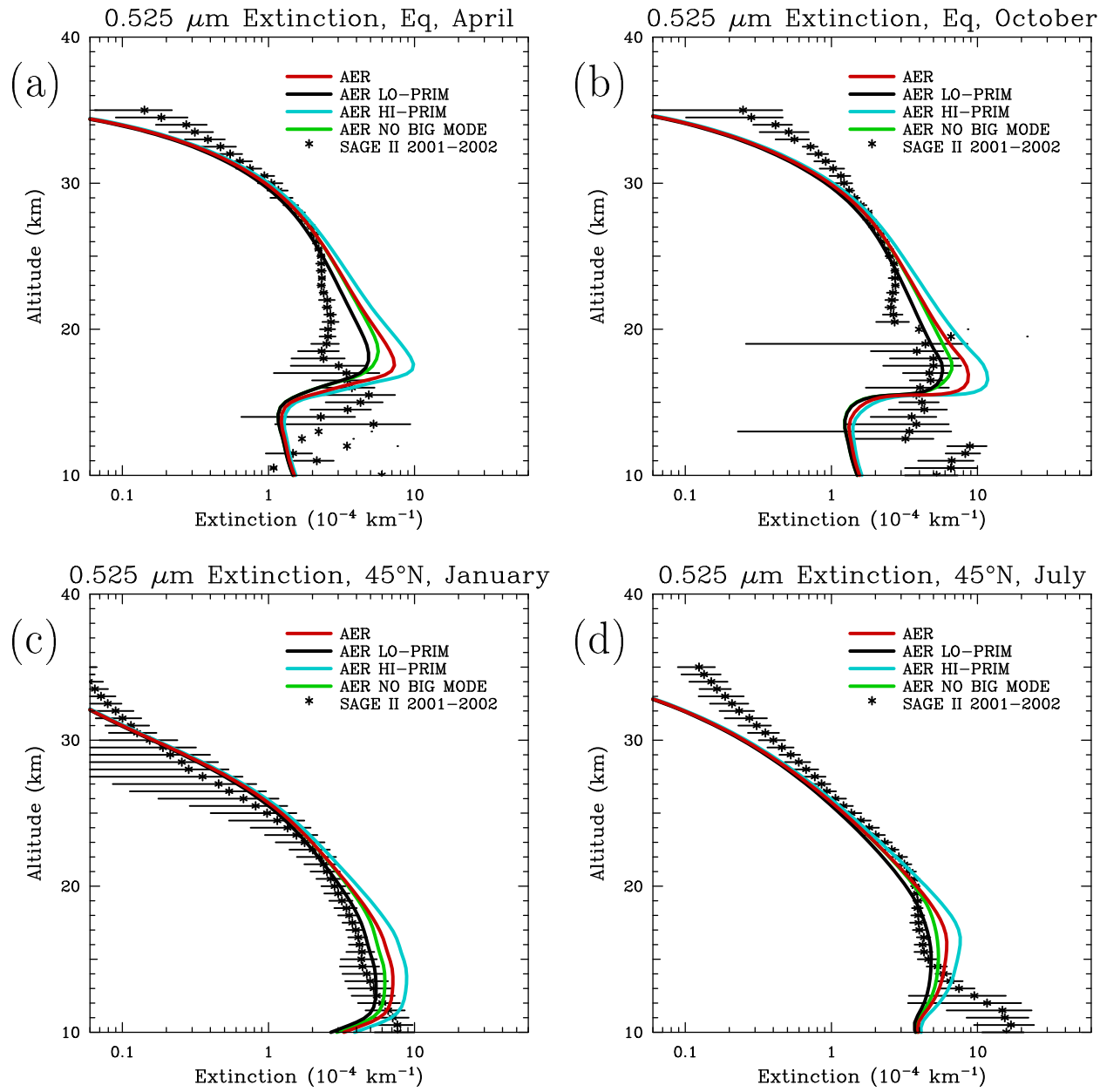

Figure 6.40: Comparison of SAGE II and calculated extinctions from the AER model at 0.525 μm in (a) April and (b) October at the equator, and in (c) January and (d) July at 45°N. Model results are shown with primary aerosol at the tropopause increased (HI-PRIM) and decreased (LO-PRIM) by two standard deviations and with the large mode (0.3-0.8 μm radius) of primary aerosol removed (NO BIG MODE).

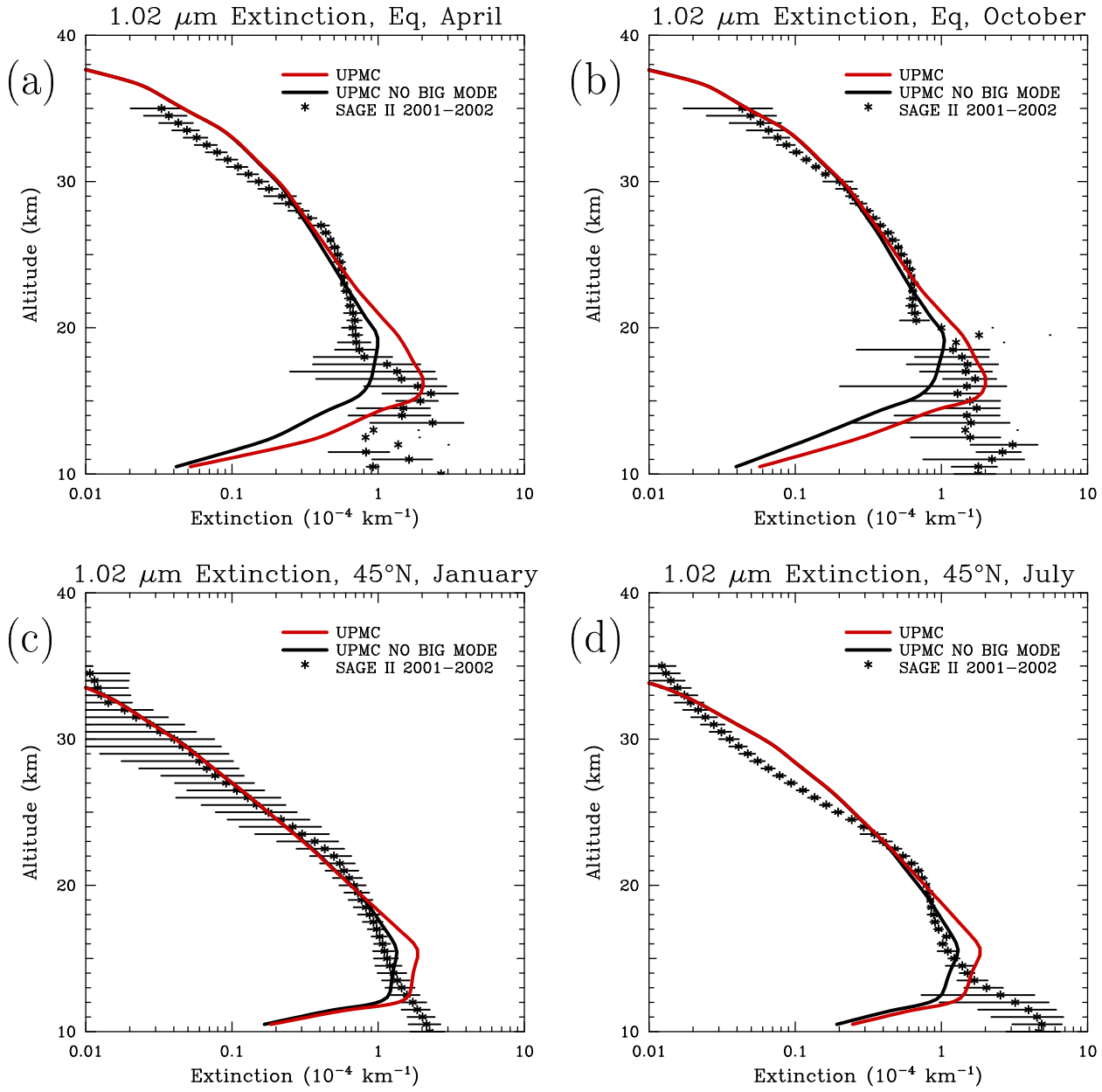

Figure 6.41: Comparison of SAGE II and calculated extinctions from the UPMC model at 1.02 μm in (a) April and (b) October at the equator, and in (c) January and (d) July at 45°N. Model results are shown for the standard model and with the large mode (0.3-0.8 μm radius) of primary aerosol removed (NO BIG MODE).

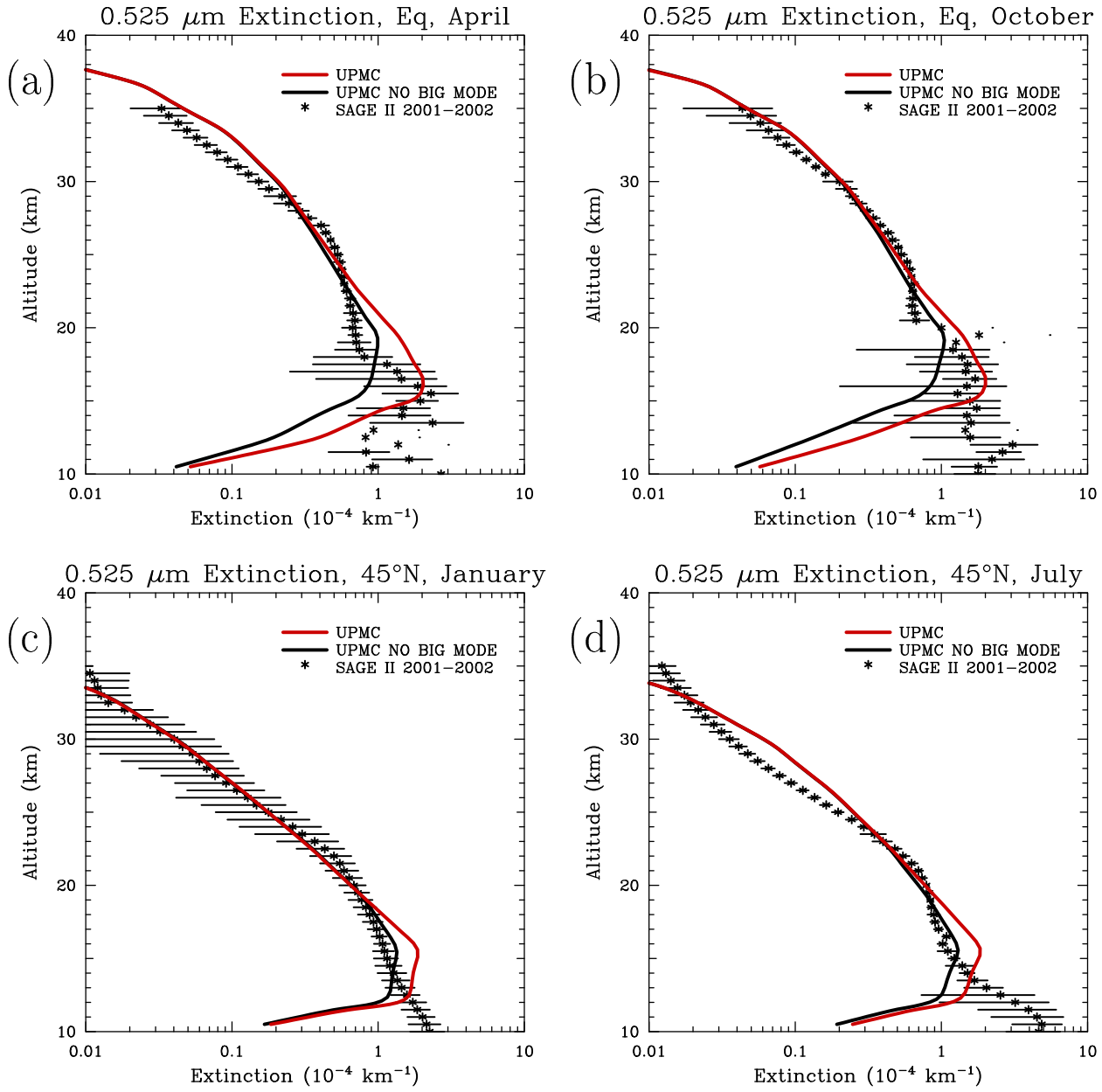

Figure 6.42: Comparison of SAGE II and calculated extinctions from the UPMC model at 0.525 μm in (a) April and (b) October at the equator, and in (c) January and (d) July at 45°N. Model results are shown for the standard model and with the large mode (0.3-0.8 μm radius) of primary aerosol removed (NO BIG MODE).

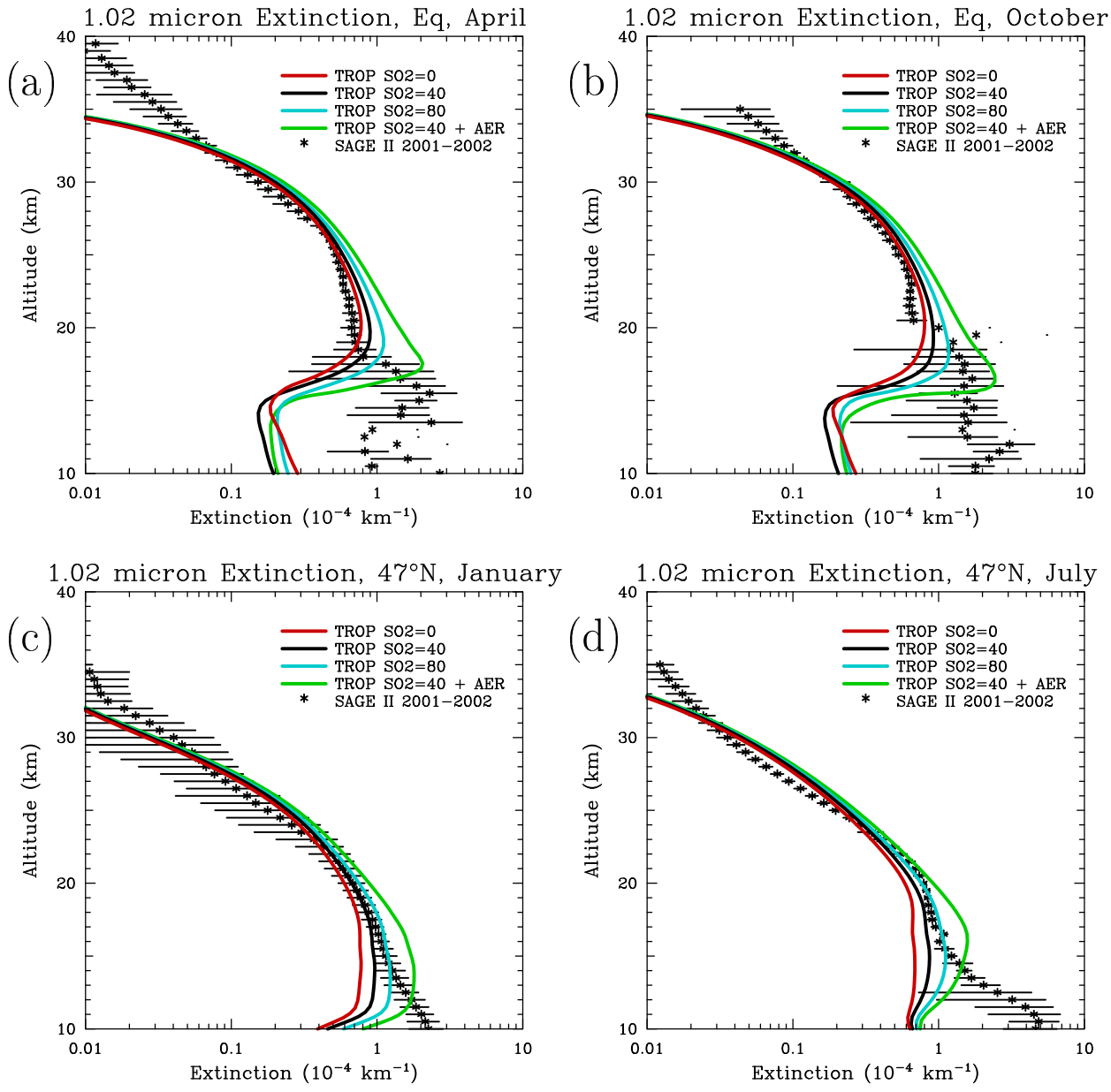

Figure 6.43: Comparison of SAGE II and calculated extinctions from the AER model at 1.02 μm in (a) April and (b) October at the equator, and in (c) January and (d) July at 45°N. Model results are shown with SO_2 in the tropical upper troposphere set to 0, 40, and 80 pptv without primary aerosol, and with 40 pptv of SO_2 in the tropical upper troposphere and primary aerosol (TROP SO2=40 + AER).

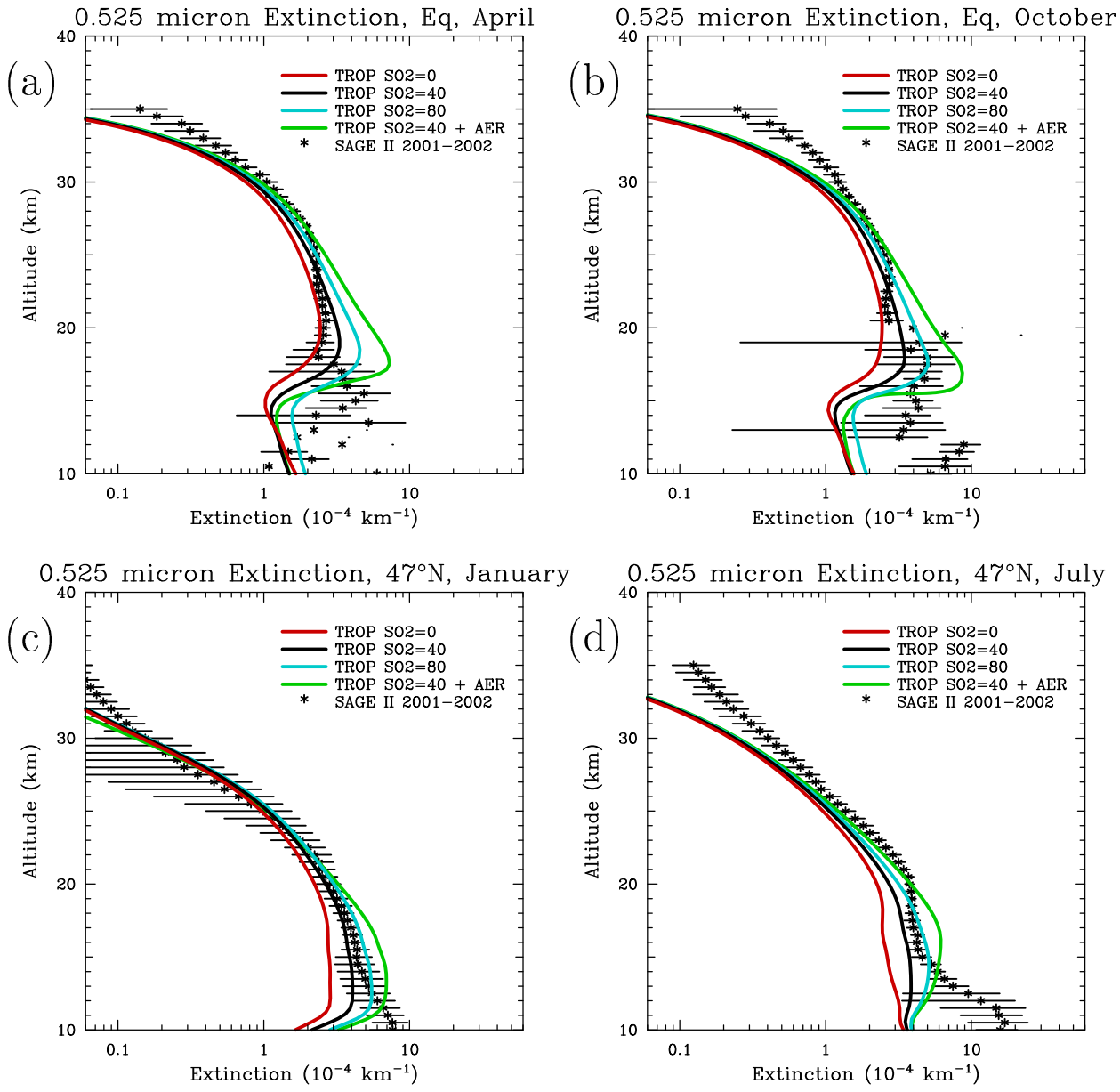

Figure 6.44: Comparison of SAGE II and calculated extinctions from the AER model at 0.525 μm in (a) April and (b) October at the equator, and in (c) January and (d) July at 45°N. Model results are shown with SO_2 in the tropical upper troposphere set to 0, 40, and 80 pptv without primary aerosol, and with 40 pptv of SO_2 in the tropical upper troposphere and primary aerosol (TROP SO2=40 + AER).

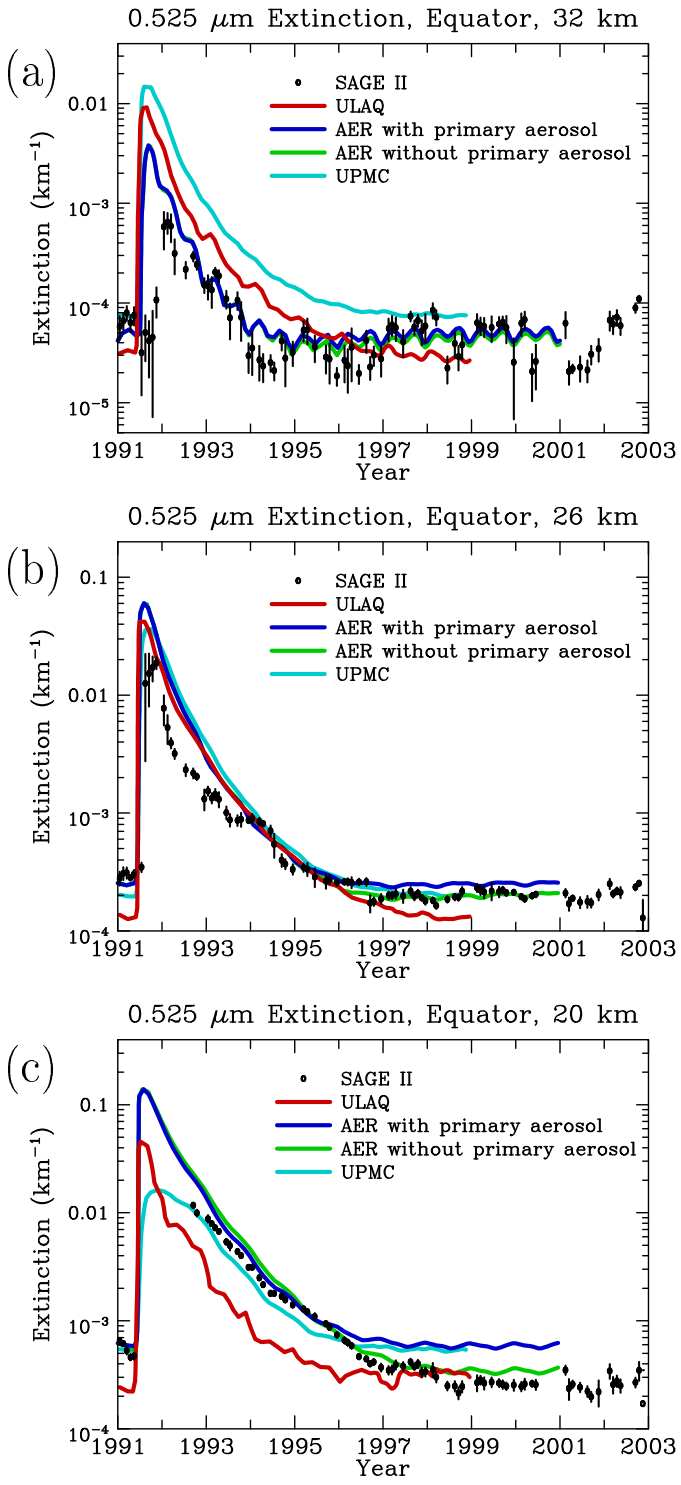

Figure 6.45: Aerosol extinction at 0.525 μm for 1991 to 2002 at (a) the equator and 32 km, (b) the equator and 26 km and (c) the equator and 20 km. SAGE II data are shown by symbols, model results by colored lines.

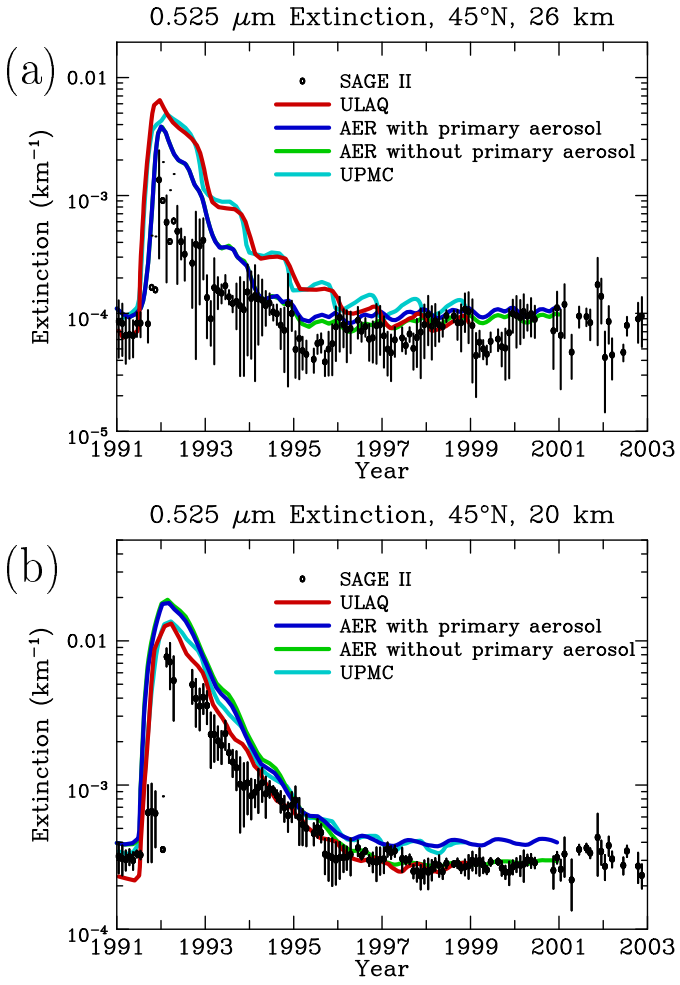

Figure 6.46: Aerosol extinction at 0.525 μm for 1991 to 2002 at (a) 45°N and 26 km and (b) 45°N and 20 km. SAGE II data are shown by symbols, model results by colored lines.

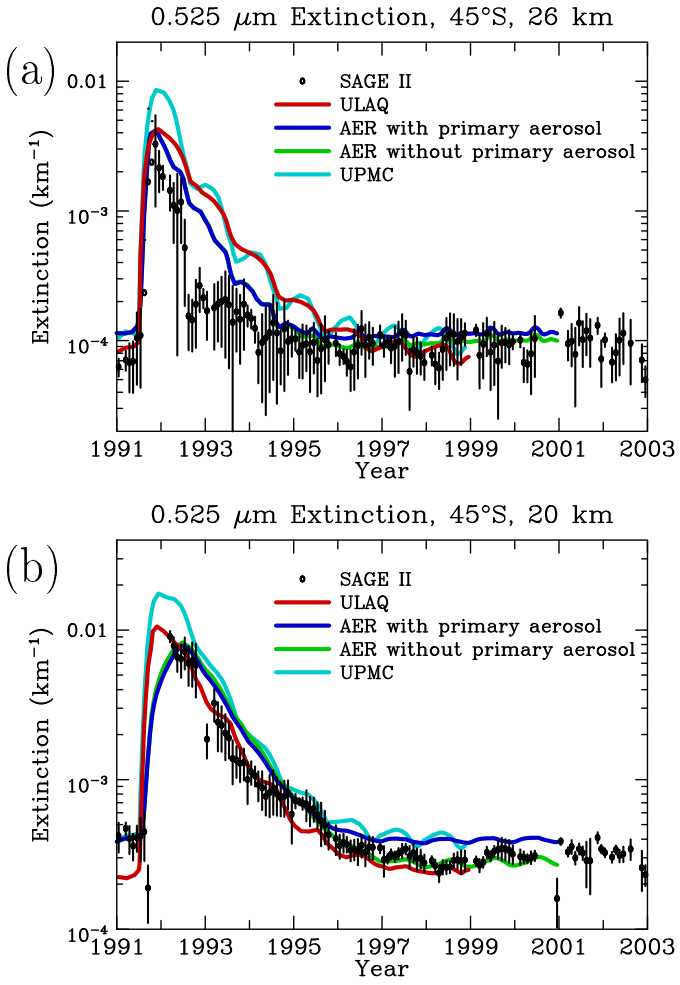

Figure 6.47: Aerosol extinction at 0.525 μm for 1991 to 2002 at (a) 45°S and 26 km and (b) 45°S and 20 km. SAGE II data are shown by symbols, model results by colored lines.

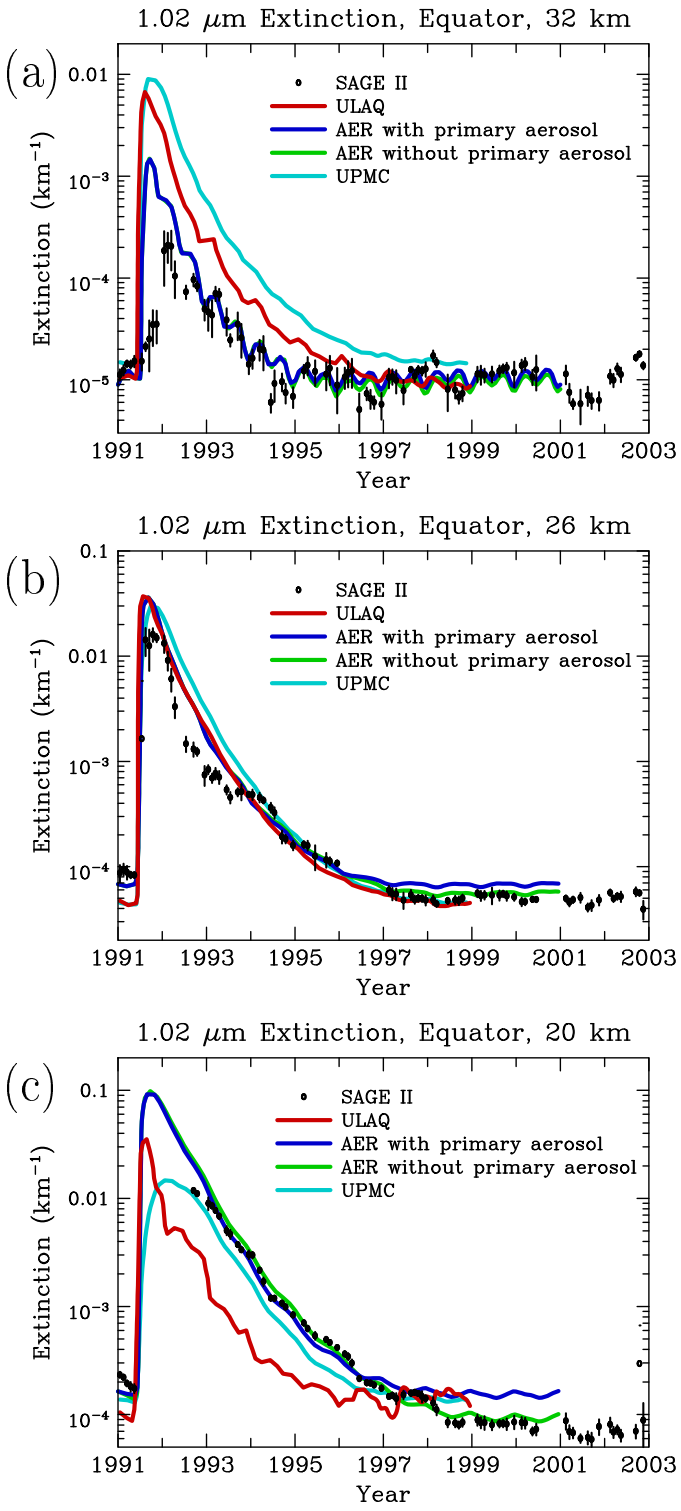

Figure 6.48: Aerosol extinction at 1.02 μm for 1991 to 2002 at (a) the equator and 32 km, (b) the equator and 26 km and (c) the equator and 20 km. SAGE II data are shown by symbols, model results by colored lines.

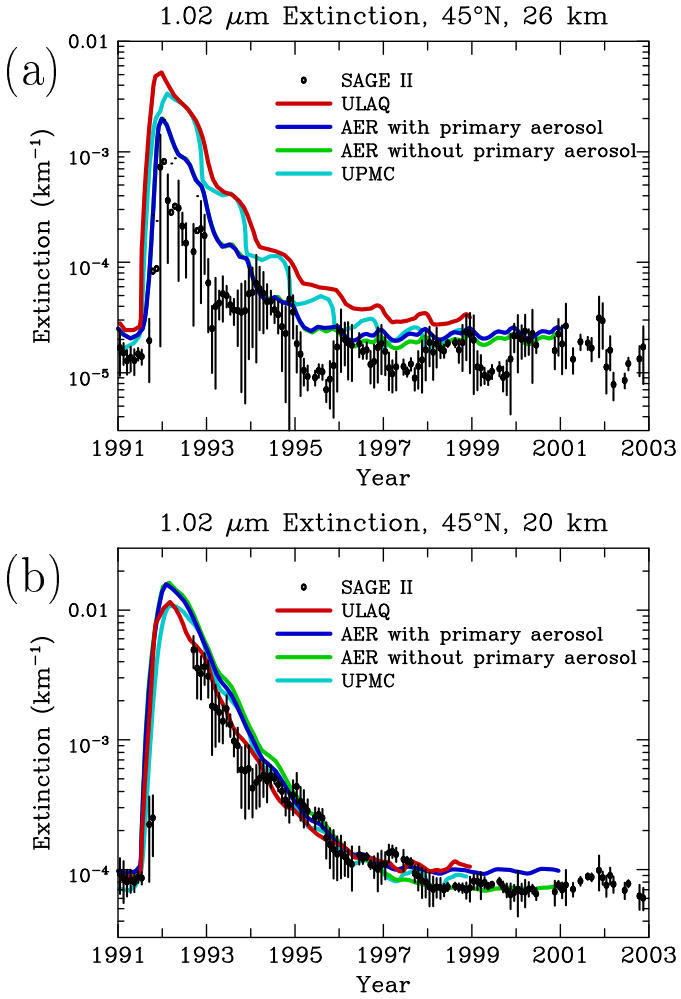

Figure 6.49: Aerosol extinction at 1.02 μm for 1991 to 2002 at (a) 45°N and 26 km and (b) 45°N and 20 km. SAGE II data are shown by symbols, model results by colored lines.

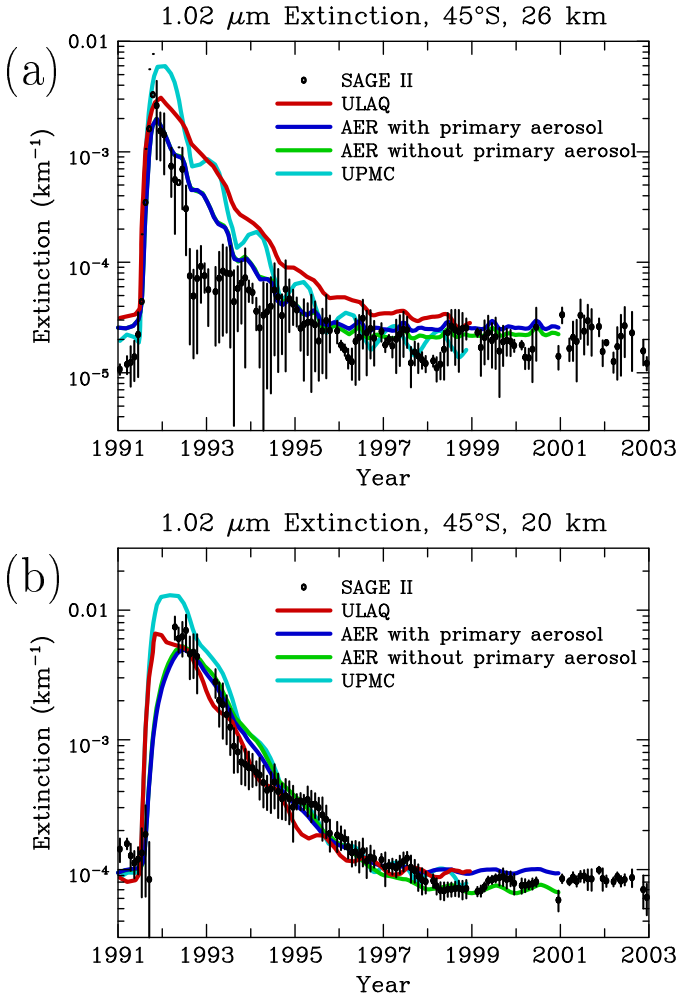

Figure 6.50: Aerosol extinction at 1.02 μm for 1991 to 2002 at (a) 45°S and 26 km and (b) 45°S and 20 km. SAGE II data are shown by symbols, model results by colored lines.

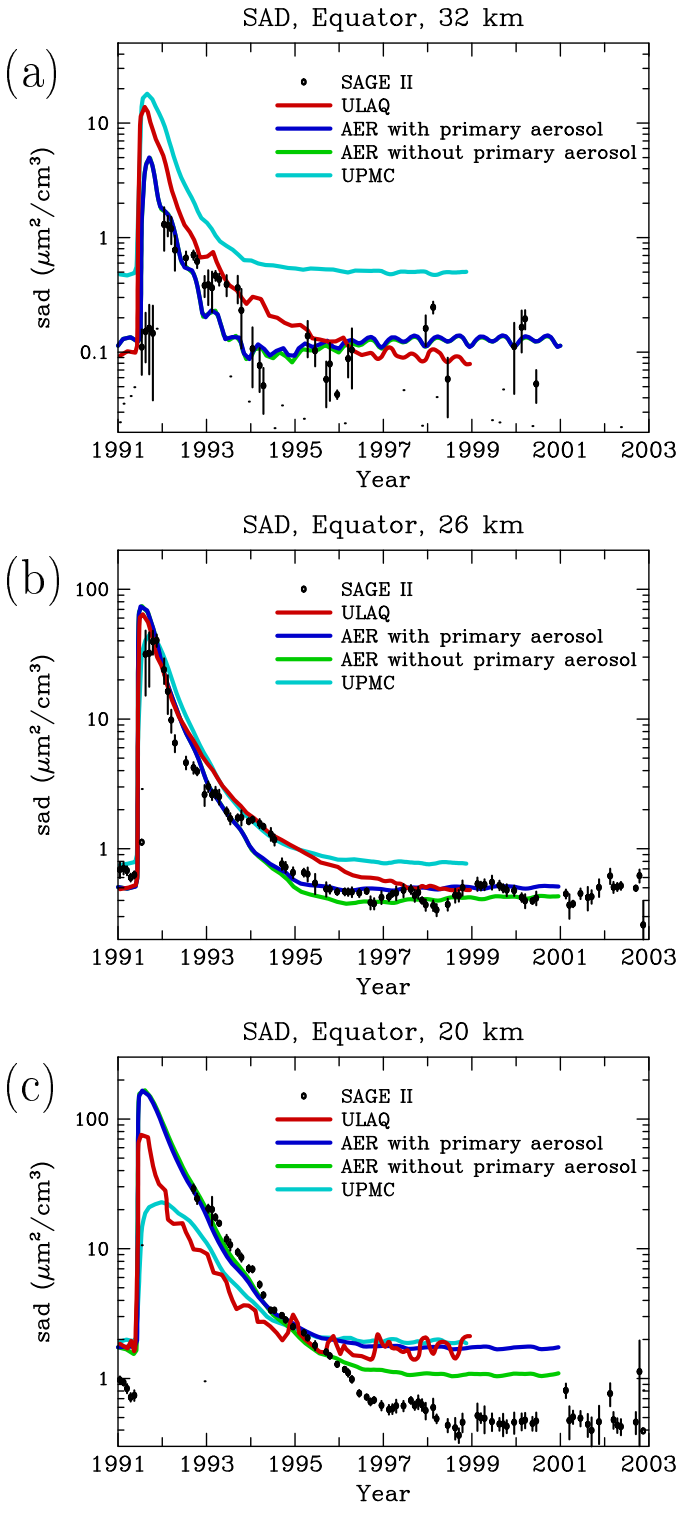

Figure 6.51: Surface area density (μm^2/cm^3) for 1991 to 2002 at the (a) equator and 32 km, (b) equator and 26 km, and (c) equator and 20 km. SAGE II results use Equation 4.1 to obtain surface area from the 1.02 and 0.525 μm extinction. Model-calculated surface area density is integrated over the model's entire size distribution.

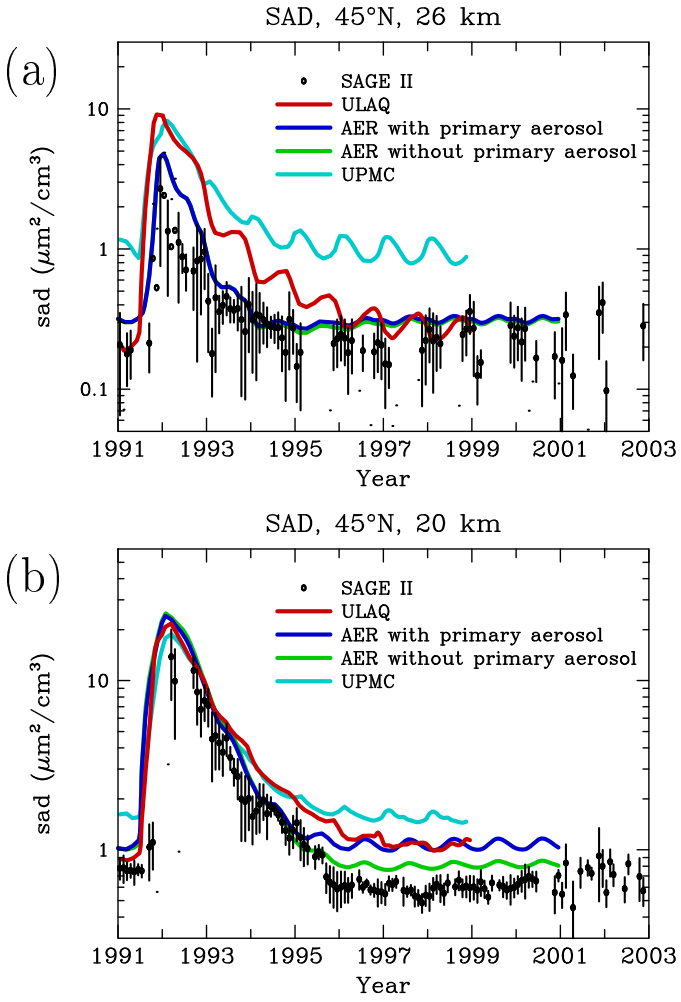

Figure 6.52: Surface area density (μm^2/cm^3) for 1991 to 2002 at (a) 45°N and 26 km and (b) 45°N and 20 km. SAGE II results use Equation 4.1 to obtain surface area from the 1.02 and 0.525 μm extinction. Model-calculated surface area density is integrated over the model's entire size distribution.

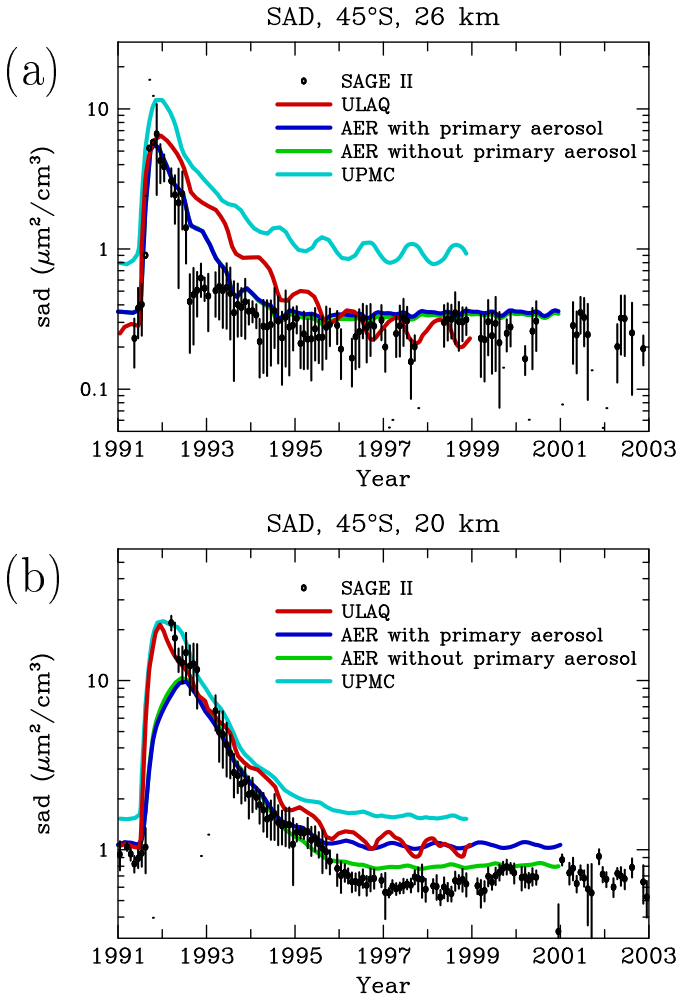

Figure 6.53: Surface area density (μm^2/cm^3) for 1991 to 2002 at (a) 45°S and 26 km and (b) 45°S 20 km. SAGE II results use Equation 4.1 to obtain surface area from the 1.02 and 0.525 μm extinction. Model-calculated surface area density is integrated over the model's entire size distribution.

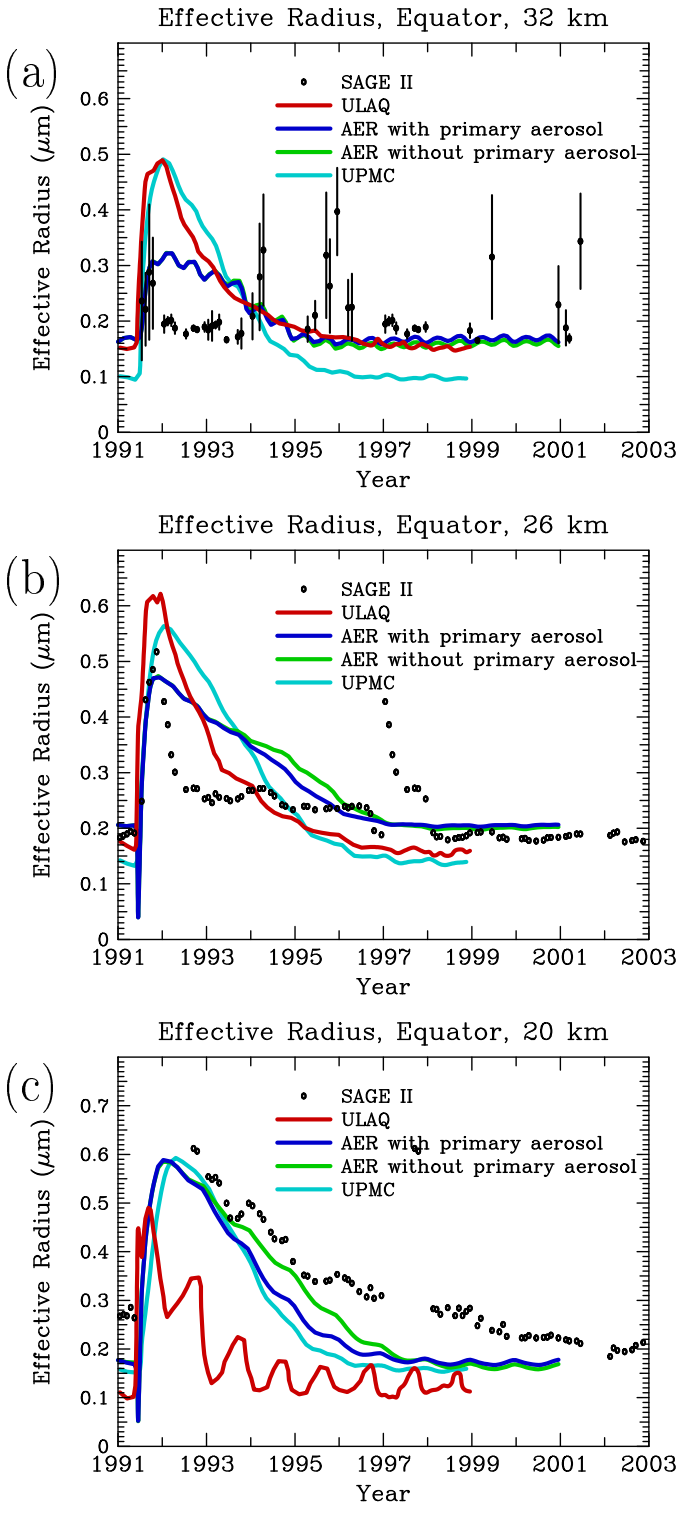

Figure 6.54: Effective radius (μm) for 1991 to 2002 at the (a) equator and 32 km, (b) equator and 26 km, and (c) equator and 20 km. SAGE II data are shown by symbols, model results by colored lines. SAGE II results use Equation 4.4 to obtain effective radius from the 1.02 μm extinction. Model-calculated effective radius is integrated over the model's entire size distribution.

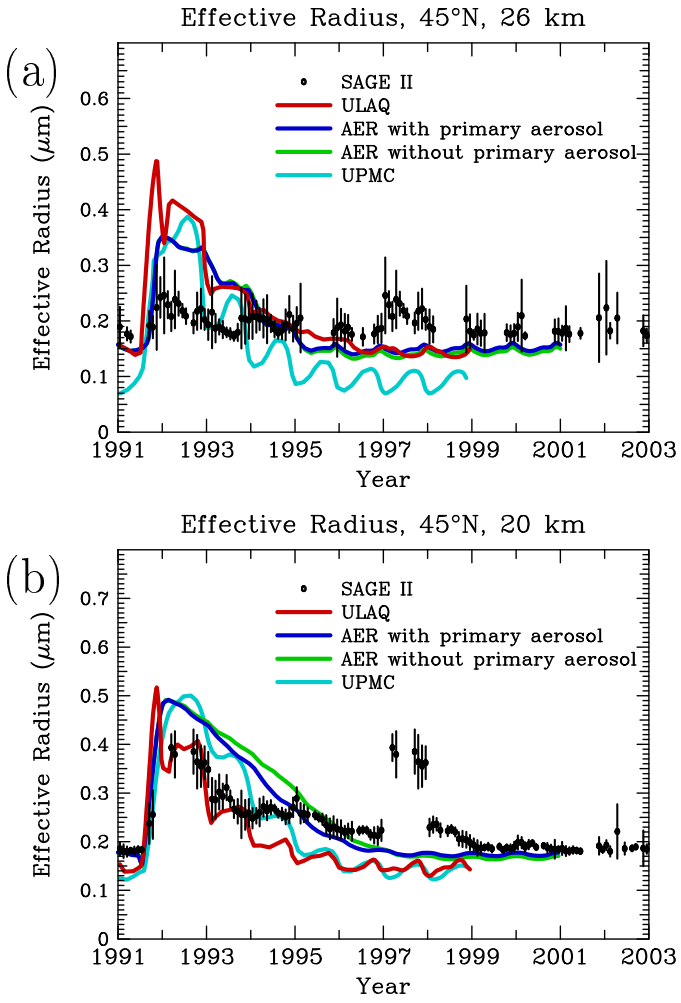

Figure 6.55: Effective radius (μm) for 1991 to 2002 at (a) 45°N and 26 km and (b) 45°N and 20 km. SAGE II data are shown by symbols, model results by colored lines. SAGE II results use Equation 4.4 to obtain effective radius from the 1.02 μm extinction. Model-calculated effective radius is integrated over the model's entire size distribution.

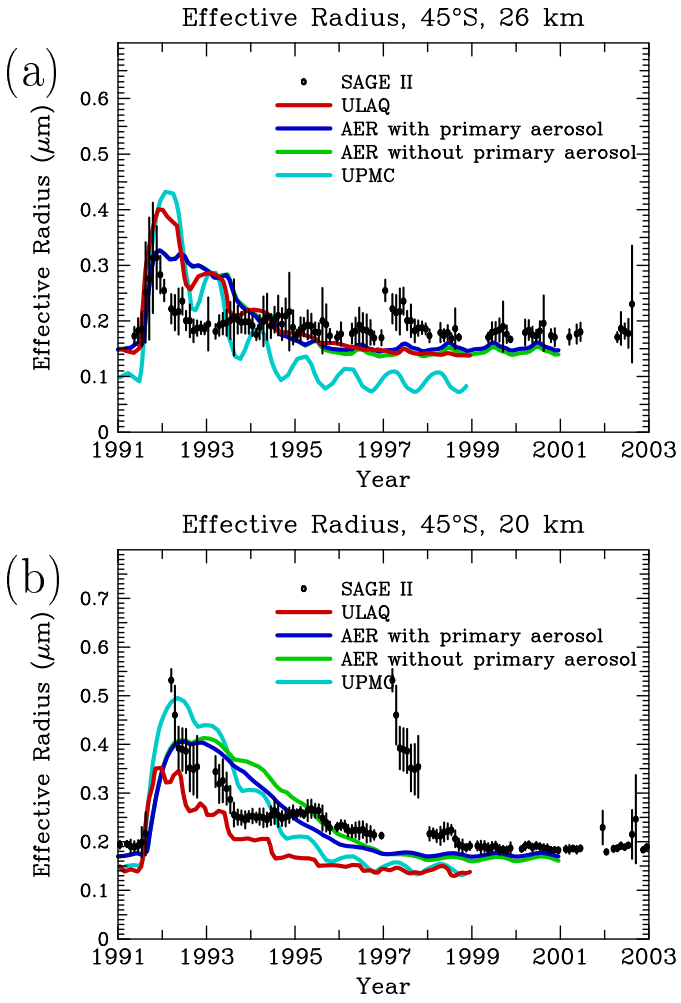

Figure 6.56: Effective radius (μm) for 1991 to 2002 at (a) 45°S and 26 km and (b) 45°S and 20 km. SAGE II data are shown by symbols, model results by colored lines. SAGE II results use Equation 4.4 to obtain effective radius from the 1.02 μm extinction. Model-calculated effective radius is integrated over the model's entire size distribution.

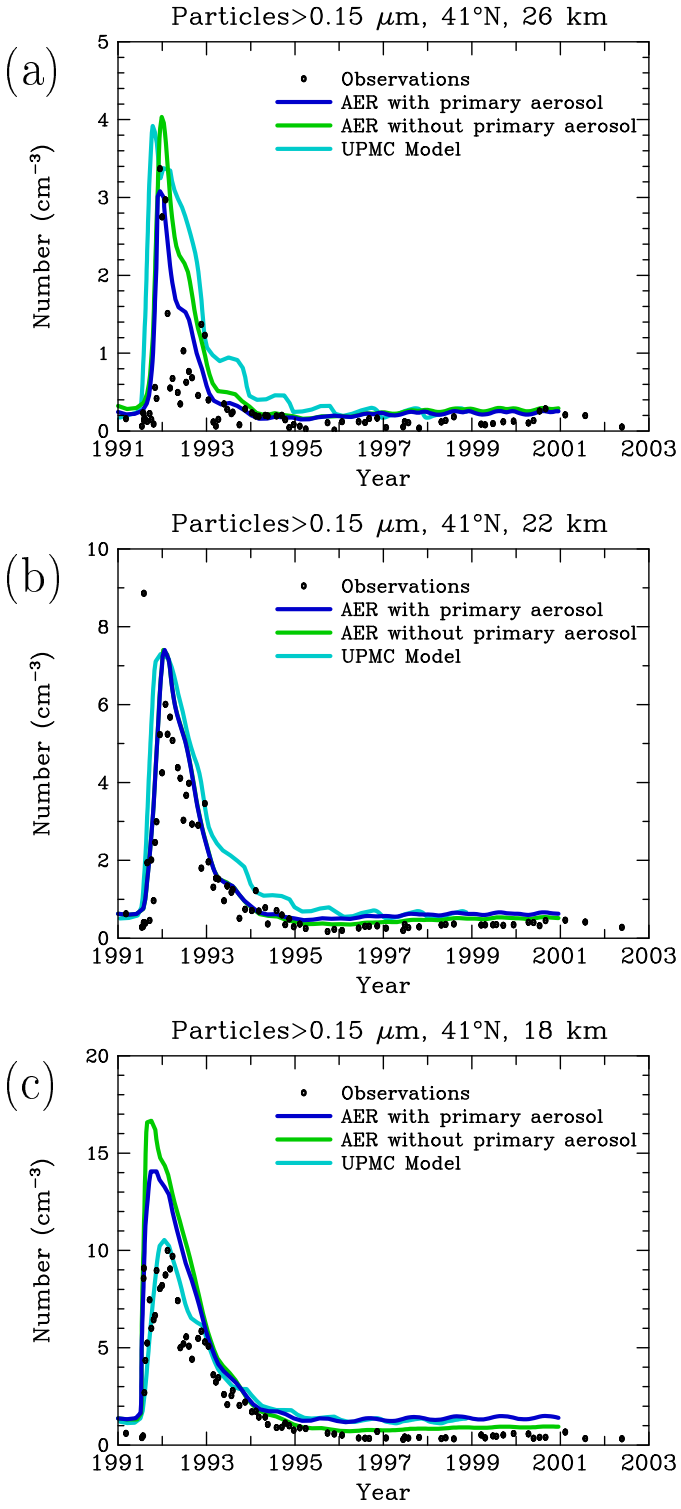

Figure 6.57: Number densities (particles/cm^3) of particles with radius greater than 0.15 μm for 1991 to 2002 at (a) 18 km, (b) 22 km and (c) 26 km in Wyoming. Observations taken at the University of Wyoming are shown by symbols, model results by colored lines.

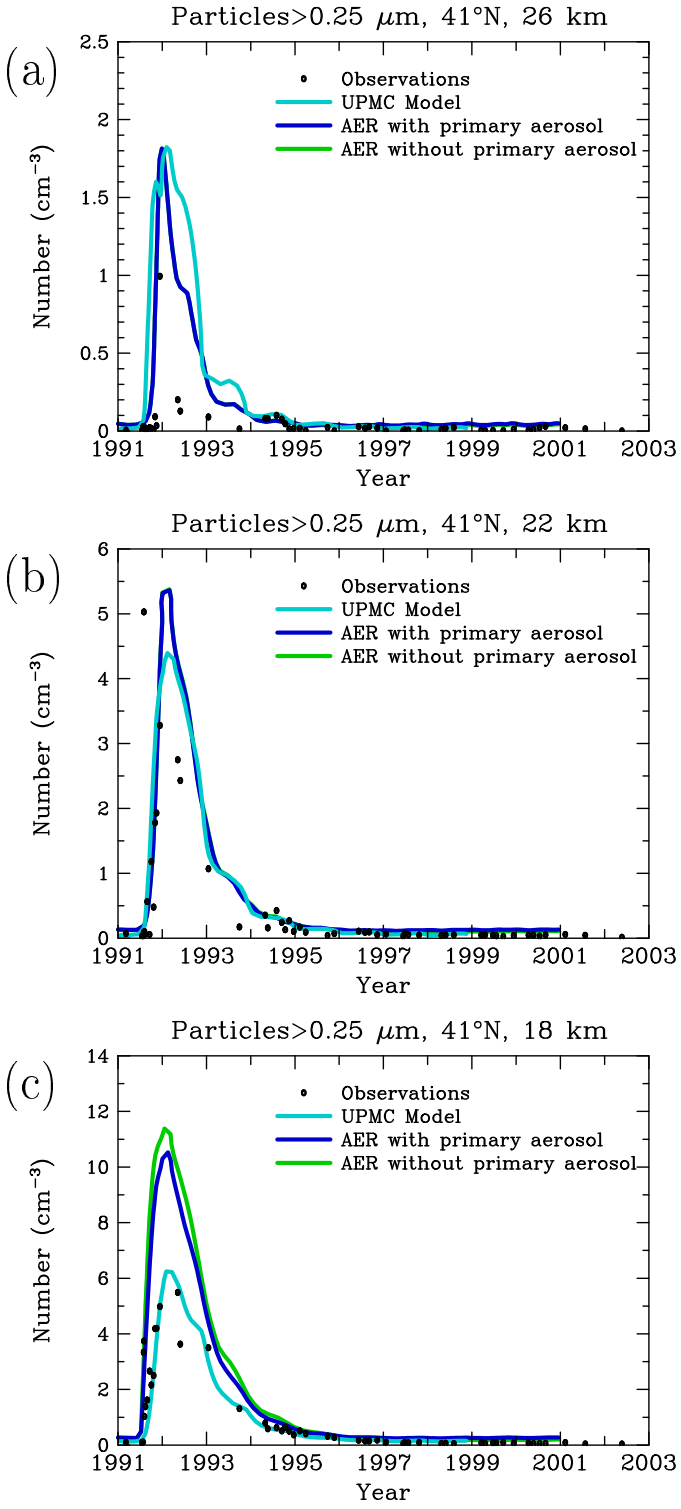

Figure 6.58: Number densities (particles/cm^3) of particles with radius greater than 0.25 μm for 1991 to 2002 at (a) 18 km, (b) 22 km and (c) 26 km in Wyoming. Observations taken at the University of Wyoming are shown by symbols, model results by colored lines.

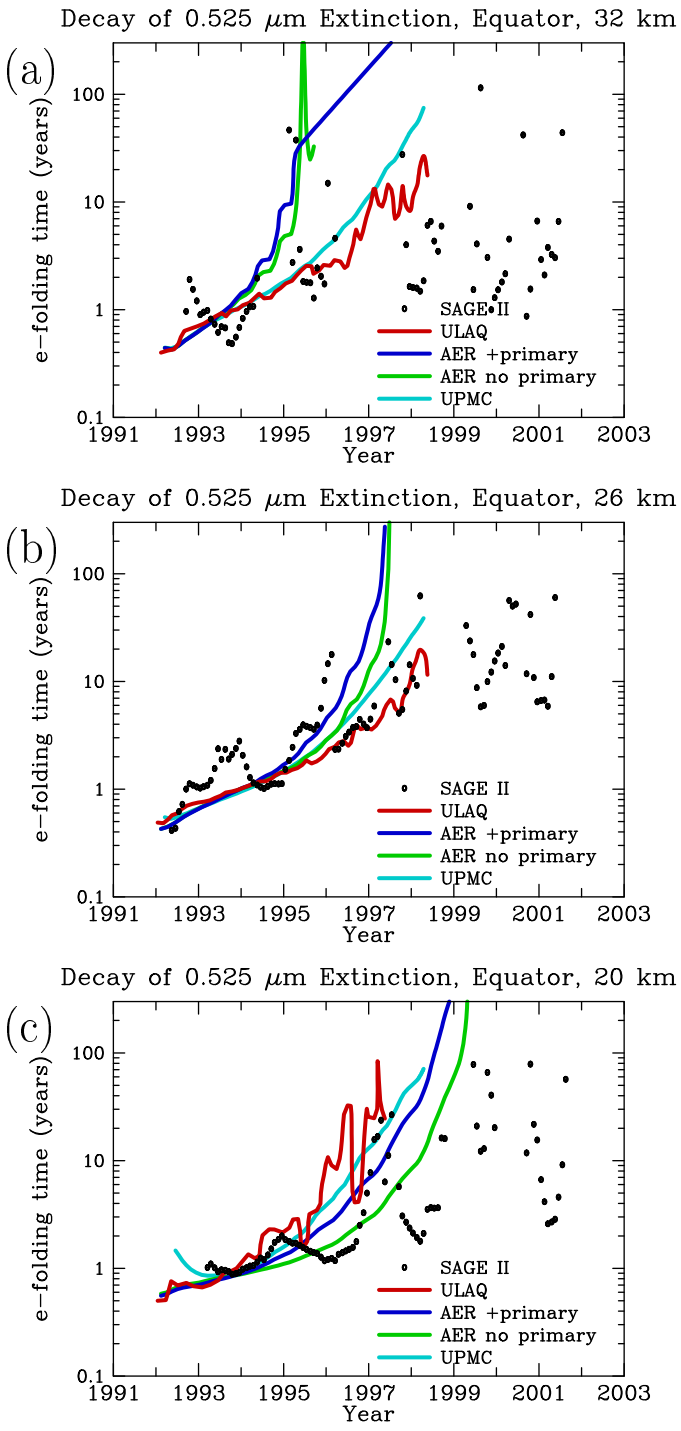

Figure 6.59: E-folding time of aerosol extinction at 0.525 μm for 1991 to 2002 at the (a) equator and 32 km, (b) equator and 26 km, and (c) equator and 20 km. SAGE II data are shown by symbols, model results by colored lines.

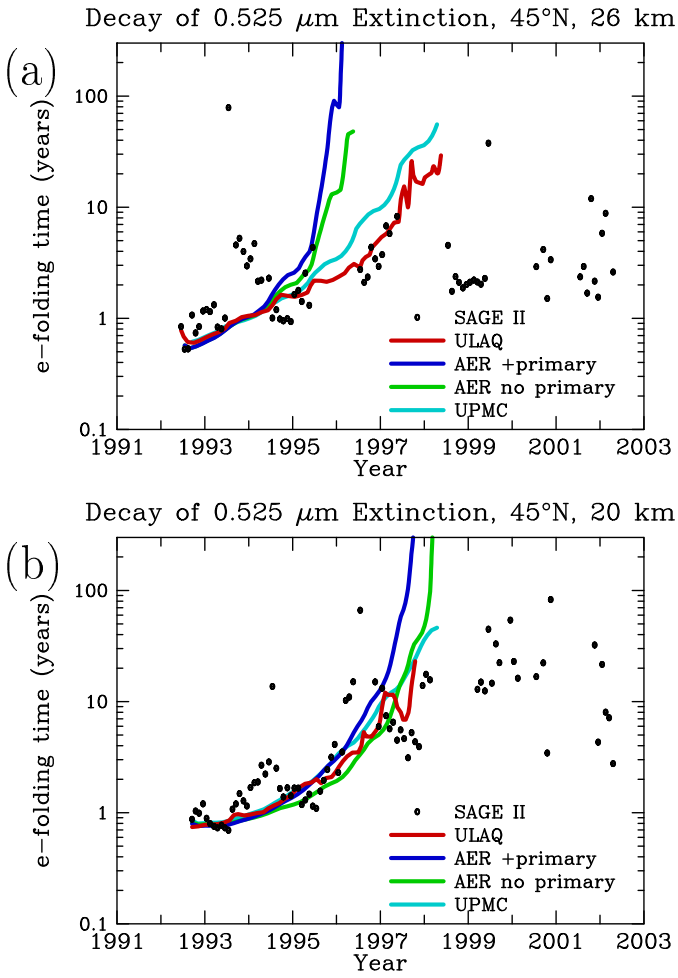

Figure 6.60: E-folding time of aerosol extinction at 0.525 μm for 1991 to 2002 at (a) 45°N and 26 km and (b) 45°N and 20 km. SAGE II data are shown by symbols, model results by colored lines.

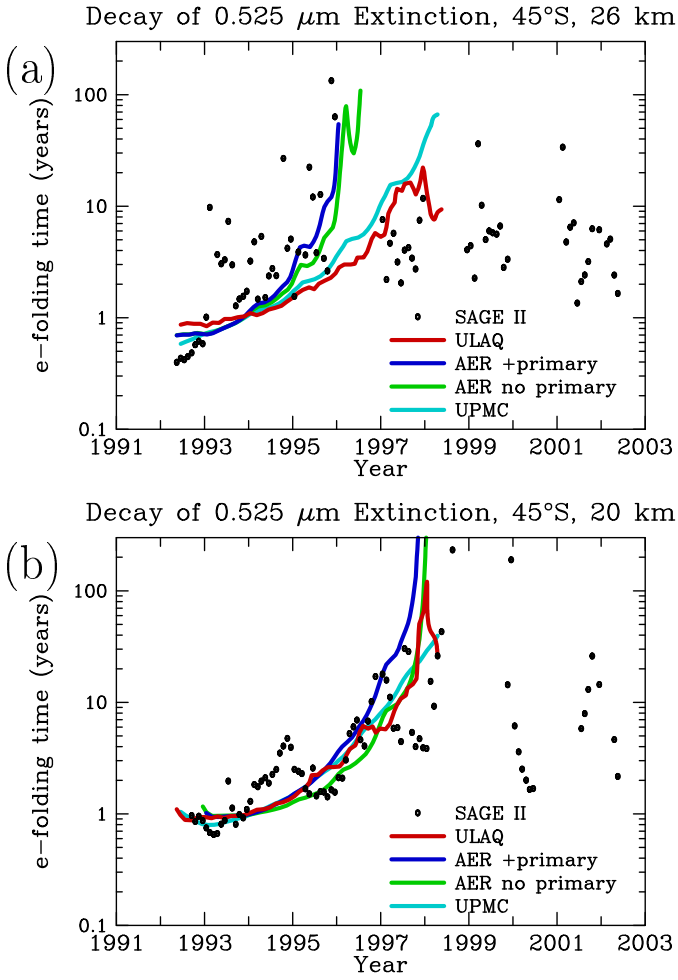

Figure 6.61: E-folding time of aerosol extinction at 0.525 μm for 1991 to 2002 at (a) 45°S and 26 km and (b) 45°S and 20 km. SAGE II data are shown by symbols, model results by colored lines.

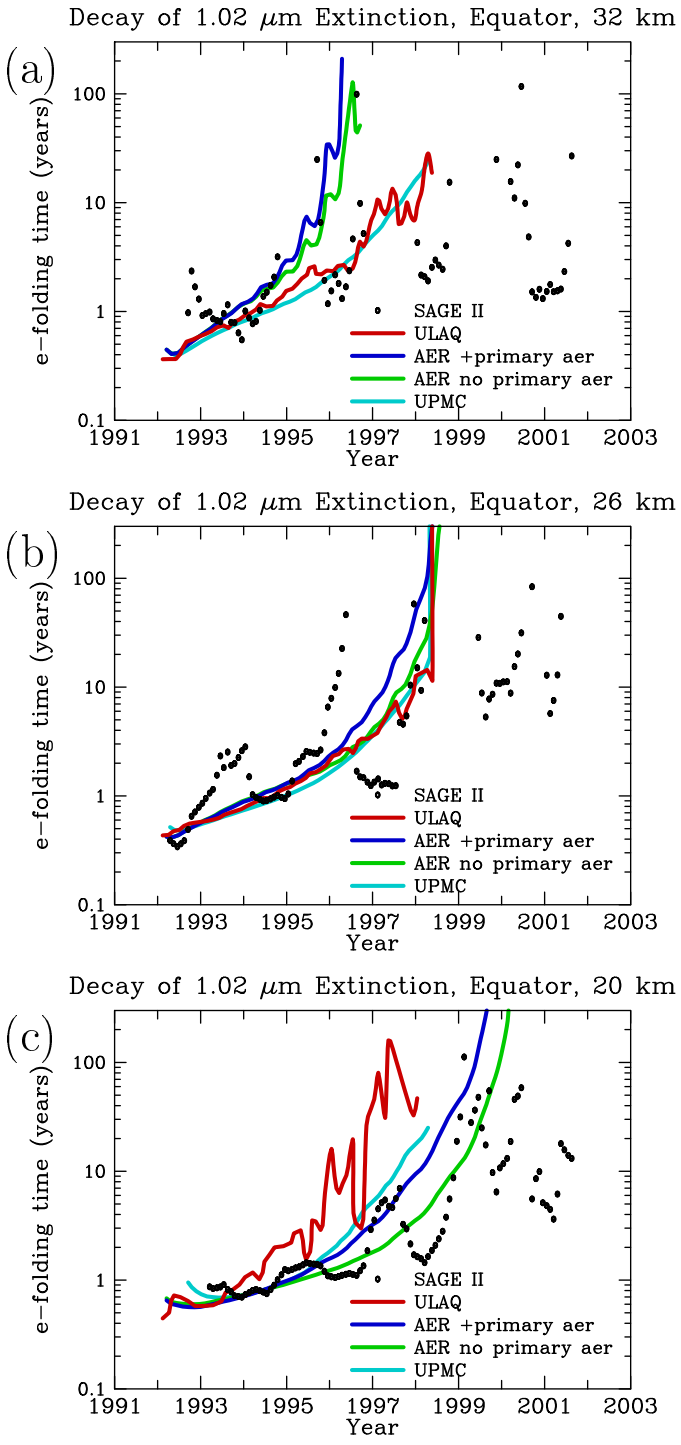

Figure 6.62: E-folding time of aerosol extinction at 1.02 μm for 1991 to 2002 at the (a) equator and 32 km, (b) equator and 26 km, and (c) equator and 20 km. SAGE II data are shown by symbols, model results by colored lines.

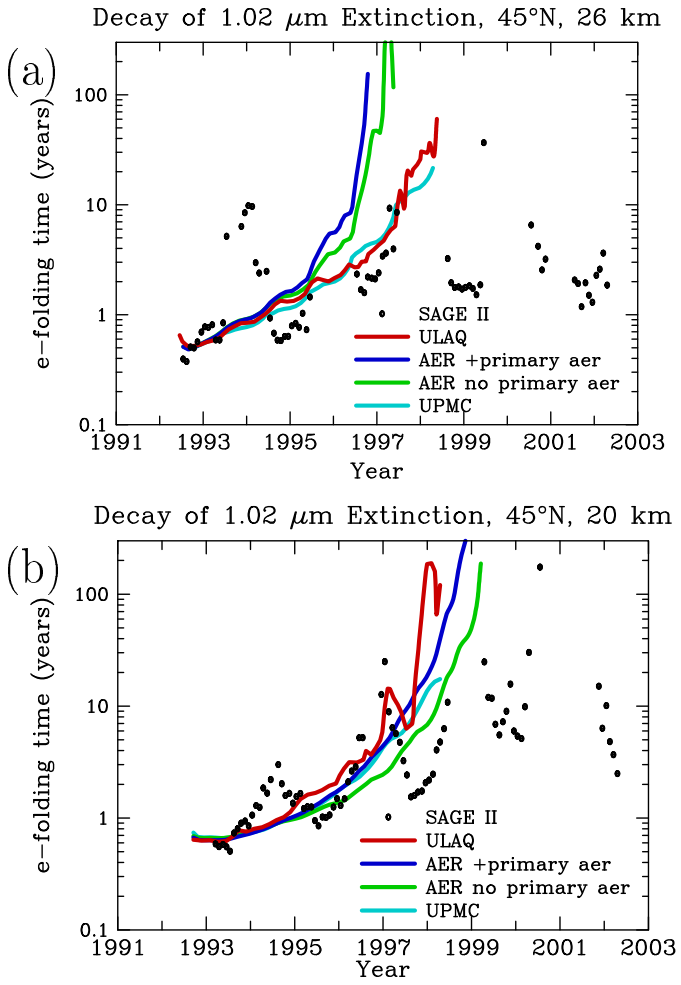

Figure 6.63: E-folding time of aerosol extinction at 1.02 μm for 1991 to 2002 at (a) 45°N and 26 km and (b) 45°N and 20 km. SAGE II data are shown by symbols, model results by colored lines.

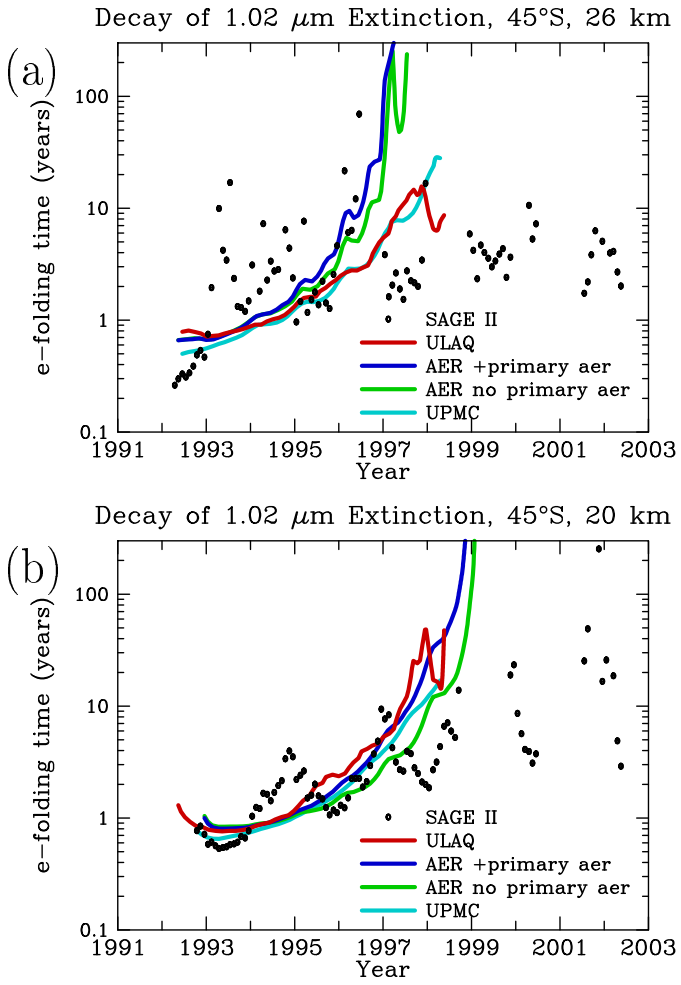

Figure 6.64: E-folding time of aerosol extinction at 1.02 μm for 1991 to 2002 at (a) 45°S and 26 km and (b) 45°S and 20 km. SAGE II data are shown by symbols, model results by colored lines.

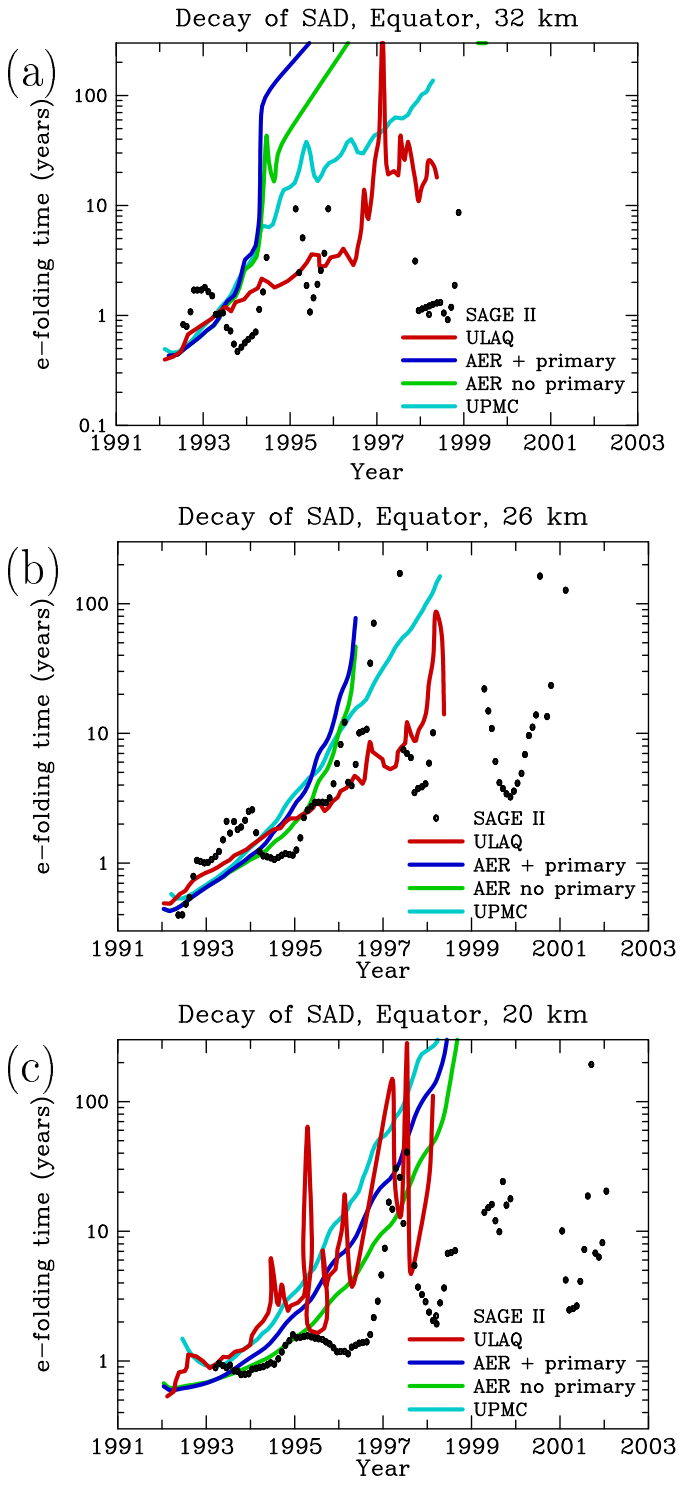

Figure 6.65: E-folding time of surface area density for 1991 to 2002 at the (a) equator and 32 km, (b) equator and 26 km, and (c) equator and 20 km. SAGE II data are shown by symbols, model results by colored lines.

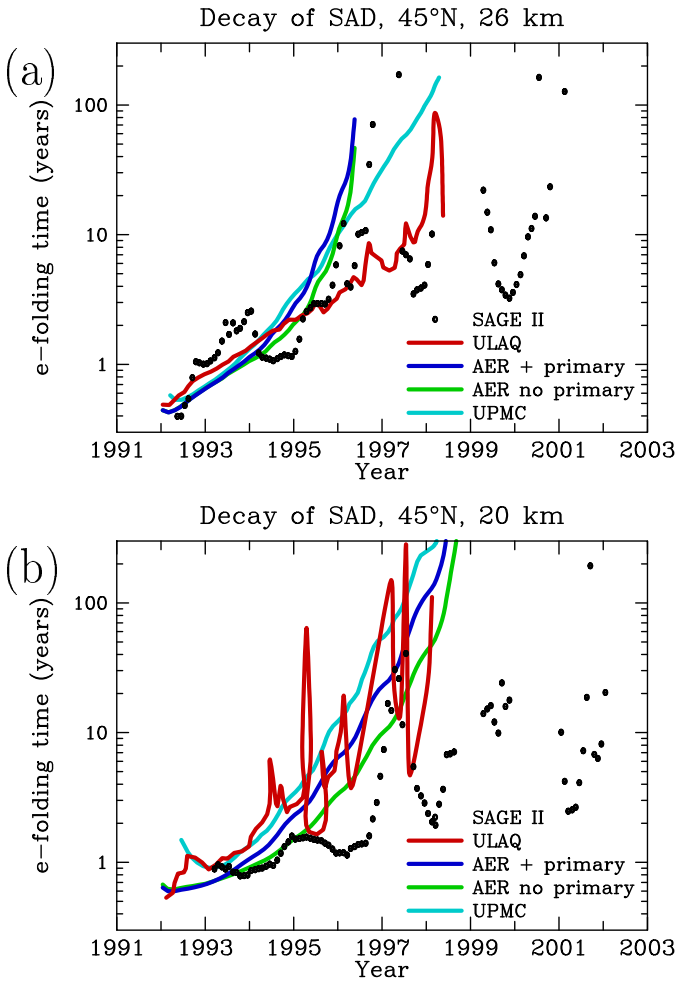

Figure 6.66: E-folding time of surface area density for 1991 to 2002 at (a) 45°N and 26 km and (b) 45°N and 20 km. SAGE II data are shown by symbols, model results by colored lines.

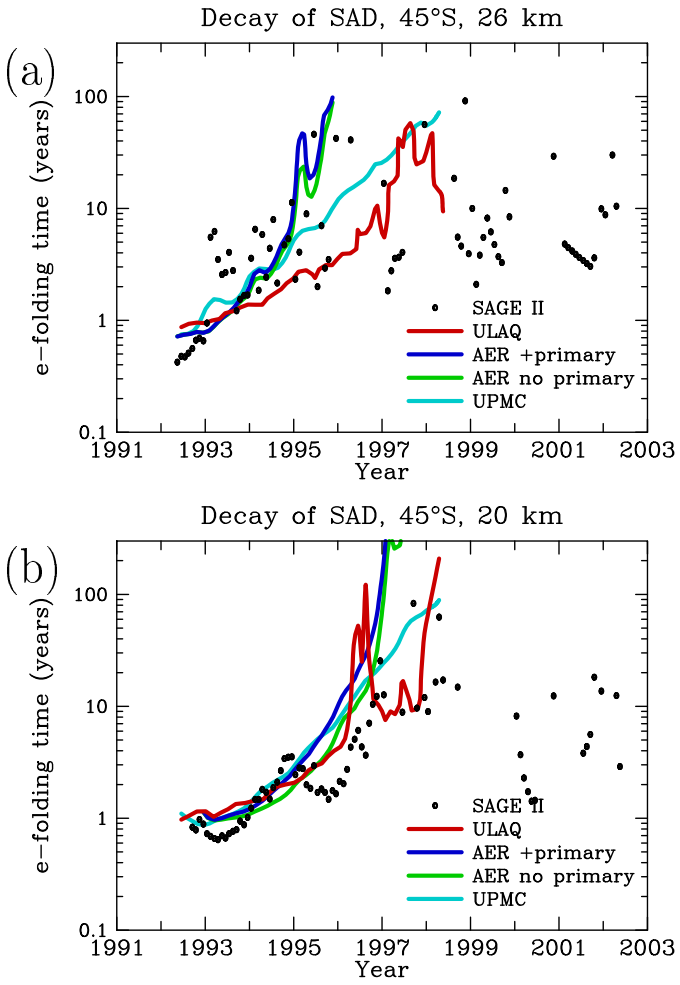

Figure 6.67: E-folding time of surface area density for 1991 to 2002 at (a) 45°S and 26 km and (b) 45°S and 20 km. SAGE II data are shown by symbols, model results by colored lines.

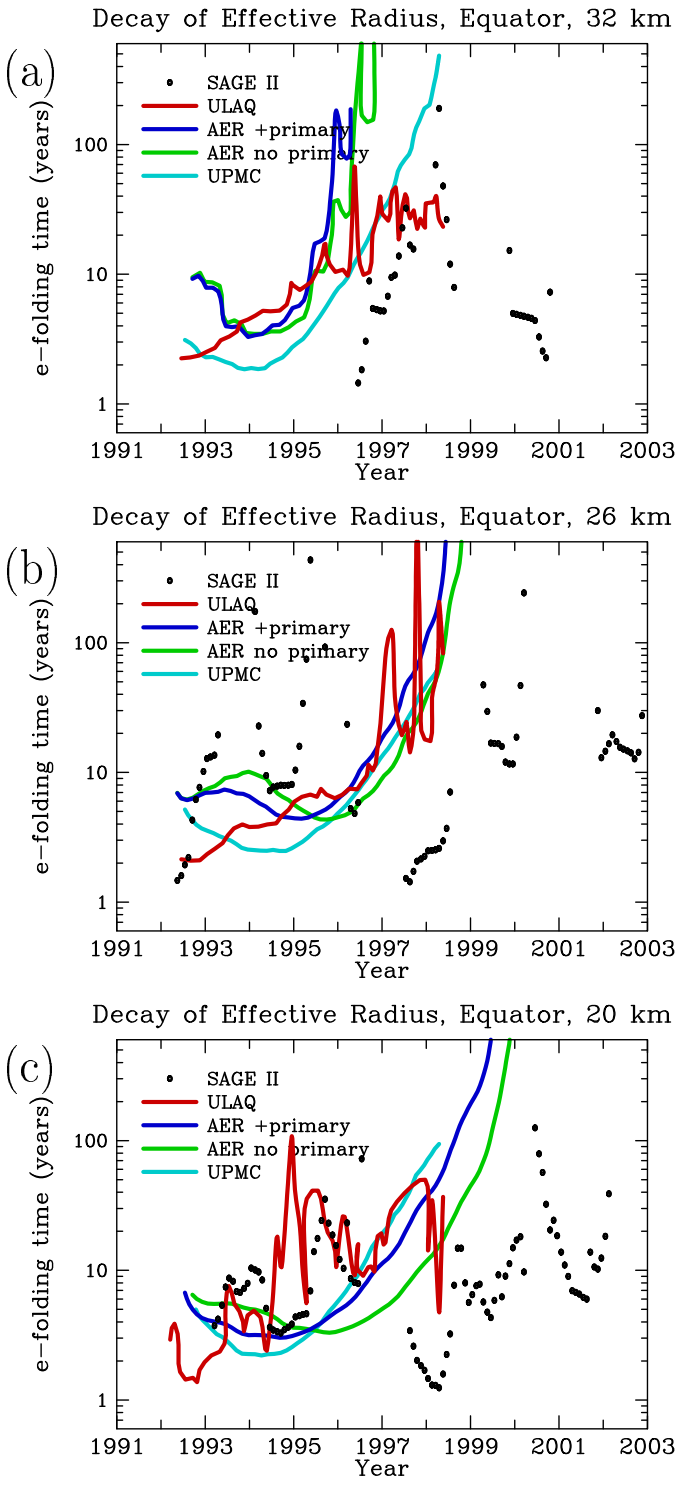

Figure 6.68: E-folding time of effective radius for 1991 to 2002 at the (a) equator and 32 km, (b) equator and 26 km, and (c) equator and 20 km. SAGE II data are shown by symbols, model results by colored lines.

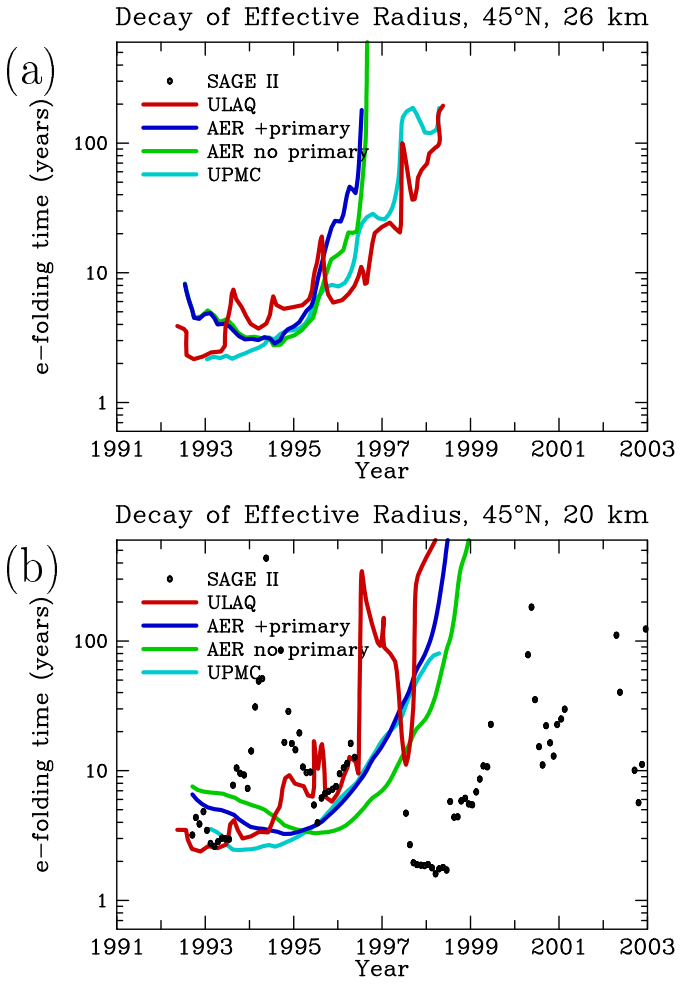

Figure 6.69: E-folding time of effective radius for 1991 to 2002 at (a) 45°N and 26 km and (b) 45°N and 20 km. SAGE II data are shown by symbols, model results by colored lines.

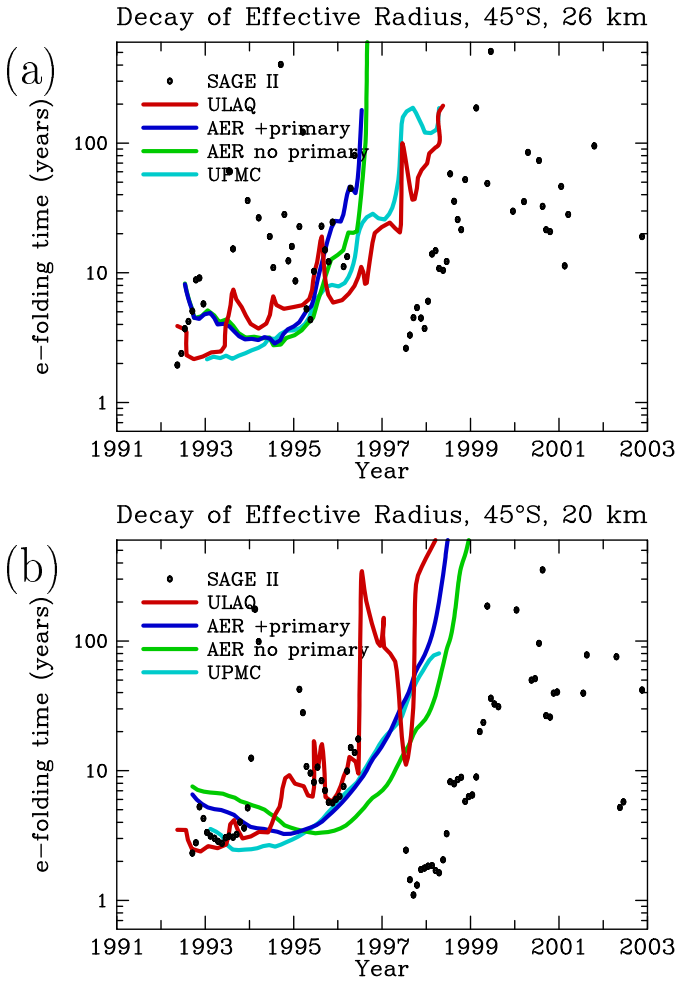

Figure 6.70: E-folding time of effective radius for 1991 to 2002 at (a) 45°S and 26 km and (b) 45°S and 20 km. SAGE II data are shown by symbols, model results by colored lines.

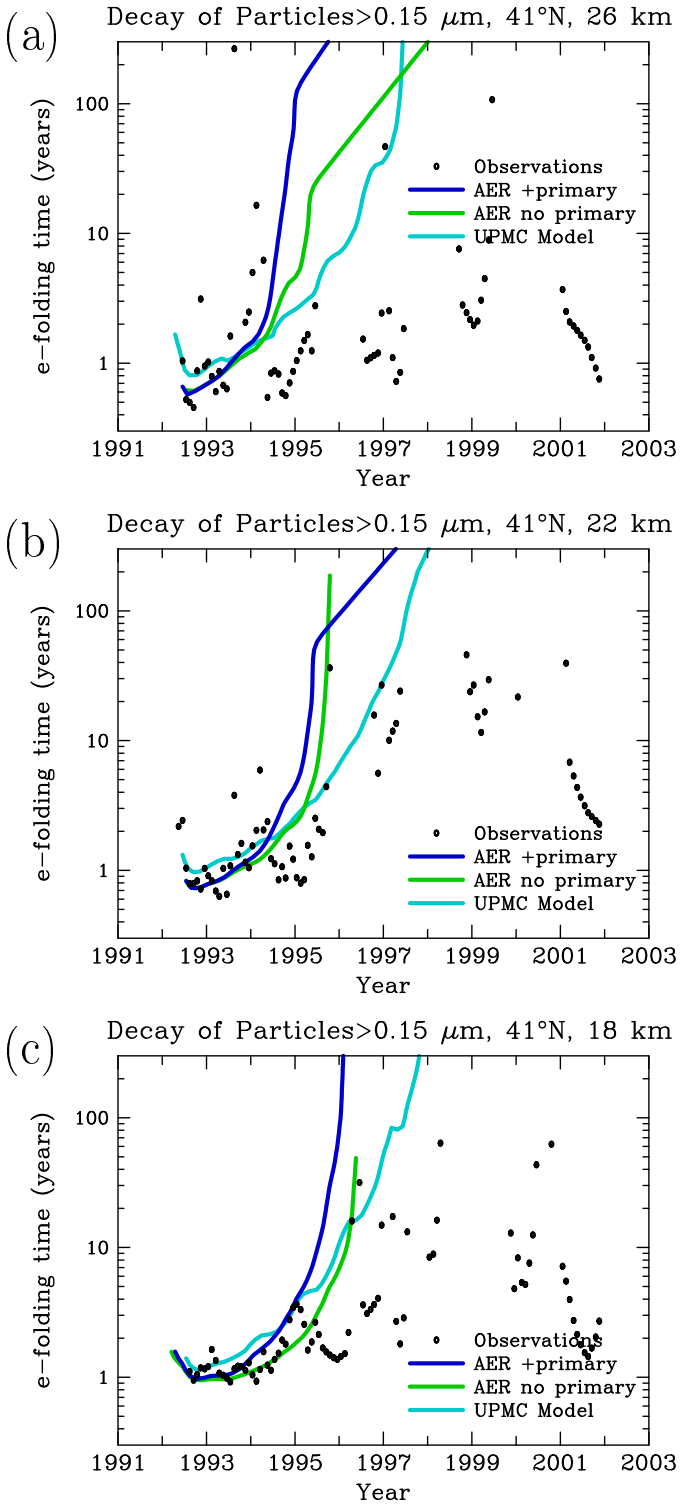

Figure 6.71: Decay of number densities of particles with radius greater than 0.15 μm for 1991 to 2002 at the (a) 18 km, (b) 22 km and (c) 26 km in Wyoming. Observations taken at the University of Wyoming are shown by symbols, model results by colored lines.

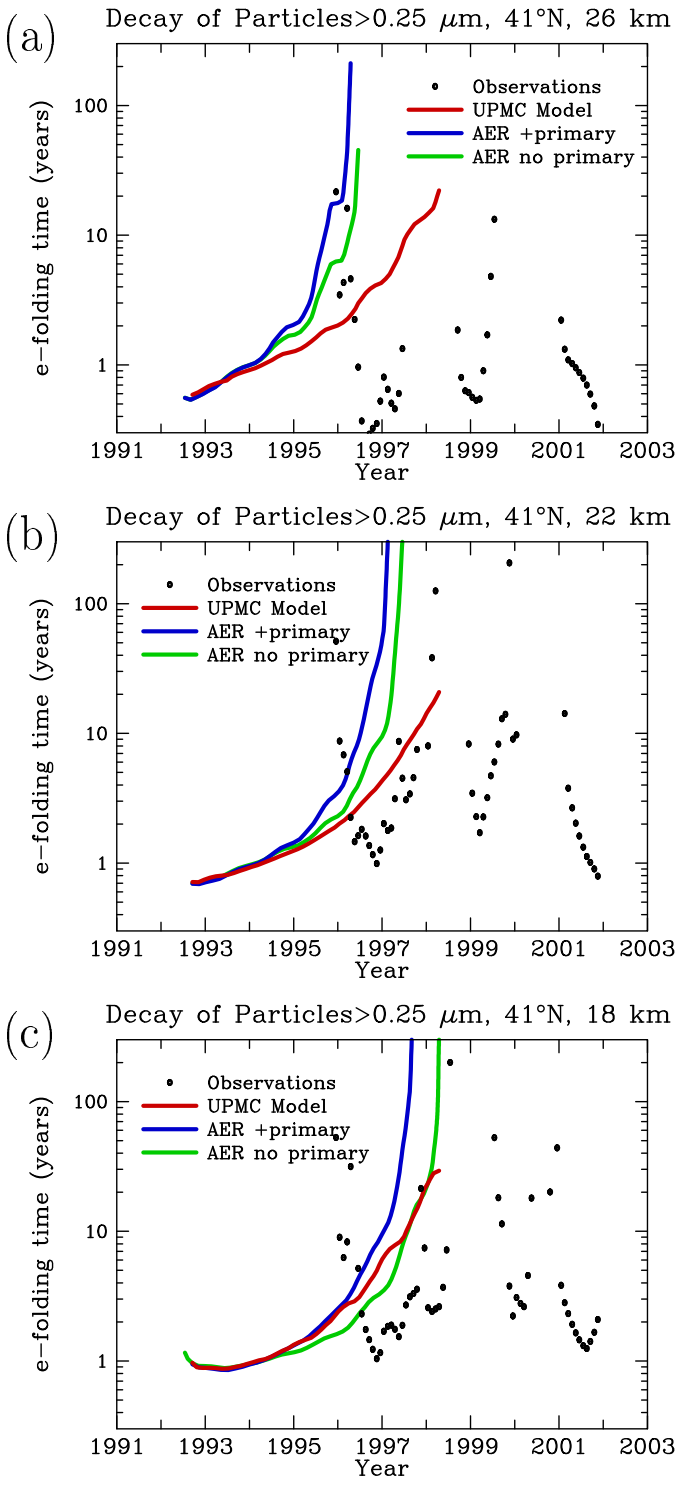

Figure 6.72: Decay of number densities of particles with radius greater than 0.25 μm for 1991 to 2002 at the (a) 18 km, (b) 22 km and (c) 26 km in Wyoming. Observations taken at the University of Wyoming are shown by symbols, model results by colored lines.